

**SERVO CONTROL OF AN UNDERACTUATED POWER
TRANSMISSION SYSTEM: ANALYSIS OF A SPUR GEAR
PAIR**

**EKSİK TAHRİKLİ GÜÇ AKTARIM SİSTEMİNİN SERVO
KONTROLÜ: BİR ÇİFT DÜZ DİŞLİNİN ANALİZİ**

ABBAS KHOSHVAGHT PIRSOLTAN

ASST. PROF. DR. CAN ULAŞ DOĞRUEK
Supervisor

Submitted to Graduate School of Sciences and Engineering of Hacettepe University
as a Partial Fulfillment to the Requirements
for the Award of the Master of Science Degree
in Mechanical Engineering

2015

ABBAS KHOSHVAGHT PIRSOLTAN' in hazırladığı “**Eksik Tahrikli Güç Aktarım Sisteminin Servo Kontrolü: Bir Çift Düz Dişlinin Analizi**” adlı bu çalışma aşağıdaki jüri tarafından **MAKİNE MÜHENDİSLİĞİ ANABİLİM DALI'** nda **YÜKSEK LİSANS TEZİ** olarak kabul edilmiştir.

Prof. Dr. Bora YILDIRIM
Başkan

Yrd. Doç. Dr. Can Ulaş DOĞRUER
Danışman

Prof. Dr. Bora YILDIRIM
Üye

Doç. Dr. Melik DÖLEN
Üye

Bu tez Hacettepe Üniversitesi Fen Bilimleri Enstitüsü tarafından **YÜKSEK LİSANS TEZİ** olarak onaylanmıştır.

Prof. Dr. Fatma SEVİN DÜZ
Fen Bilimleri Enstitüsü Müdürü

This work named "**Servo Control of an Underactuated Power Transmission System: Analysis of a Spur Gear Pair**" by **ABBAS KHOSHVAGHT PIRSOLTAN** has been approved as a thesis for the **MASTER OF SCIENCE DEGREE IN MECHANICAL ENGINEERING** by the below mentioned Examining Committee Members.

Prof. Dr. Bora YILDIRIM
Head

Asst. Prof. Dr. Can Ulaş DOĞRUER
Supervisor

Prof. Dr. Bora YILDIRIM
Member

Assoc. Prof. Dr. Melik DÖLEN
Member

This thesis has been approved as a thesis for the **MASTER OF SCIENCE DEGREE IN MECHANICAL ENGINEERING** by Board of Directors of the Institute for Graduate School of Science and Engineering.

Prof. Dr. Fatma SEVİN DÜZ
Director of the Institute of
Graduate School of Science and Engineering

ETHICS

In this thesis study, prepared in accordance with the spelling rules of Institute of Graduate Studies in Science of Hacettepe University,

I declare that

- all the information and documents have been obtained in the base of the academic rules
- all audio-visual and written information and results have been according to the rules of scientific ethics
- In case of using others works, related studies have been cited in according with the scientific standards
- all cited studies have been fully referenced
- I did not do any distortion in the data set
- and any part of this thesis has not been presented as another thesis study at this or any other university.

15/12/2015

ABBAS KHOSHVAGHT PIRSOLTAN

ABSTRACT

SERVO CONTROL OF AN UNDERACTUATED POWER TRANSMISSION SYSTEM: ANALYSIS OF A SPUR GEAR PAIR

Abbas KHOSHVAGHT PIRSOLTAN

Master of Science Degree, Department of Mechanical Engineering

Supervisor: Asst. Prof. Dr. Can Ulaş DOĞRUER

December 2015, 108 pages

Among many types of gears, spur gears have the highest efficiency. This type of gears need less space than any other gears and they produce lower axial thrust. So, they have a much simple bearing system. Spur gears yield less heat, and manufacturing of them is simpler than others. Transmission error (TE) is one of the disadvantages of spur gearboxes. TE are caused by many factors, but the most important factor is mesh stiffness variation. When a pair of gears are rotating, according to the value of contact ratio, the number of contact teeth are constantly changing from m to $m + 1$ (m =minimum number of teeth in contact). This variation in the number of teeth in contact causes high changes in total stiffness. As a result, it causes transmission errors. Researchers have developed different methods to eliminate or minimize the transmission error. In this study, a control method has been developed. In this method by using a control law, system can regulate output of gearbox.

Here, gear parametric design method is done in Solidworks program. It is possible to generate different spur gears with different teeth numbers, module, tooth wide, and pressures angle. All parameters of gears are in accordance with conventional mathematical and geometric equations of gear design. Involute curves on the base

circle are designed according to Involute equation. Also, typical spur gearbox is designed to have gear pair with real parameters.

Gears mesh stiffness is computed by using both analytical and numerical (Finite Element) methods. Mesh stiffness computation is based on the theory of energy stored in the material. Deflection value is obtained based on the applied moment, and stiffness is calculated by using that method. The results of the analytical and finite element methods are compared with each other.

Control system design for regulation and linearization of gearbox output are done according to the theory of trajectory tracking. Trajectory tracking of transmission error curve is done by the method of underactuated multibody system. In this method, output is measured by sensors. The system is linearized and the remaining linear portion of the dynamics is controlled with a PI controller. Factors such as the number of teeth, gear base circle diameter, material, weight, geometry, and transmission ratio are effective in system responses.

The results show that the method of underactuated multibody system is effective in regulation gearbox output. When this control law is used to control the torque input acting on the designed gearbox, the output will be quite uniform, transmission error will be minimized, and vibration and noise will be decreased.

Keywords: Spur Gear, Transmission Error, Servo Control, Underactuated Multibody Systems, Spur Gear Dynamics

ÖZ

EKSİK TAHRİKLİ GÜÇ AKTARIM SİSTEMİNİN SERVO KONTROLÜ: BİR ÇİFT DÜZ DİŞLİNİN ANALİZİ

Abbas KHOSHVAGHT PIRSOLTAN

Yüksek Lisans, Makina Mühendisliği Bölümü

Tez Danışmanı: Yrd. Doç. Dr. Can Ulaş DOĞRUER

Aralık 2015, 108 sayfa

Düz dişliler diğer dişlilerin karşılaştırıldığında en yüksek verime sahip oldukları görülür. Bu tür dişliler daha dar alanda kullanılabilir ve yataklara aksenal kuvvet uygulamaz. Düz dişlilerin yatak sistemleri diğer dişlilere göre daha basittir. Düz dişliler çalışma sırasında daha az ısı üretir ve imalatı daha basittir. Bu tür dişlilerin en büyük dezavantajları iletim hatası sayılır. İletim hatası birçok nedenden olabilir. En önemli nedeni iki dişli arasındaki esneklik katsayısının zaman ile değişimidir. Bir çift dişli döndüğü zaman dişli ve çarkın değme oranına göre temas halinde olan dişlerin sayısı m ile $m + 1$ (m =temas halinde olan dişlerin sayısı) arası değişir. Bu temas halinde olan dişlerin sayısındaki değişiklik esneklik katsayısında büyük değişikliğe neden olur ve sonuçta iletim hatası oluşur. Araştırmacılar iletim hatalarının kaldırılması veya azalması için farklı yöntemler geliştirmişler. Bu çalışmada bir kontrol yöntemiyle iletim hatasının etkisinin azaltılmasına çalışıldı. Bu yöntemde sistem kontrolcüsü dişli kutusunun çıkış milindeki hataları.

Dişli tasarımında Solidworks'ta parametrik tasarım yöntemi kullanılmıştır. Bu program vasıtası ile farklı ölçülerde, modüllerde, basınç açısı ve farklı diş sayısında düz dişliler üretilebilir. Dişlilerin tüm değişkenleri konvansiyonel matematiksel ve

geometrik denklemlere uyumlu tasarlanmıştır. Temel dairenin üzerinde çizilen involute eğrileri, involute denklemlerle çizilmiştir. Dişlilerin esneklik katsayısı hem analitik ve hem sayısal (sonlu elemanlar) yöntemlerle hesaplanmıştır; esneklik katsayısı hesaplamaları malzemede depolanan enerji teorisi dayanır. Moment altında oluşan eğilmenin miktarını ölçerek veya hesaplayarak yukarıdaki yöntemlerle esneklik katsayısı hesaplanmıştır. Analitik ve sayısal yöntemlerin sonuçları karşılaştırılmıştır.

Dişli kutusunun çıkış milin hızını düzenlemek için kontrol sistemi yörünge izleme teorisi kullanılmıştır. İletim hataları eğrisinin yörünge izlemesi eksik tahrikli sistem yöntemiyle yapılmıştır. Bu yöntemde giriş ve çıkış milleri algılayıcı le ölçülür. Sistemde PI denetleyici kullanılmıştır. Diş sayısı, temel daire çapı, malzeme, dişli ağırlığı, geometri ve aktarma oranı gibi faktörler sistemin sonucunda etkilidir. Sonuçlar uygulanan eksik tahrikli sistem yönteminin dişli kutusunun çıkışının kararlı hale getirilmesinde etkin olduğunu göstermektedir. Bu kontrol yöntemi giriş torkunu kontrol ederek çıkış mil hareketi oldukça düzenlenir ve iletim hatasını oldukça azalır ve titreşim ve gürültünün azalmasına da neden olur.

Anahtar sözcükler: Düz Dişli, İletim Hatası, Servo kontrol, Eksik Tahrikli Dinamik Sistem, Düz Dişli Dinamiği

ACKNOWLEDGMENTS

I would like to give my sincere appreciation to my committee members who have made unique contributions to this dissertation. I am blessed to have Asst. Prof. Dr. Can Ulaş DOĞRUER as my supervisor. I admire his extraordinary help with this dissertation. I would also like to thank the other two members of my dissertation committee, Prof. Dr. Bora YILDIRIM and Assoc. Prof. Dr. Melik DÖLEN for their enthusiastic assistance which helped improving the quality of this research.

I am very grateful to my parents for their prayers, encouragement, and support.

Finally, I send special appreciations to my dear wife, Leila Hashempour, for her unconditional love and support through the years in my graduate education. She did make it all possible by her encouragement and willingness to tolerate my education.

Table of Contents

| | Page |
|---|-------------|
| ABSTRACT | v |
| ACKNOWLEDGMENTS | ix |
| TABLE OF CONTENTS | x |
| LIST OF TABLES | xv |
| LIST OF FIGURES | xvi |
| SYMBOLS AND ABBREVIATIONS | xxiii |
| NOMENCLATURE | xxiv |
| 1. INTRODUCTION | 1 |
| 1.1. General Introduction | 1 |
| 1.2. Torsional Mesh Stiffness | 2 |
| 1.3. Transmission Error | 2 |
| 1.4. Finite Element Analysis (FEA) | 3 |
| 1.5. Regulation of Gear Transmission Noises | 4 |
| 1.6. Thesis Scope | 4 |
| 1.7. Outline of Thesis | 5 |
| 2. Literature Review and Background | 6 |
| 2.1. Introduction | 6 |
| 2.2. Analytical Method Analysis | 8 |
| 2.3. Finite Element Analysis | 9 |
| 2.4. Experimental Transmission Error Evaluation | 9 |
| 2.5. Reduction of Noises and Transmission Error Methods | 9 |
| 2.6. Conclusion | 11 |
| 3. Parametric Design of Spur Gear | 12 |
| 3.1. Introduction | 12 |
| 3.2. Parametric Design of Spur Gear | 12 |
| 3.2.1. Involute Curve Used for Spur Gears | 13 |
| 3.3. Conclusion | 16 |
| 4. Numerical and Analytical Evaluation of Mesh Stiffness of Gear | 17 |
| 4.1. Introduction | 17 |
| 4.2. Computation of Mesh Stiffness of Gear Using Finite Element Methods | 17 |
| 4.2.1. Contact | 19 |

| | |
|---|----|
| 4.2.2. Meshing..... | 21 |
| 4.2.3. Loading..... | 22 |
| 4.2.4. Material..... | 23 |
| 4.2.5. Case Studies..... | 24 |
| 4.3. Evaluation of Mesh Stiffness of Gear Using Analytical Methods | 27 |
| 4.3.1. Calculation of Hertzian Contact Stiffness | 28 |
| 4.3.2. Calculation of Total Mesh Stiffness | 29 |
| 4.4. Conclusion: Comparison Between Results of Analytic Method and Numerical Method (Finite Element Method) | 34 |
| 5. Spur Gear Pairs Transmission Error Regulation | 41 |
| 5.1. Introduction..... | 41 |
| 5.2. Trajectory Tracking of Multibody Systems | 42 |
| 5.2.1. Fully Actuated Multibody Systems (FAMS) | 42 |
| 5.2.2. Underactuated Multibody Dynamics | 43 |
| 5.2.2.1. Underactuated Multibody Systems Analysis | 43 |
| 5.2.3. Normal Form of Input-Output | 43 |
| 5.2.4. Linearization | 44 |
| 5.2.5. Model Inversion and Feedforward Control..... | 45 |
| 5.2.6. Systems with Collocated Output..... | 46 |
| 5.2.6.1. Input-Output Normal Form..... | 46 |
| 5.2.6.2. Linearization | 47 |
| 5.2.6.3. Model Inversion and Feedforward Control..... | 49 |
| 5.3. Dynamic Model of a Spur Gear Pair..... | 49 |
| 5.3.1. Dynamic Model of a Spur Gear Pair Supported by Elastic Shafts and Bearing: Model with Sliding Friction, Backlash and Manufacturing Error | 50 |
| 5.3.2. Simplification of 6 DOF Model and Assumptions..... | 51 |
| 5.3.3. Dynamic Model of a Spur Gear Pair: Model without Sliding Friction, Backlash, Elastic Shafts and Bearing and Profile Error Free | 52 |
| 5.3.4. Nonlinear Dynamic Model of a Spur Gear Pair with Variable Mesh Stiffness Changing with Position..... | 53 |

| | |
|--|----|
| 5.4. Analysis of Underactuated Multibody Systems: Servo Control of a Spur Gear Pair..... | 55 |
| 5.4.1. Systems with Collocated Output: 2 DOF Spur Gear Pair Model..... | 55 |
| 5.4.2. Input-Output Normal Form..... | 56 |
| 5.4.3. Input-Output Linearization | 57 |
| 5.4.4. Model Inversion and Feedforward Control..... | 58 |
| 5.5. Pole Placement: Error Dynamics..... | 60 |
| 5.5.1. Transfer Function of a Single Mass System with PID controller | 61 |
| 5.5.1.1. Error Dynamics..... | 61 |
| 5.5.1.2. Parametric Study on PI Gains: The Effect of K_p on Error Dynamics | 61 |
| 5.5.1.3. Parametric Study on PI Gains: The Effect of K_I on Error Dynamics | 62 |
| 5.5.1.4. Rule of Thumb to Select PI Gains | 62 |
| 5.5.1.5. Desired PID Controller Gains: K_D, K_p, K_I | 62 |
| 5.5.1.6. Selected PID Controller Gains..... | 63 |
| 5.6. Conclusion..... | 68 |
| 6. Simulation Model: MATLAB Simulink Model of a Spur Gear Pair..... | 69 |
| 6.1. Introduction..... | 69 |
| 6.2. An Overview of MATLAB Simulink Model..... | 69 |
| 6.3. Inside the MATLAB Simulink Model: Simulink Model of a Spur Gear Pair | 71 |
| 6.3.1. Reference Velocity Profile | 71 |
| 6.3.2. Inverse Kinematic Model | 72 |
| 6.3.3. Inverse Dynamic Model | 73 |
| 6.3.4. System Model: Nonlinear Spur Gear Pair Model..... | 76 |
| 6.3.5. Error Dynamics: PID Controller | 81 |
| 6.4. Conclusion..... | 81 |
| 7. Results: Simulation..... | 85 |

| | |
|--------------------------------------|-----|
| 7.1. Introduction..... | 85 |
| 7.2. A Strategy for Simulations..... | 86 |
| 7.2.1. Case Study-1..... | 86 |
| 7.2.2. Case Study-2..... | 88 |
| 7.2.3. Case Study-3..... | 90 |
| 7.3. Simulation Results..... | 92 |
| 7.3.1. Result of Case Study-1..... | 94 |
| 7.3.2. Result of Case Study-2..... | 97 |
| 7.3.3. Result of Case Study-3..... | 100 |
| 7.4. Conclusion..... | 103 |
| 8. Conclusion and Future Work..... | 104 |
| 8.1. Conclusion and Future Work..... | 104 |
| REFERENCES..... | 105 |
| CURRICULUM VITAE..... | 108 |

List of Tables

| | Page |
|--|-------------|
| Table 4.1. General Property of Structural Steel Material | 24 |
| Table 4.2 General Parameters of Gear Pairs | 25 |
| Table 5.1. Determined PI Gains | 63 |
| Table 5.2. PI Gains..... | 63 |
| Table 7.1. Data related to MATLAB Simulink Model 1 | 87 |
| Table 7.2. Data related to MATLAB Simulink Model 2 | 89 |
| Table 7.3. Data related to MATLAB Simulink Model 3 | 91 |

List of Figures

| | Page |
|--|-------------|
| Figure 1.1. The Torsional Mesh Stiffness k for two Complete Mesh Cycle of Gear Pair..... | 2 |
| Figure 1.2. Finite Element Model of a Mating Gear Pair..... | 3 |
| Figure 2.1. Torsional Model (Two-DOF Model) | 8 |
| Figure 2.2. Single-DOF Model | 8 |
| Figure 2.3. Finite Element Model | 9 |
| Figure 2.4. Regions of Single-Tooth, Double-Tooth and Triple-Tooth Loading in Low Contact Ratio and High Contact Ratio Gears | 10 |
| Figure 3.1. How Equation of an Involute Curve (Two Branches of an Involute Curve) is Drawn | 14 |
| Figure 3.2. Sketch of Necessary Construction Circles of a Spur Gear | 14 |
| Figure 3.3. Involute Tooth Profile of a Spur Gear | 14 |
| Figure 3.4. Parametric Equations of Gear | 15 |
| Figure 3.5. Involute Curve Equations and Parameters Which Generate Tooth Involute Curves | 16 |
| Figure 4.1. Gears Body Course Mesh and Refinement by Mesh Sizing Method at the Contact Points | 19 |
| Figure 4. 2. Gears Body Course Mesh and Refinement by Mesh Sizing Method at Contact Points | 19 |
| Figure 4. 3. Teeth Contact Faces | 20 |
| Figure 4. 4. Ground-Body Revolute Joint | 21 |
| Figure 4. 5. Hex Dominant Meshing Method | 21 |
| Figure 4. 6. Meshing Details | 22 |
| Figure 4. 7. Analysis Settings Details | 23 |
| Figure 4. 8. Rotation Steps | 23 |
| Figure 4. 9. Joint Probe Results | 26 |
| Figure 4. 10. Angular Deformation of Pinion and Gear | 26 |
| Figure 4.11. Maximum Stress Zone of Pinion and Gear..... | 27 |
| Figure 4.12. Line of Action and Parameters of a Gear Pair | 29 |
| Figure 4.13. Elastic Force on Tooth | 31 |
| Figure 4.14. Single-Contact Teeth Mating | 33 |

| | |
|--|----|
| Figure 4.15. Two-Contact Teeth Mating | 33 |
| Figure 4.16. Comparison of total Mesh Stiffness against Analytic Method and Numerical Method Evaluations of Gear Pair Case 1 | 35 |
| Figure 4.17. Comparison of Total Mesh Stiffness against Analytic Method and Numerical Method Evaluations of Gear Pair Case 2 | 36 |
| Figure 4.18. Comparison of total Mesh Stiffness against Analytic Method and Numerical Method Evaluations of Gear Pair Case 3 | 36 |
| Figure 4.19. Comparison of total Mesh Stiffness against Analytic Method and Numerical Method Evaluations of Gear Pair Case 4 | 37 |
| Figure 4.20. Comparison of total Mesh Stiffness against Analytic Method and Numerical Method Evaluations of Gear Pair Case 5 | 37 |
| Figure 4.21. Comparison of Total Mesh Stiffness against Analytic Method and Numerical Method Evaluations of Gear Pair Case 6 | 38 |
| Figure 4.22. Comparison of Total Mesh Stiffness against Analytic Method and Numerical Method Evaluations of Gear Pair Case 7 | 38 |
| Figure 4.23. Comparison of Total Mesh Stiffness against Analytic Method and Numerical Method Evaluations of Gear Pair Case 8 | 39 |
| Figure 4.24. Comparison of Total Mesh Stiffness against Analytic Method and Numerical Method Evaluations of Gear Pair Case 9 | 39 |
| Figure 4.25. Comparison of Total Mesh Stiffness against Analytic Method and Numerical Method Evaluations of Gear Pair Case 10 | 40 |
| Figure 5.1. Graphical Representation of the Input-Output Normal Form of Underactuated Multibody Systems..... | 44 |
| Figure 5.2. Graphical Representation of Feedforward Control of Underactuated Multibody Systems | 45 |
| Figure 5.3. CAD Model of a Single-Stage Spur Gear Pair | 48 |
| Figure 5.4. The Lumped-Parameter Dynamic Model of a Spur Gear | 50 |
| Figure 5.5. Simplified 2-DOF Spur Gear Pair Model | 54 |
| Figure 5.6. A Typical Mesh Stiffness Element: Nonlinearity Due to Change in the Number of Teeth in Contact | 54 |
| Figure 5.7. Block Diagram of the Controller and the Gear System..... | 60 |
| Figure 5.8. Error Dynamics Response to Unit Impulse Input: Effect of K_p | 64 |
| Figure 5.9. Error Dynamics Response to Unit Impulse Input: Effect of K_I | 65 |
| Figure 5.10. Unit Impulse Input Control Surface..... | 66 |

| | |
|---|----|
| Figure 5.11. Desired Error Dynamics Response to Unit Impulse Input: $K_p = 40, K_i = 4$ | 67 |
| Figure 6.1. General Outlook of MATLAB Simulink Model of a Spur Gear Pair | 70 |
| Figure 6.2. Reference Velocity Profile Block | 72 |
| Figure 6.3. Signal Builder for Acceleration | 72 |
| Figure 6.4. Inverse Kinematic Model | 73 |
| Figure 6.5. Inverse Dynamic Model | 74 |
| Figure 6.6. Inverse Dynamic Model: Gear Model | 75 |
| Figure 6.7. Inverse Dynamic Model: Gear Damper/ Stiffness Model | 77 |
| Figure 6.8. Inverse Dynamic Model: Pinion Model | 78 |
| Figure 6.9. Inverse Dynamic Model: Pinion Damper/ Stiffness Model | 78 |
| Figure 6.10. System Model | 80 |
| Figure 6.11. System Model: Pinion Model | 80 |
| Figure 6.12. System Model: Gear Model | 82 |
| Figure 6.13. System Model: Gear Damper/ Stiffness/ Sensor Model | 83 |
| Figure 6.14. Error Dynamics | 84 |
| Figure 6.15. Error Dynamics: PI Controller | 84 |
| Figure 7.1. Mesh Stiffness Curve with Three FFT Harmonics | 86 |
| Figure 7.2. Mesh Stiffness Curve with Five FFT Harmonics | 86 |
| Figure 7.3. Loading Curve | 88 |
| Figure 7.4. Acceleration Curve | 88 |
| Figure 7.5. Loading Curve | 90 |
| Figure 7.6. Acceleration Curve | 90 |
| Figure 7.7. Loading Curve | 92 |
| Figure 7.8. Acceleration Curve | 92 |
| Figure 7.9. Transmission Error | 94 |
| Figure 7.10. Input Torque | 94 |
| Figure 7.11. Acceleration Curve of Pinion | 95 |
| Figure 7.12. Velocity Curve of Pinion | 95 |
| Figure 7.13. Position Curve of Pinion | 95 |
| Figure 7.14. Velocity Curve of Gear | 96 |
| Figure 7.15. A Close Look at Velocity Curve of Gear | 96 |
| Figure 7.16. Position Curve of Gear | 96 |
| Figure 7.17. Transmission Error | 97 |

| | |
|---|-----|
| Figure 7.18. Input Torque | 97 |
| Figure 7.19. Acceleration Curve of Pinion | 98 |
| Figure 7.20. Velocity Curve of Pinion | 98 |
| Figure 7.21. Position Curve of Pinion | 98 |
| Figure 7.22. Velocity Curve of Gear | 99 |
| Figure 7.23. A Close Look at Velocity Curve of Gear | 99 |
| Figure 7.24. Position Curve of Gear | 99 |
| Figure 7.25. Transmission Error | 100 |
| Figure 7.26. Input Torque | 100 |
| Figure 7.27. Acceleration Curve of Pinion | 101 |
| Figure 7.28. Velocity Curve of Pinion | 101 |
| Figure 7.29. Position Curve of Pinion | 101 |
| Figure 7.30. Velocity Curve of Gear | 102 |
| Figure 7.31. A Close Look at Velocity Curve of Gear | 102 |
| Figure 7.32. Position Curve of Gear | 102 |

Symbols and Abbreviations

| | |
|--------------|--|
| AGMA | American Gear Manufacturers Association |
| CAD | Computer Aided Design |
| DF | Dynamic Factor |
| DIN | Deutsches Institut für Normung |
| DMF | Dynamic Mesh Force |
| DOF | Degree Of Freedom |
| DTE | Dynamic Transmission Error |
| FAMS | Fully Actuated Multibody Systems |
| FE | Finite Element |
| FEA | Finite Element Analysis |
| FOS | Factor of Safety |
| I-ONF | Input-Output Normal Form |
| ISO | International Organization for Standardization |
| LDM | Load Distribution Model |
| LDP | Load Distribution Model |
| LOA | Line of Action |
| NLC | Non-Linear Control |
| OLOA | Off-line of Action |
| PI | Proportional Integral |
| PID | Proportional Integral Derivative |
| TE | Transmission Error |
| UAMS | Underactuated Multibody Systems |
| FFT | Fast Fourier Transform |

Nomenclature

| | |
|------------|------------------------------------|
| k | Mesh stiffness |
| $k(t)$ | Time-varying Mesh stiffness |
| Z | Gear ratio |
| θ_p | Angular rotation of the pinion |
| θ_g | Angular rotation of gear |
| c | Viscous damper |
| T_1 | Pinion torque |
| T_2 | Gear torque |
| θ_1 | Pinion angular position |
| θ_2 | Gear angular position |
| I_1 | Pinion moment of inertia |
| I_2 | Gear moment of inertia |
| r_1 | Pinion base radii |
| r_2 | Gear base radii |
| d_f | Dedendum circle diameter |
| P | Diametral pitch of the gear |
| φ | Pressure angle |
| m | Module |
| N_1 | Number of pinion teeth |
| N_2 | Number of gear teeth |
| i | Reduction ratio |
| E | Young's modulus |
| ν | Poisson' ratio |
| k_h | Hertzian-contact stiffness |
| B | Tooth width |
| U_h | Potential energy (Hertzian energy) |
| F | Acting force in contact point |
| U_s | Shear energy |
| U_a | Axial compressive energy |

| | |
|------------|---|
| U_b | Bending compressive energy |
| k_s | Effective shear stiffness |
| k_a | Effective axial stiffness |
| k_b | Effective bending stiffness |
| α_1 | Pressure angle |
| α_2 | The half of the base tooth angle |
| k_t | Total effective mesh stiffness |
| $k_{t,i}$ | Total effective mesh stiffness of pinion or gear |
| θ_d | Two teeth contact angular displacement angle of pinion |
| θ_s | Single tooth contact angular displacement angle |
| M | Generalized mass matrix |
| k | Generalized Coriolis vector |
| g | Generalized applied forces |
| \bar{B} | Squared input matrix |
| q | Generalized coordinate |
| f | Degrees of freedom |
| u | Projects the inputs |
| y | Desired trajectories of the generalized coordinates |
| $h(q)$ | Tracking in the task space or tracking in the operational space |
| H | Jacobian matrix of the system output |
| \bar{h} | Local acceleration of Jacobian matrix of the system output |
| z | Coordinates of the input-output normal form |
| x | Original coordinates |
| η | Additional coordinates |
| ξ | First part of the coordinate transformation |
| P | The matrix of velocity dependent forces |

CHAPTER 1

INTRODUCTION

1.1. General Introduction

Spur gears are known to be the simplest type of gears which can transmit rotary motion, torque, and convert speed between parallel shafts. When two spur gear pair are assembled to transmit torque between parallel shafts, prediction of the dynamic behavior of spur gears is vital to monitor the condition of the gears. This analysis covers a broad range of interest: transmission error (TE), load sharing ratio, distortion field variation etc. When involute profiles of spur gears are manufactured with zero error (e.g. manufacturing tolerances are very tight and there is no load) a pair of pinion and gear, both of them are spur gears, are expected to work with zero TE. When the same gear pair is studied under loading, a different behavior becomes significant; it is seen that the mesh stiffness of each gear changes into the meshing cycle. This changes in torsional stiffness causes error in angular rotation of the gear body [2]. Angular velocity of the pinion would be transmitted to the output shaft with error due to the deformation of gear bodies and tooth profile errors.

Vibration and noise reduction has been an important concern, when powertrains and gear mechanisms are designed. When the roots of this problem (e.g. vibration and noise is searched for) it is observed that change in the stiffness of a meshing teeth is the fundamental source that causes gear vibration and noise. The mesh stiffness of gear tooth changes by varying the teeth in contact; this can be seen in Figure 1.1.

This the mesh stiffness may cause instability and lead to severe vibration under harsh operating conditions. In reference [3,4] it has been experimentally shown that large amplitude of vibration caused by parametric instability is observed when the frequency is equal to twice of the natural frequency (secondary instability) or the natural frequency (primary instability). Furthermore, tooth deflections and TE has been adversely affected by mesh stiffness variation. To a large extent, excessive gear resonance is basically excited by the harmonics of TE [5, 6, and 7].

1.2. Torsional Mesh Stiffness

Torsional mesh stiffness of gears can be calculated approximately as the ratio of load and the total elastic rotation of the gear. In the above definition, total angular rotation is defined as the angle through which a gear turns due to bending, shearing and contact of the gear teeth when it is meshed with a fixed mating gear. Each tooth pair may be thought of as a spring attached to a spur gear body, where number of contacted pairs alternates between single-tooth-pair contact and double-tooth-pair contact. When low contact ratio gear are examined, the torsional mesh stiffness can be modeled by springs where one spring is used to model one tooth in contact and two parallel spring is used to model two teeth in contact [2].

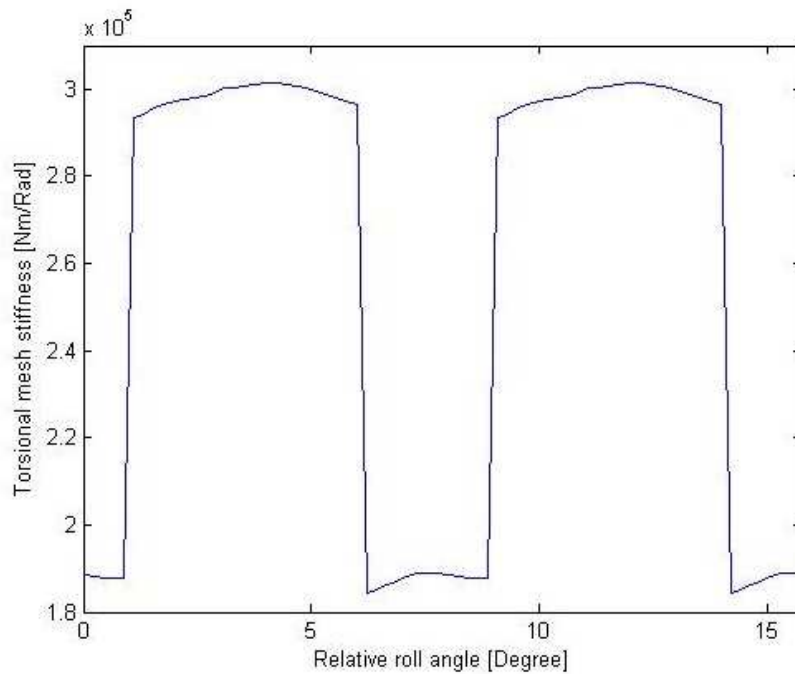


Figure 1.1. The Torsional Mesh Stiffness k for two Complete Mesh Cycle of a Gear Pair.

1.3. Transmission Error

Welbourn [8] defines TE as the difference of real position of the output shaft and the position it was supposed to be if the gear drive were perfectly. When angular units are used, the equation for transmission error is written as

$$TE = \theta_g - (Z)\theta_p \quad (1.1)$$

where Z denotes the transmission ratio of gear pair and θ_g and θ_p denotes the rotation of the output and input shaft (Rad), respectively. The above definition can be used when the system is loaded dynamically or statically, and this definition is

valid for both loaded and unloaded gears. When gears are unloaded, TE results from errors in the involute profile of pinion and gear, spacing errors, and run out. Also, assembly errors, such as errors in alignment, and static and dynamic deflections of the shaft and bearings at the support can stimulate TE's. However, that the torsional stiffness of gears changes all over the mesh, is considered to be at the root of this undesired error in transmission. This phenomena lies at the heart of dynamic analysis of spur gears and it is said to be the basic reason which causes TE, even when gears with the ideal involute profiles are loaded [2, 9].

1.4. Finite Element Analysis (FEA)

In this thesis, in order to design gear's geometry, Autodesk Inventor and Solidworks Programs were used. First, geometry of a teeth is drawn using proper module, number of teeth and gear width parameters. These values are computed by using realistic loading conditions and mechanics of material science that accounts for the failure mode of gears under static and dynamic loading; in this respect, fatigue failure has been accounted for, using basic machine design approaches. Then, in the finite element (FE) software, solid model, which is generated in previous step, is meshed with a rough FE meshing step. The result is a FE model of a typical spur gear pair which was meshed in Ansys software is given in Figure 1.2.

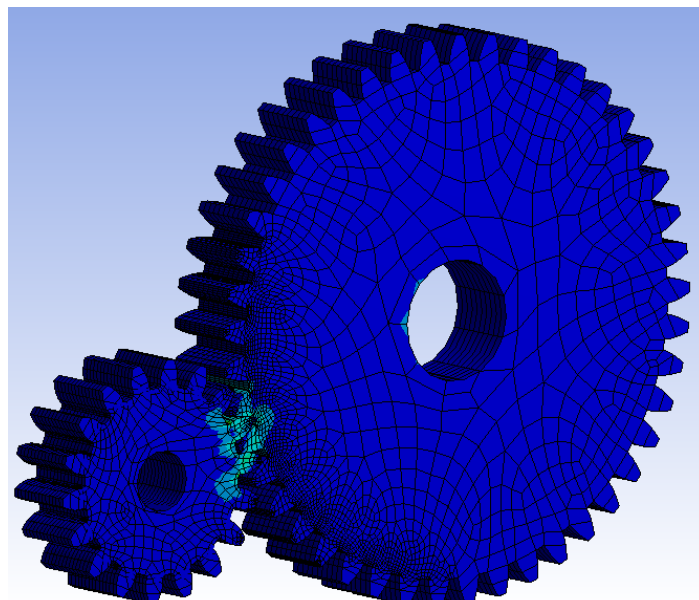


Figure 1.2. FE Model of a Mating Gear Pair.

1.5. Regulation of Gear Transmission Noises

In previous section, it has been answered to the following question; how solid model of a gear pair is generated and how mesh stiffness is calculated. To do that, first a mathematical model must be developed. Many researchers have proposed a dynamic model of spur gears. By using these models, a pair of gears can be simulated on a computer.

The model that is selected will help us to simulate the spur gear pairs which is under the guidance of a control method that is develop in this thesis; a nonlinear controller will be developed to regulate the output speed of the gear mechanism; while this is being done, several factors should be accounted for. When a pair of elastic spur gear pair is loaded, elastic vibration modes superimposed on the rigid-body mode. When the related literature is searched for, it is seen that these type of elastic mechanisms are best classified into underactuated multibody system category. Thus techniques that are used in underactuated multibody systems, are adopted and used here to control the elastic modes of a gear pair. The aim is to regulate the output speed of the gear so that unwanted oscillations are eliminated.

1.6. Thesis Scope

In this thesis, first of all, a pair of spur gears is designed using analytical methods, then mesh stiffness cycle curve is obtained using finite element method and analytical method given in [24]. Finally, nonlinear control techniques and trajectory control methods are applied to minimize transmission errors. When transmission error is eliminated, a proper gearbox made of spur gears without excessive vibration can be designed.

The main approach is to modulate the input torque such that it compensate the change in mesh stiffness. However, if adaptive nonlinear control techniques are not used, this requires that change in the mesh stiffness is known in advance of the operation. Hence, it is assumed that the gearbox is analyzed by a finite element software and gears are mounted in a gearbox with high precision. This allows us to predict the geometry of the mechanical system in advance. Thus the change in mesh stiffness which is inherently nonlinear, can be predicted and canceled by a feedforward loop. This leaves us with a linear dynamics which can be controlled by

pole placement techniques. Hence, any acceleration and velocity profile can be tracked easily.

1.7. Outline of Thesis

This thesis is arranged as; in first chapter, a general introduction was made, and tried to highlight the significance of the research and objectives that will be pursued. The definition of torsional mesh stiffness for spur gear in mesh, and gear transmission error are given. In chapter two, a critical review of the state of the literature related to this research is made. This chapter contains a significant number of relevant and pertinent publications on the subject of contact analysis and it documents a vast amount of literature on mathematical models of gear dynamics, FE analysis of mesh stiffness, measurements techniques for vibration analysis, and noise control. In chapter three, CAD model, which is used to design a gearing model is studied. In chapter four, analytical methods and numerical methods are used to compute mesh stiffness, mesh stiffness of a number of gear pairs with different number of teeth, different modules and different transmission ratio are calculated, and these results are compared against each other to validate the numerical method. In chapter five, a spur gear pair's dynamic model supported by elastic shafts, bearing is given. Control law is designed to track a reference velocity profile when flexible multi body systems are studied. At the end of this chapter, this general approach is simplified to a particular control law for a pair of elastic spur gears. In chapter six, MATLAB Simulink model is constructed using the mathematical model developed in previous chapter. Various items of the Simulink model is explained by referring to the mathematical equations. In chapter seven, conclusions are drawn and the contribution of this thesis to dynamic analysis of spur gears research with an emphasis on the active vibration control are presented. Finally, some recommendations for future works is given.

CHAPTER 2

Literature Review and Background

2.1. Introduction

Noise control, vibration analysis and dynamic analysis of gear models has been studied intensively, in the past. In the last century, the interest in static and dynamic analysis of gears ranges from vibration analysis and noise control to transmission errors and stability analysis. The primary interest in gear analysis may be summarized as; study of transmission efficiency, stress analysis, computation of loads acting on the other machine component, computation of noise emitted into working medium, detection of fault and estimation of fatigue life, condition monitoring, computation of natural frequencies of the system, study of whirling of rotors. The primary interest in gear analysis is to develop methods to control and limit TE of gearing systems to a minimum possible value.

A number of different model has been proposed by different researchers; these models show significant variations not only in the effects included, but also in the primary assumptions that is made.

In this thesis, models with tooth compliance are studied. The following aspects of the problem is focused; contact stress and mesh stiffness analysis of the gear models. The elasticity of the bearings and shafts are ignored. In these types of models, the gear system is generally modelled as a single-degree of freedom spring-mass system (Figure 2.1 and 2.2). In this model, gears are represented by rigid wheels that are connected to each other along the line of action (LOA) through a number of elements that are intended to represent the flexibility. The first element is the periodically time-varying gear mesh stiffness $k(t)$, The second element is a viscous damper c that is intended to represent the energy losses at the gear mesh.

When solution of the dynamic equation of a gear system is examined, it is observed that analytical techniques and/or numerical methods have been used to solve these differential equations; some of the researchers have used analytical methods where others used finite element models.

It has been known for long years that transmission error is a main reason of gear vibration. To this end, profile modification is a common practice to control

transmission error and excessive vibration. A group of investigators has studied teeth modifications to reduce (or if possible) to eliminate the transmission error in a gearing system; Teeth modification approaches includes modification of involute profile, asymmetric teeth modification, and teeth tip modification. Modified geometry of teeth of an asymmetric teeth design which is a combined double-crowned teeth and an involute profile was proposed to stabilize and regulate the bearing contact and to get a reduced magnitude shape of transmission errors. The result of symmetric and asymmetric spur gears stress analysis have been favorable. Because it has been shown that transmission error and bending stresses of an asymmetric spur gear has been reduced [10]. In 2013 Del Rincon et al. [29] developed a model for the analysis of forces in contact and spur gear transmissions. They computed transmission error, meshing stiffness and load sharing factor for different loading conditions, center distance and mounting distances. Chen and Shao [30] proposed a model to study the relationship between gear errors and mesh stiffness, and loaded static transmission errors.

A group of researchers [11] has developed a software to study the dynamic behavior of gears using numerical methods. Dynamic behavior of gears was studied, these type of gears can be used in in wind turbine gearbox application which demands for high performance. Software has been used to compare the performance of conventional gears and asymmetric teeth gears. In this respect, a gear pair can be designed and analyzed with these system, for example transmitted torque, dynamic load, frequency spectra of static transmission error. can be studied with use of those program.

Some researchers [12] proposed a spur gear pair's 6-DOF nonlinear time-varying dynamic model to study the influence of the elasticity of the supporting elements (e.g. shaft and bearings) on the dynamic response. The dynamic model is coupled with a quasi-static contact model which includes the gear mesh stiffness and a damper, modelling the energy dissipative characteristics of the gear bodies. This nonlinear dynamic model was used to compute dynamic tooth forces, and the dynamic transmission error (DTE).

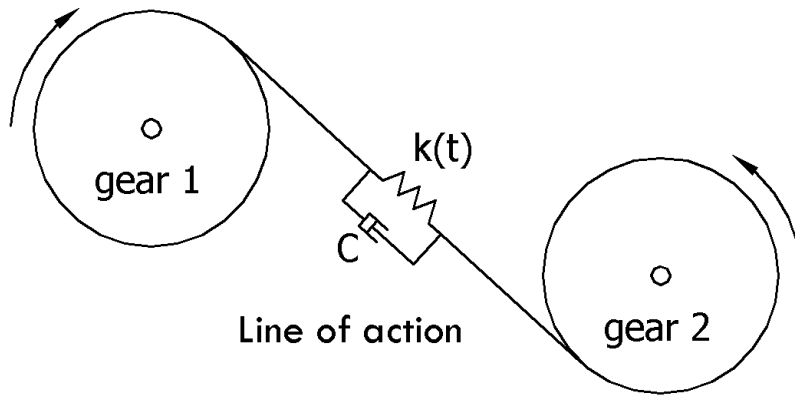


Figure 2.1. Torsional Model (Two-DOF Model) [13].

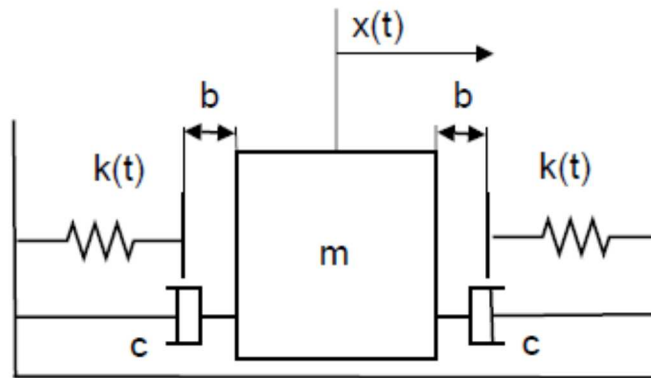


Figure 2.2. Single-DOF Model [13].

2.2. Analytical Method Analysis

At the first step of the analysis, mesh stiffness of a single spur tooth pair has to be calculated. This mesh stiffness is used in gear mesh interface of the discrete dynamic model of a spur gear pair, note that this dynamic model is the basis of all mathematical models. In 2011, Zaigang Chen [15], proposed an analytical method to calculate the mesh stiffness. The analytical method proposed in [15, 16] is used in this thesis to reduce the time required for analysis and simulation. Before this analytical method is used, it was cross-checked with an advanced finite element model of spur gear pair under quasi-static loads. It is seen that the results are promising and analytical methods can be used with reasonable accuracy. The most important features of the time-varying mesh stiffness can be captured by using the results of this analytical method.

2.3. Finite Element Analysis

In 2014, Roy, Kumar, and Kiran [17] investigated the contact pressure of spur gear, using Finite Element Analysis (FEA) method in ANSYS 14.5 program. They designed different spur gear pairs with different module set, using Solidworks program then they imported these models to ANSYS. These models were analyzed by using ANSYS Workbench to compute stress and contact pressure. They explained how to do analysis of mating spur gear pair in ANSYS Workbench. They compared the results of FEA method against analytical methods. In 2015 Temis et al. [38] simulated gear systems by using dynamic FE analysis method. They did analysis in different rotation speed of gears and found time-varying mesh stiffness of gear systems.

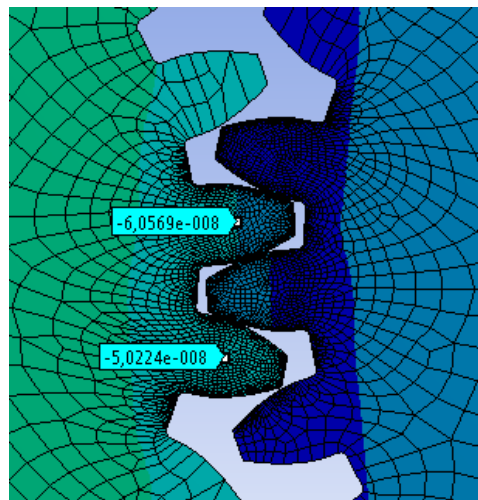


Figure 2.3. Finite Element Model.

2.4. Experimental Transmission Error Evaluation

In 1995 Blankenship et.al [6] used a laboratory testing device to investigate transmission error experimentally for gear pair. At first, they examined gear pair, then placed it on a testing device and tests were made on it. For this test, they designed gears according to AGMA class 14.

2.5. Reduction of Noises and Transmission Error Methods

In 2005, Tammina, Kahraman, and Vijayakar [18] studied the relationship between two basic parameter of spur gear pairs: DTE and dynamic factor (DF). They tried to predict dynamic behavior of gears by studying a simplified discrete model and a FE-based deformable body model. Dynamic factors and dynamic TE were computed

when loads were applied on tooth. They calculated TE for different contact ratios, different torques, and rotation speed. They compared model dataset (predicted), with experimental data where modified tooth profile of gear, and unmodified tooth profile of gear were used. In 1997 Amabili and Rivola [28] used single-DOF model with mesh stiffness to study steady-state response of a low-contact ratio spur gear pair. In 2000 Theodossiades and Natsiavas [31] investigated of a gear-pair system dynamics with backlash and mesh stiffness. Mesh stiffness models with different complexity have been considered in gear analysis; some of these models are as simple as being a constant value for a typical mesh cycle and others take into account the true characteristics of mesh stiffness i.e. time-varying stiffness. In 1996 Velez and Maatar [32] developed an advanced lumped-parameter model to study the influence of mounting and assembly error such as eccentricity, and linear profile modification on gear dynamics. In 2011 Faggioni et al. [33] developed an optimization method to reduce gear vibration by modifying gear's profile. In 2012, Palmer and Fish [19] first explained the physical reasons that causes TE and then proposed a theory that explains the underlying dynamics of TE. They discussed several methods that can be used in design phase. These methods can be used to modify the teeth profile geometry and to determine force sharing. They investigated the effect of modification in the profile of a spur gear's teeth, and the effect of tip modification on TE. They discussed three tip relief methods which are commonly used in the industry: i) a 2-D mapping model to show transmission error, ii) a 3-D FEA calculation, and iii) a 3-D linear mesh stiffness evaluation method.

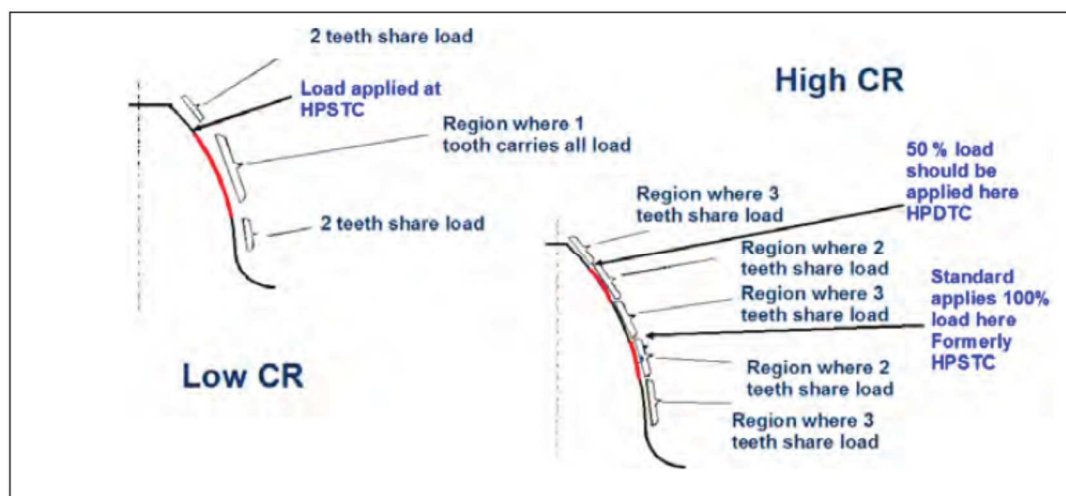


Figure 2.4. Regions of Single-Tooth, Double-Tooth and Triple-Tooth Loading on Low Contact Ratio and High Contact Ratio Gears [18].

In 2007, Faggioni, et.al. [13] proposed a method to modify gear profile that decreases system vibrations. In order to study the spur gear dynamic behavior, they used a non-linear dynamic model. They examined two different cost functions. One of the functions is based on dynamic behavior and the other function is based on quasi-static loading. In order to find the ideal profile modifications (which minimize amplitude of the vibration of gearing system) they proposed a Random-Simplex algorithm. The optimization algorithm output are: estimation of the best profile of spur gear teeth, including tip modification, and modification of the root profile.

In 2000 Chen and Brennan [34] developed a network of actuators to cancel the gear vibration by generating secondary forces using three actuators positioned on the gear.

2.6. Conclusion

In this chapter, previous studies related to gear dynamics were reviewed. According to former studies, researchers have proposed various methods of analysis of gear pairs. It is seen that a large number of researchers have studied errors and transmission errors. They have been able to simulate the behavior of gear pairs by providing dynamic models. By using these models they have been able to reduce transmission errors. Finally, it is seen that some of them have presented methods and design approaches for correcting errors and transmission errors. Most researchers have tried to change the curve form on teeth. Some have been able to reduce the Transmission errors by the change of curve form on teeth. Some of these changes were created only on the involved side of tooth and the other side is unchanged.

CHAPTER 3

Parametric Design of Spur Gear

3.1. Introduction

When gear teeth are designed, AGMA and DIN mathematical and geometrical equations can be used. The existing commercial software was used to reduce the process of computer calculations and increase the speed of design. For this purpose, Solidworks software was used because it has parametric design utility which makes the design process to be handled in a concise way.

3.2. Parametric Design of Spur Gear

Involute gearing has found many applications in industry. The advantages of involute profile can be listed as:

- it is simple to change tooth thickness and center distance,
- the tools which are used to produce involute gears, can be produced with high precision
- nonstandard involute gears can be produced by using standardized tools (which is originally devised for standard gears) and,
- change in gear center distance does not result in transmission errors [20].

Hence, tooth profile of a spur gear is generated as an involute curve. When a spur gear is modeled, the first step is to draw the dedendum circle whose diameter is defined by Equation (3.1)

$$d_f = 2 \left[r_1 - \left(\frac{0.025}{p} \right) \right] \quad (3.1)$$

where d_f is the dedendum circle diameter, r_1 is the theoretical limit radius, and P is the diametral pitch of the gear. Despite the fact that theoretical limit radius is not used in in gear modeling, in order to find the form diameter, it is an essential parameter.

In order to find the form diameter, it is required that a group of other parameters are fixed, which can be done by using a series of equations [14]. When this circle is extruded to the gear's specified thickness, it gives the solid model of a blank gear.

Then, teeth are added to this blank gear. A new sketch is created on one of the gear's flat faces, this new sketch is used as a reference geometry for the involute tooth. In this sketch, pitch circle, outside diameter circle, and base circle are drawn, centers of all these circles are fixed at the origin of the blank.

3.2.1. Involute Curve Used for Spur Gears

Consider the specific case when the base circle is evolute, for this particular case, the spur gear's tooth profile is the involute curve. The evolute base circle of radius r_b (see Figure 3.1), is considered to be the base circle. Figure 3.1 shows two involute curve which are clockwise and counterclockwise. They are produced by starting from point M_o of the line that rolls over the involute base circle counterclockwise and clockwise, respectively. Each branch shows its own side of the tooth.

Equation 3.2 can be used to compute the base diameter. The involute curve originates at the gear's base circle. The involute curve is usually expressed by parametric equations shown below (see Equations 3.3-a, and 3.3-b for counterclockwise curve and Equations 3.4-a, and 3.4-b for clockwise). In the following equations, D_b denotes the base diameter, D denotes the pitch diameter, φ denotes the pressure angle and r_b denotes the base radius. The magnitudes of θ in the equations are used to express an initial displacement of involute generator line which draws the curve.

$$D_b = D \cdot \cos \varphi \quad (3.2)$$

Parametric involute equations are given below:

$$x(t) = r_b(\cos t + t \sin t) \quad (3.3-a)$$

$$y(t) = r_b(\sin t - t \cos t) \quad (3.3-b)$$

$$x(t) = r_b[\cos(-t - \beta) - t \sin(-t - \beta)] \quad (3.4-a)$$

$$y(t) = r_b[\sin(-t - \beta) + t \cos(-t - \beta)] \quad (3.4-b)$$

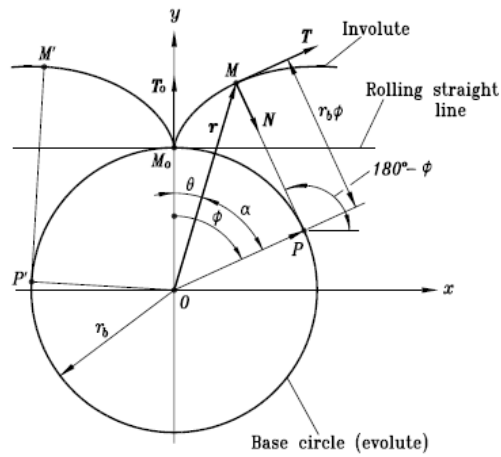


Figure 3.1. How an Involute Curve (Two Branches of an Involute Curve) is Drawn.

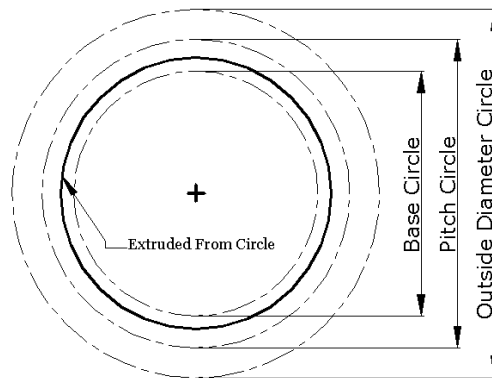


Figure 3.2. Sketch of the Necessary Construction Circles of a Spur Gear.

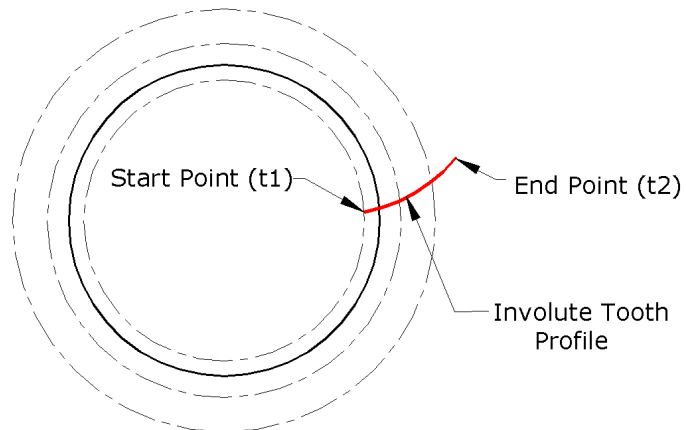


Figure 3.3. Involute Tooth Profile of a Spur Gear.

A center line must be drawn to finish the tooth involute profile. Equation (3.5) defines the half thickness of tooth which shows parameters of half tooth. Parameter t denotes the distance of involute curve from tooth center line along the pitch diameter.

$$t = \pi / (2 \cdot p) \quad (3.5)$$

Equation (3.6) defines the teeth grooves, Equation 3.7 defines gear root diameter, and Equation 3.8 defines fillet radius of depth of teeth.

$$h_t = \frac{2.2}{P} + 0.05 \quad (3.6)$$

$$D_R = D_0 - 2h_t \quad (3.7)$$

$$r_f = 0.1P \quad (3.8)$$

In the above equations, P denotes the diametral pitch and D_0 denotes the outside diameter.

In order to create the solid model of a spur gear, these equations and gear parameters must be inserted in “Equations, Global Variables, and Dimensions” box. This dialog box and those equations can be used to generate different size and teeth number of spur gears as show in Figure 3.4.

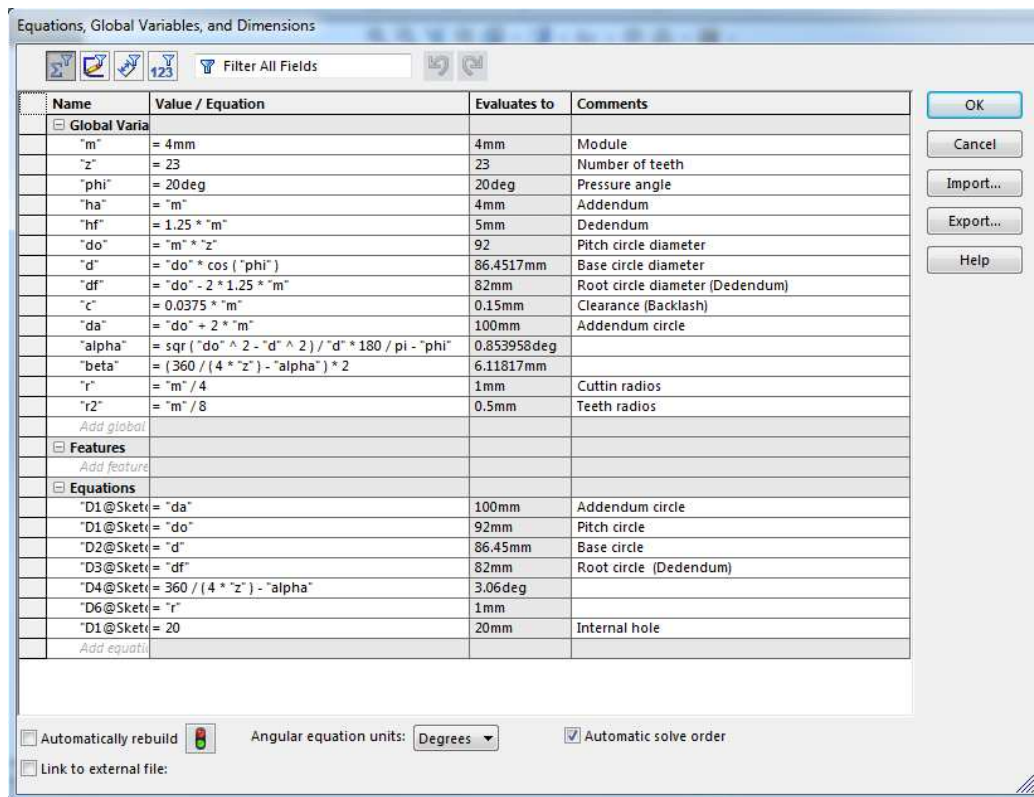


Figure 3.4. Parametric Equations of Gear

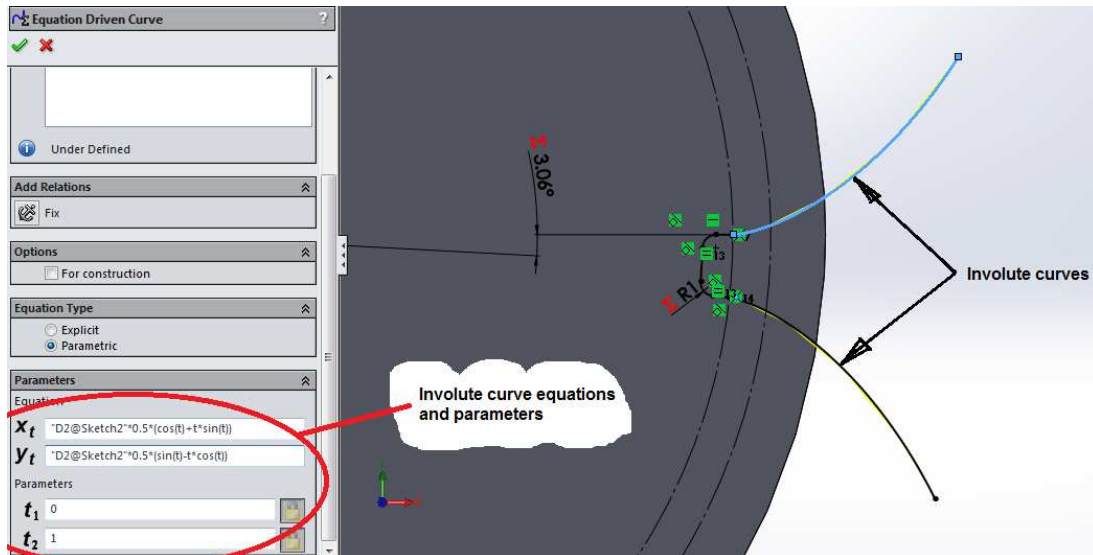


Figure 3.5. Involute Curve Equations and Parameters Which Generate Tooth Involute Curves.

3.3. Conclusion

In this chapter, gear design and involute curve equations which are used in the Solidworks, are explained. The parameters in the “Equation Global Variables and Dimensions Environment” were entered into the program. The result completely agrees with the mathematical and geometrical equations of gear design. To design several models with different sizes and number of teeth, it is sufficient to change the values of tooth, module, pressure angle, and the hole diameter of gear in the “Equation Global Variables and Dimensions Environment”. The result is a solid model of the desired gear body.

CHAPTER 4

Numerical and Analytical Evaluation of Mesh Stiffness of Gear

4.1. Introduction

In this chapter, models of spur gear with tooth compliance are studied. Since mesh stiffness is a prerequisite for the upcoming simulations in the subsequent chapters, in this chapter it was focused on the computation of contact stress and mesh stiffness. As it was stated above, this mesh stiffness will be used in the gear mesh interface as a nonlinear spring constant. It is evident that this nonlinear spring constant is the backbone of all dynamic analysis of the models. In order to simplify the dynamic model, it is assumed that the elasticity of the bearings and shafts, etc., are negligible, if their impact on the analysis is compared to the effect of mesh stiffness. When the related literature is reviewed, it is seen that, in these types of studies, the system is generally modelled as a single-DOF system.

These models include the potential energy storing elements which causes tooth deformation. There are research papers in which single-contact tooth and two-contact tooth gear pair models have been examined. When two-contact teeth models are studied, the contact stress analysis and meshing stiffness computation are often done together. In these methods, the system is modeled as a spring mass system which is a SDOF system. In this group, the main characteristics compliance is due to the gear tooth deformation, and other mechanical parts of gear are assumed to be rigid. In this section, by using two method, meshing stiffness of a spur gear pair will be calculated:

- FE method,
- Analytical method given in [24].

4.2. Computation of Mesh Stiffness of Gear Using FE Method

In order to compute the mesh stiffness, a family of spur gear pair models were generated using Solidworks and these solid models were imported to ANSYS program. The imported models were analyzed in ANSYS Workbench to compute meshing stresses and the deformation of gear bodies. These ANSYS analysis results were compared to analytical method results. Also, the ANSYS analysis

results; (meshing stiffness), were imported to Matlab Simulink model based control law to regulate the gear noise and transmission error.

This chapter presents a detailed 3-D FE model which is employed to calculate torsional mesh stiffness and static transmission error. Solidworks program is used to design parametric 3-D model of a spur gear pair and “ANSYS Workbench Static Structural” tab in “System Toolbox”, is used to make finite element analysis. After solid model of gears are imported into ANSYS, the bodies are meshed (see Figure 4.1). The refinement is realized by using mesh sizing methods in ANSYS Workbench. The constraints, contact elements and torque are added to the model (see Figure 4.2). Then the program solves the model.

In order to determine the mesh stiffness, a quasi-static method is used to simulate [21]. The stiffness is calculated at successive angular positions of the gears (a number of points along the $2PI/N_2$ angle was considered). Therefore, gears have to be rotated to successive positions, before the model is solved. This will be done in ANSYS Workbench automatically by using the revolute joint and selecting rotational magnitude for type field and creating tabular degree values. The following results are extracted from the model during the automated post processing:

- deformation,
- torsional mesh stiffness,
- contact zone gears.

The mesh stiffness k is defined as the quotient of input load T (Nm) and gear rotation, TE (rad) [21].

$$k = \frac{T}{TE} \quad (4.1)$$

In general, a spur gear pair has m or $m + 1$ tooth pairs in contact. This implies a change in the total gear mesh stiffness. As a result, the stiffness coefficient in the equation of motion is a function of time or rotation angle, which causes parametric excitation of the transmission error. The transmission error will increase rapidly and the gear teeth will lose contact, at certain intervals of rotational speeds [22]. To get a smooth transmitted motion, these intervals of rotational speeds must be avoided.

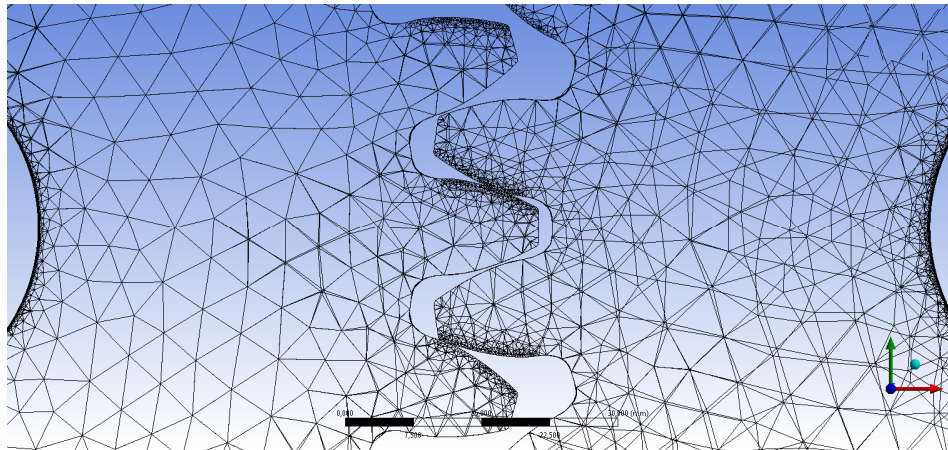


Figure 4.1. Gears Body Course Mesh and Refinement by Mesh Sizing Method at the Contact Points.

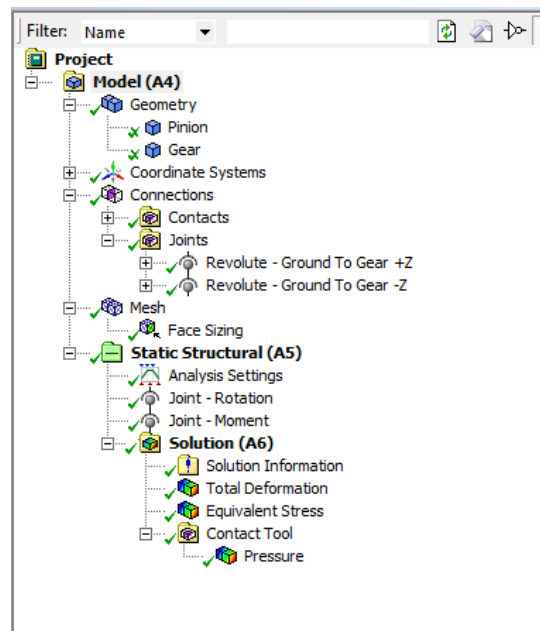


Figure 4.2. Gears Body Course Mesh and Refinement by Mesh Sizing Method at the Contact Points.

4.2.1. Contact

If the two bodies are in static equilibrium, the contact between two components or bodies is a static phenomenon. If not, the contact is a dynamic phenomenon. Dynamic contact modeling and equations are often much more complicated than static modeling and equations. In other words, most of engineering applications are dynamic. Nevertheless, many of that processes can be solved as static for simplicity. In situations friction effect may be neglected for simplicity because its

force is so small. So, a special case of general contact may occur as a frictionless contact.

A mathematical model of contact problems involves systems of inequalities or non-linear equations. In addition, among other factors, modelling of friction is completely difficult, and chemical and physical properties of the material, motion, and the temperature of the contacting surface.

The type of gear contacts is selected frictionally and the magnitude of friction coefficient is considered to be zero. Here, surfaces that are contacted with each other are determined. As shown in Figure 4.3, contact surfaces of driver gear is introduced into software as a contact body and contact surfaces of driven gear is introduced as a target body. Behavior of contact is set as symmetric and in formulation section Augmented Lagrange is selected. It is used revolute joint Body-Ground for gear central hole. Here, it is used revolute joint to do the analysis in different angle positions.

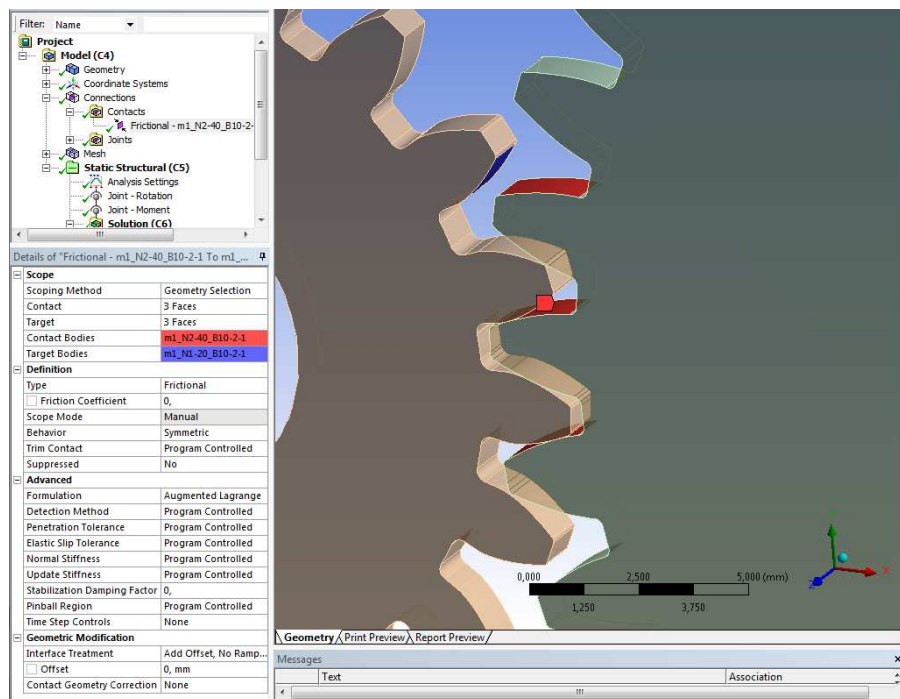


Figure 4.3. Teeth Contact Faces.

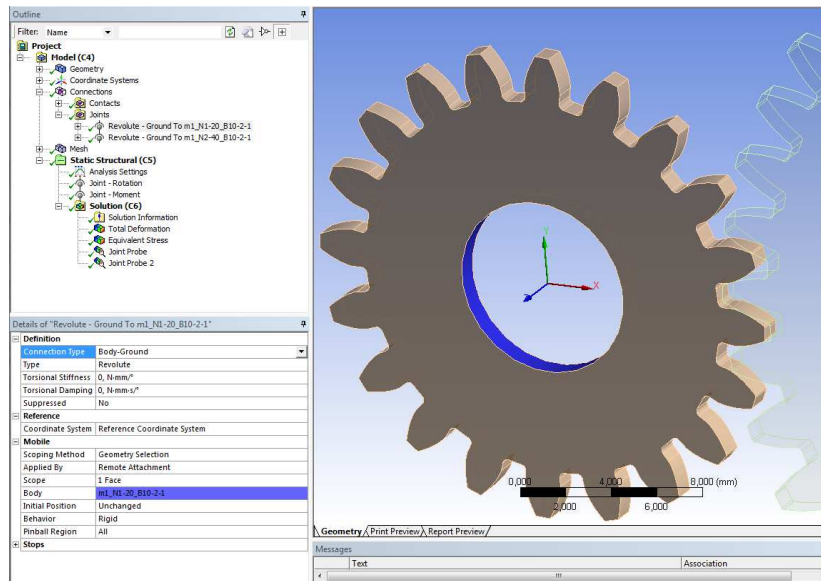


Figure 4.4. Ground-Body Revolute Joint.

4.2.2. Meshing

For gear meshing, mesh section parts that are in contact will be fined. By Face Sizing selection, at first gears contact surfaces are meshed in so fine magnitude. Then for gears hole surface the magnitude of Element Size is selected slightly larger than the surface of teeth. For example, Element Sizing for gear tooth surface with 1 mm module is selected as 0.01 mm and for gear central hole surface it is selected as 0.1 mm. To determine the type of meshing elements Hex Dominant Method was used. As well as to enhance the accuracy of analysis Element Midside Nodes was used.

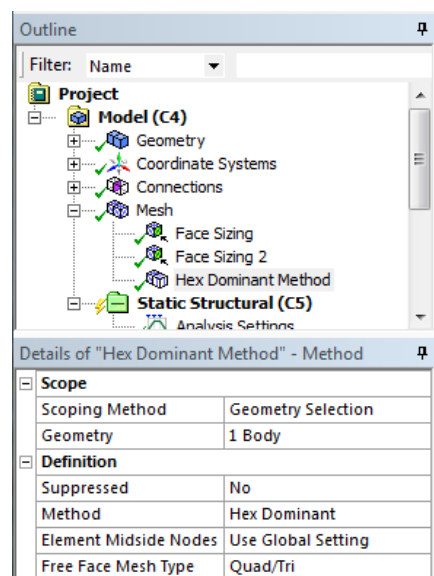


Figure 4.5. Hex Dominant Meshing Method.

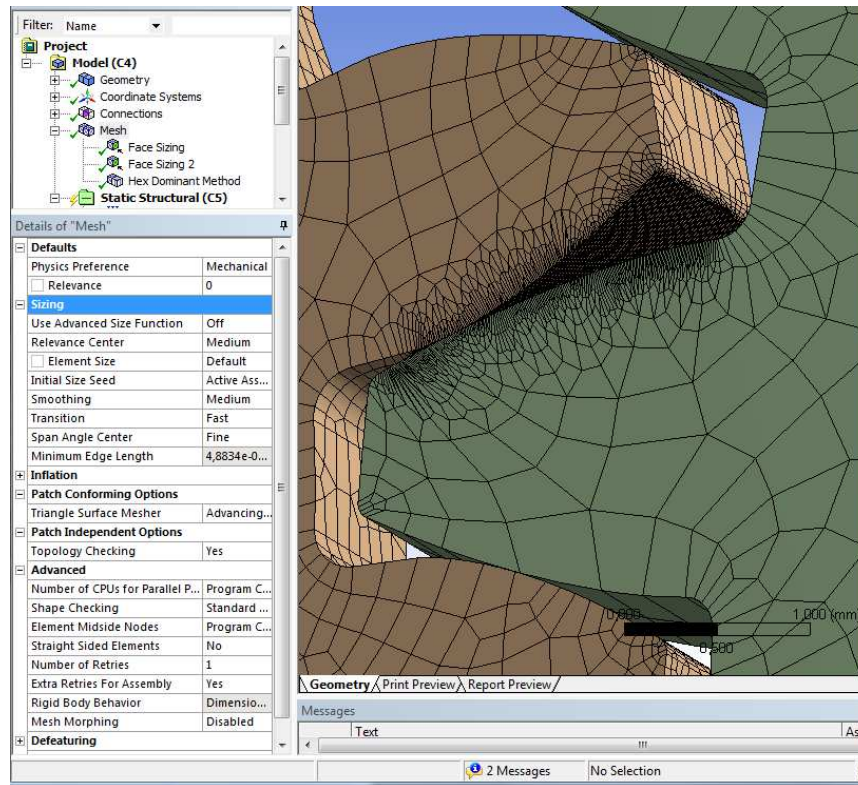


Figure 4.6. Meshing Details.

4.2.3. Loading

To set quasi-static analysis step, in Analysis Setting section the settings should be done in order to do the analysis process in small steps intervals. The behavior of gear teeth in contact at all the teeth is the same, because of that the analysis were done in the amount of rotation of a tooth. In Analysis Setting section, the number of step is adjusted to the desired value. In this project, the Number of Steps from 9 to 30 were adjusted.

To set the motion and load for both gears joint load is selected. In Detail of Joint Load, rotation type for driver gear and moment type for driven gear are selected. The magnitude for driver gear is selected as tabular and at the bottom right of the screen motion values are entered. Motion values are small steps which are form 0 to $2\pi/N$. The amount of moment (N.mm) at driven gear will be fixed.

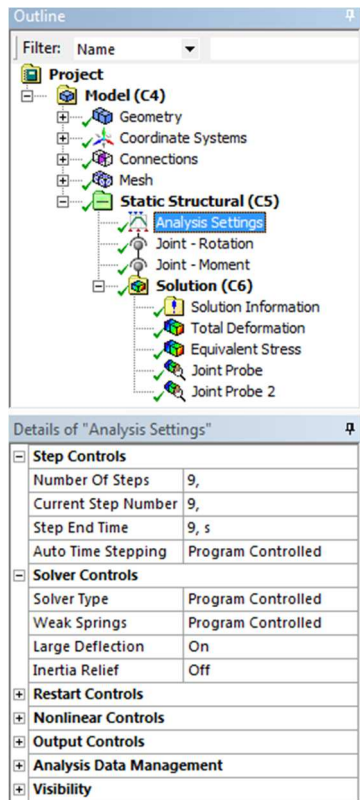


Figure 4.7. Analysis Settings Details.

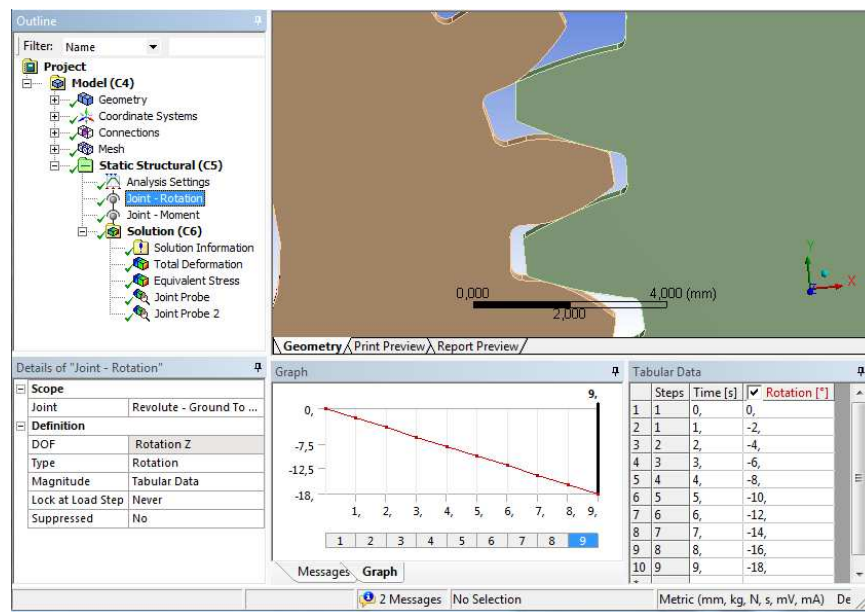


Figure 4.8. Rotation Steps.

4.2.4. Material

In this work, structural steel is used as the material of models. The general properties of this steel material are given in Table 4.1.

Table 4.1. General Property of Structural Steel Material (ANSYS Engineering Data).

| Material Property | Value | Unit |
|-------------------|---------|-------------------|
| Density | 7850 | Kg/m ³ |
| Poisson Ratio | 0.3 | - |
| Young's Modulus | 2 E+11 | Pa |
| Tensile Yield | 2.5 E+8 | Pa |
| Tensile Ultimate | 4.6 E+8 | Pa |

4.2.5. Case Studies

The selection of cases is as follows: For various modules with different numbers of teeth of the pinion and gear are investigated. For this reason, cases with five different modules and for each module two cases with different teeth number for the pinion and different gear were selected. In this work, torsional deformation of gear pairs which have module in the range of 1, 2, 3, 5, and 6 *mm* and transmission ratio in the range between 1:1.2 and 1:3.5 were investigated. On the pinion and gear bodies, the number of teeth varies from 18 to 63. In all models pressure angle was set to 20°. The parameters of gear pairs are given in Table 4.2. The maximum stress, deformed model, and mesh stiffness diagram for the cases given in Table 4.2 are shown in Figure 4.10-4.21.

Table 4.2 General Parameters of Gear Pairs

| Variable | Symbol | Case 1 | Case 2 | Case 3 | Case 4 | Case 5 | Case 6 | Case 7 | Case 8 | Case 9 | Case 10 |
|--------------------------------|----------------------|--------|--------|--------|--------|--------|--------|--------|--------|--------|---------|
| Module (mm) | m | 1 | 1 | 2 | 2 | 3 | 3 | 5 | 5 | 6 | 6 |
| Number of pinion teeth | N1 | 20 | 20 | 22 | 22 | 18 | 18 | 20 | 20 | 25 | 25 |
| Number of gear teeth | N2 | 40 | 60 | 33 | 38 | 45 | 63 | 30 | 35 | 30 | 42 |
| Reduction ratio | i | 1:2 | 1:3 | 1:1.5 | 1:1.73 | 1:2.5 | 1:3.5 | 1:1.5 | 1:1.75 | 1:1.2 | 1:1.68 |
| Pressure angle | a₀ | 20° | 20° | 20° | 20° | 20° | 20° | 20° | 20° | 20° | 20° |
| Center to center distance (mm) | | 30 | 40 | 55 | 60 | 94.5 | 121.5 | 125 | 137.5 | 165 | 201 |
| Internal hole of pinion (mm) | | 8 | 8 | 8 | 8 | 15 | 15 | 20 | 20 | 25 | 25 |
| Internal hole of gear (mm) | | 10 | 8 | 10 | 10 | 30 | 30 | 25 | 25 | 30 | 42 |
| Gear width (mm) | | 20 | 20 | 20 | 20 | 20 | 20 | 20 | 20 | 20 | 20 |
| Contact ratio | | 1.635 | 1.671 | 1.627 | 1.642 | 1.633 | 1.661 | 1.605 | 1.622 | 1.633 | 1.668 |
| Young's modulus of pinion (Pa) | E1 | 2 E+11 | 2 E+11 | 2 E+11 | 2 E+11 | 2 E+11 | 2 E+11 | 2 E+11 | 2 E+11 | 2 E+11 | 2 E+11 |
| Young's modulus of gear (Pa) | E2 | 2 E+11 | 2 E+11 | 2 E+11 | 2 E+11 | 2 E+11 | 2 E+11 | 2 E+11 | 2 E+11 | 2 E+11 | 2 E+11 |
| Poisson's ratio of pinion | ν1 | 0.3 | 0.3 | 0.3 | 0.3 | 0.3 | 0.3 | 0.3 | 0.3 | 0.3 | 0.3 |
| Poisson's ratio of gear | ν2 | 0.3 | 0.3 | 0.3 | 0.3 | 0.3 | 0.3 | 0.3 | 0.3 | 0.3 | 0.3 |

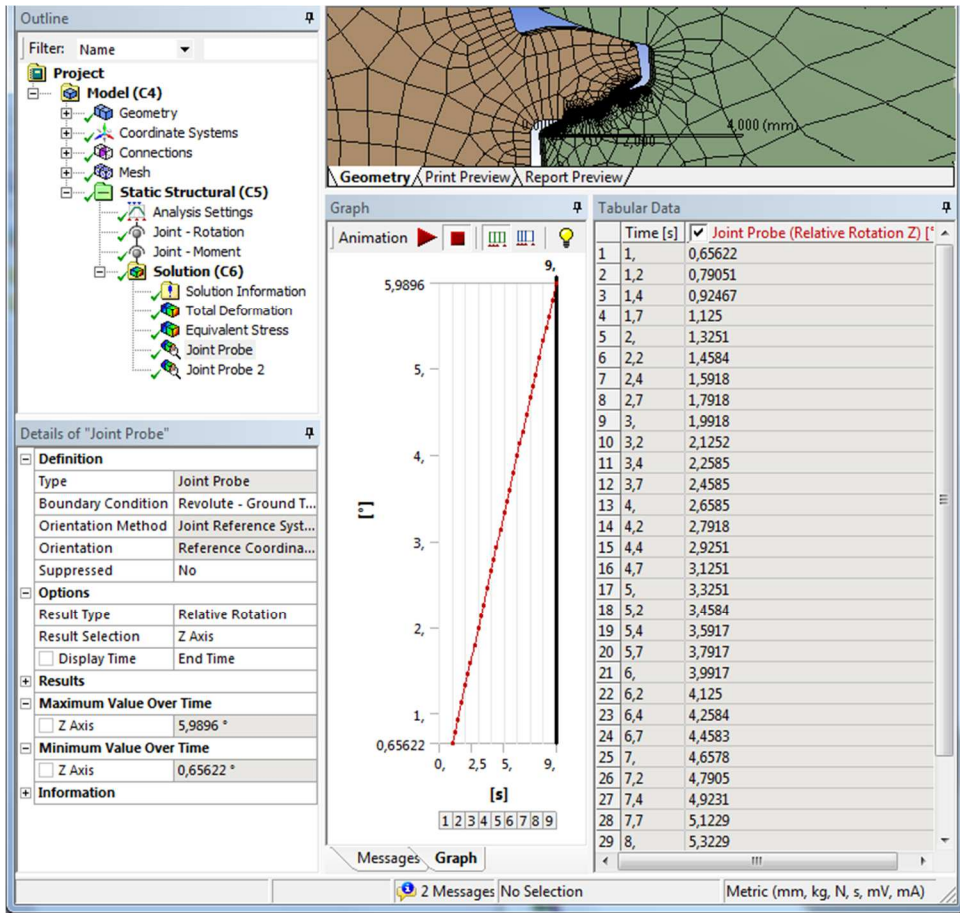


Figure 4.9. Joint Probe Results.

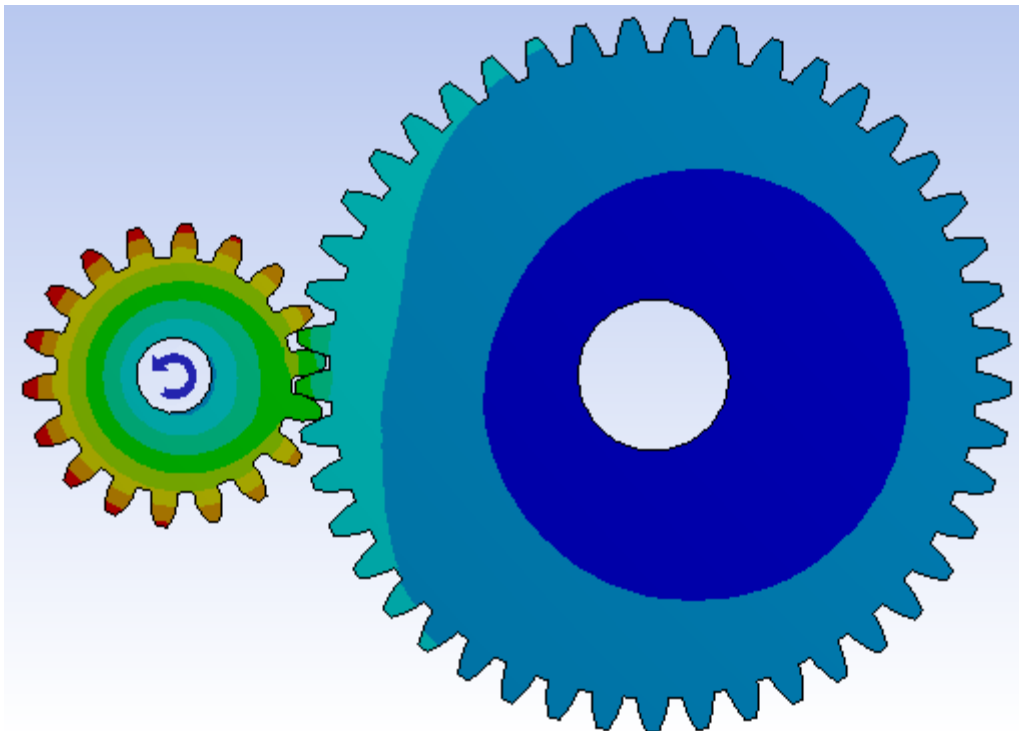


Figure 4.10. Angular Deformation of Pinion and Gear.

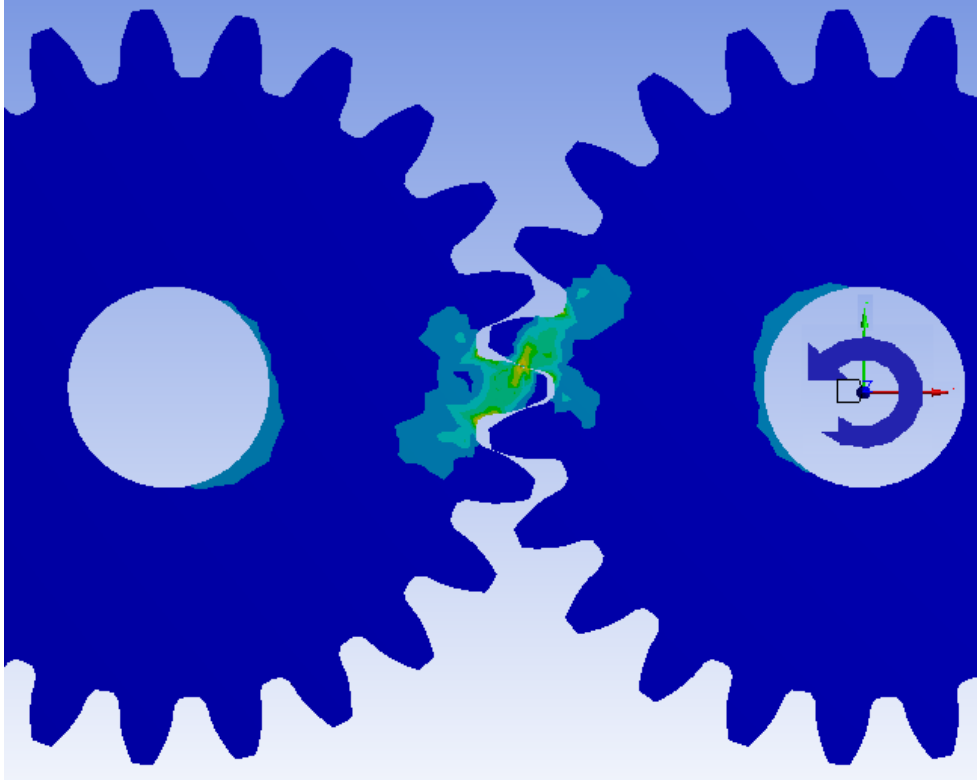


Figure 4.11. Maximum Stress Zone of Pinion and Gear.

4.3. Evaluation of Mesh Stiffness of Gear Using Analytical Methods¹

To calculate tooth and gear body deflection and bending stress, AGMA, DIN and ISO standards conventional formulas can be utilized.

To determine teeth contact stress the Hertz equation is given by,

$$\sigma_c = \sqrt{\frac{F(1 + \frac{R_1}{R_2})}{R_1 B \pi \left[\frac{(1 - \nu_1^2)}{E_1} + \frac{(1 - \nu_2^2)}{E_2} \right] \sin \alpha_0}} \quad (4.2)$$

In equation 4.2 parameters are: contact stress σ_c , pinion pitch radii R_1 , gear pitch radii R_2 , force F , pressure angle ϕ , face width B , pinion material Young's moduli E_1 , gear material Young's moduli E_2 , pinion material Poisson ratio J_1 , gear material Poisson ratio J_2 . By applying factor of safety (FOS) maximum stress is calculated by equation 4.3

¹ This section of chapter 5 was inspired from reference [24]. Author of this thesis does not claim any credit for the derivation of equations and the final results. The sole purpose of this chapter is to show that analytical methods can be used to compute mesh stiffness. In the rest of the chapter analytical method [24] will be used to accelerate the speed of simulations.

$$\sigma_a = \frac{\sigma_c}{FOS} \quad (4.3)$$

Value of FOS can be taken from design handbooks or can be calculated according to chapter 4. Torque equation is given by

$$T = F \cdot R_s \quad (4.4)$$

Where T is Torque, R_s is gear shaft diameter, and F is force.

4.3.1. Calculation of Hertzian Contact Stiffness

When isotropic elastic material for both pinion and gear bodies is used according to Hertzian law, compression of two bodies can be approximated by two paraboloids in the proximity of the contact. In this approximation, the error will be under 0.5% [23, 24]. The Hertzian-contact stiffness of a gear pairs along the entire action line will be constant. The Hertzian-contact stiffness is independent of the position of the contact. The equation of this constant is defined as

$$k_h = \frac{\pi EB}{4(1 - \nu^2)} \quad (4.5)$$

where E is Young's modulus, B is tooth width and ν is Poisson's ratio of gears materials. The potential energy (Hertzian energy) which is stored in the proximity of contact point will be calculated from

$$U_h = \frac{F^2}{4k_h} \quad (4.6)$$

Where F is acting force in contact point and k_h is the effective Hertzian stiffness in a similar direction along with the force .

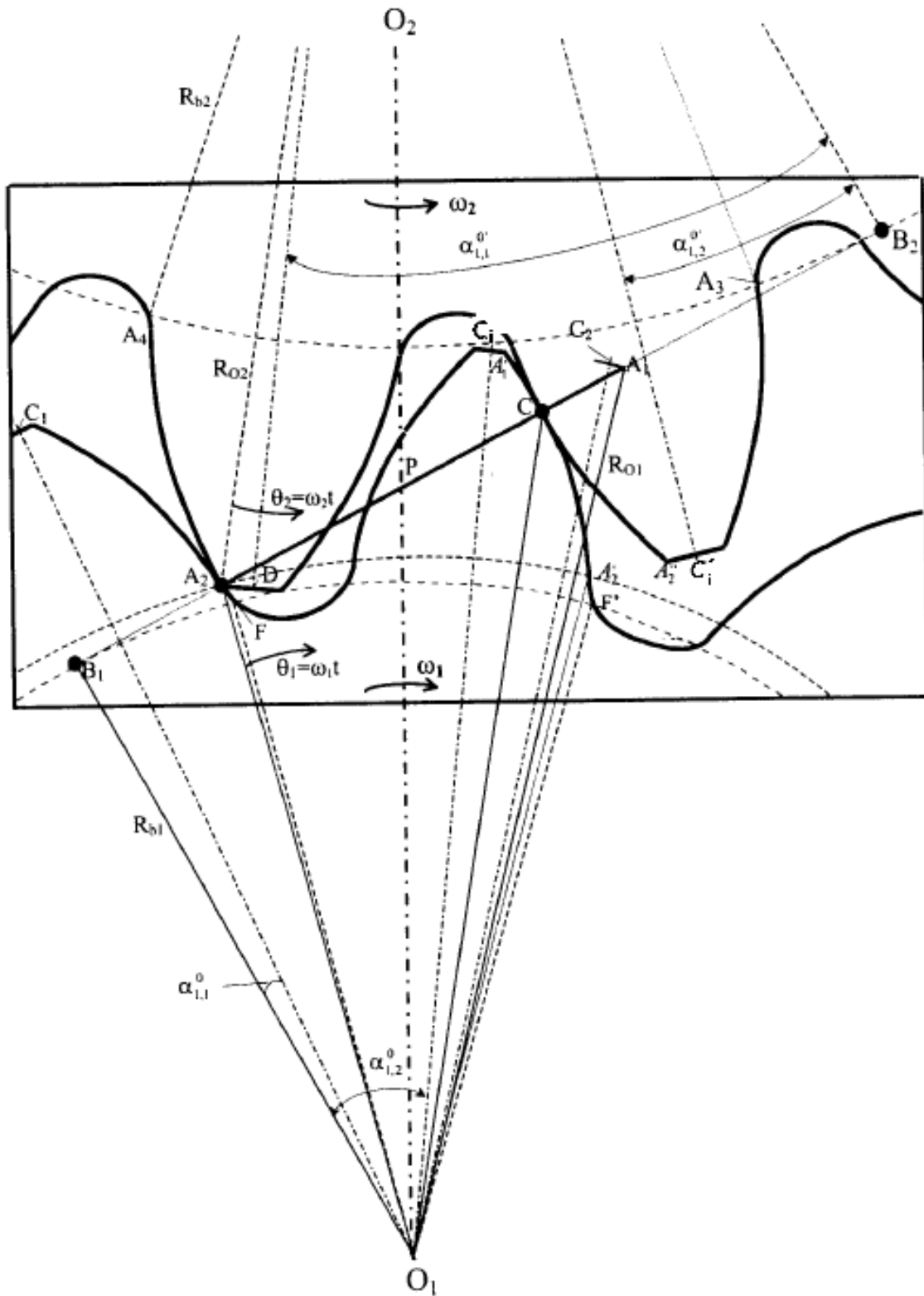


Figure 4.12. Line of Action and Parameters of a Gear Pair [24].

4.3.2. Calculation of Total Mesh Stiffness

The shear, axial and bending compressive energies which are stored in tooth respectively are expressed by

$$U_s = \frac{F^2}{4k_s} \quad (4.7)$$

$$U_a = \frac{F^2}{4k_a} \quad (4.8)$$

$$U_b = \frac{F^2}{4k_b} \quad (4.9)$$

where k_s , k_a , and k_b are the effective shear, axial stiffness, and bending compressive stiffness respectively in a similar direction along with F . The perpendicular component forces of force F is calculated as

$$F_a = F \sin\alpha_1 \quad (4.10)$$

$$F_b = F \cos\alpha_1 \quad (4.11)$$

where F_a causes bending and axial compressive effect, and F_b causes shear and bending effect in teeth and α_1 is pressure angle. The torque M is calculated as

$$M = F_a h \quad (4.12)$$

where h is the perpendicular distance between the forces applied at the point on tooth and the symmetry central line of tooth, see Figure 5.9. Perpendicular distance h can be calculated by

$$h = R_b [(\alpha_1 + \alpha_2) \cos\alpha_1 - \sin\alpha_1] \quad (4.13)$$

where R_b is the radii of base circle and α_2 is the half of the base tooth angle, see Figure 4.23. The distance d between the forces applied at the point and the tooth root is calculated by

$$d = R_b [(\alpha_1 + \alpha_2) \sin\alpha_1 + \cos\alpha_1 - \cos\alpha_2] \quad (4.14)$$

It is assumed that, the tooth on the gear is a cantilevered beam, and also assume that the deflection of body is zero. The bending potential energy according to beam theory can be expressed by

The equation of A_x and G is defined as

$$A_x = 2h_x B \quad (4.19)$$

$$G = \frac{E}{2(1 + \nu)} \quad (4.20)$$

When G, F_b , and dx is substituted in equation (4.18) and simplify it, the result can be expressed as

$$\frac{1}{k_s} = \int_{-\alpha_1}^{\alpha_2} \frac{1.2(1 + \nu)(\alpha_2 - \alpha) \cos \alpha \cos^2 \alpha_1}{EB[\sin \alpha + (\alpha_2 - \alpha) \cos \alpha]} d\alpha \quad (4.21)$$

axial compressive energy can be calculated by

$$U_a = \int_0^d \frac{F_a^2}{2EA_x} dx \quad (4.22)$$

$$\frac{1}{k_a} = \int_{-\alpha_1}^{\alpha_2} \frac{(\alpha_2 - \alpha) \cos \alpha \sin^2 \alpha_1}{2EB[\sin \alpha + (\alpha_2 - \alpha) \cos \alpha]} d\alpha \quad (4.23)$$

The total stored potential energy in a pair of spur gear by single tooth contact expressed by

$$\begin{aligned} U_t &= \frac{F^2}{2k_t} = U_h + U_{b1} + U_{s1} + U_{a1} + U_{b2} + U_{s2} + U_{a2} \\ &= \frac{F^2}{2} \left(\frac{1}{k_h} + \frac{1}{k_{b1}} + \frac{1}{k_{s1}} + \frac{1}{k_{a1}} + \frac{1}{k_{b2}} + \frac{1}{k_{s2}} + \frac{1}{k_{a2}} \right) \end{aligned} \quad (4.24)$$

In above, equation (4.24) pinion and gear subscript are denoted by 1 and 2 respectively. In the similar direction with the force F , the total effective mesh stiffness of a spur gear pair is k_t can be expressed by

$$k_t = \frac{1}{\frac{1}{k_h} + \frac{1}{k_{b1}} + \frac{1}{k_{s1}} + \frac{1}{k_{a1}} + \frac{1}{k_{b2}} + \frac{1}{k_{s2}} + \frac{1}{k_{a2}}} \quad (4.25)$$

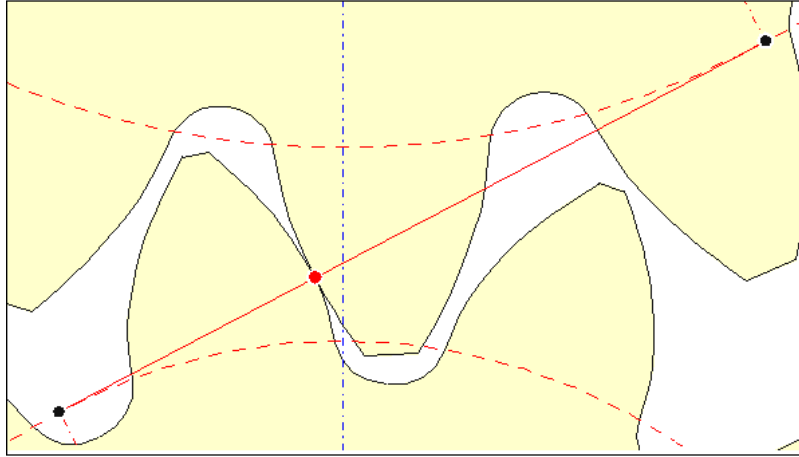


Figure 4.14. Single-Contact Teeth Mating [25]

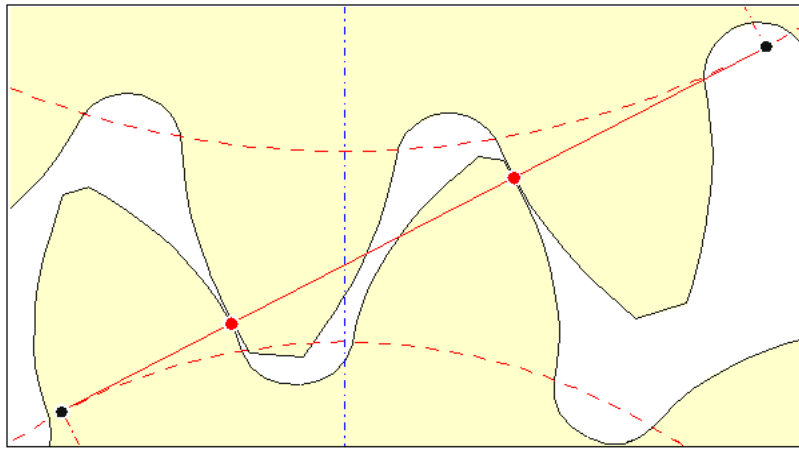


Figure 4.15. Two-Contact Teeth Mating [25].

The calculation of double teeth/ single tooth contact mesh stiffness ($k_{t,i}$) can be expressed by

$$k_{t,i} = \frac{1}{\frac{1}{k_h} + \frac{1}{k_{b1,i}} + \frac{1}{k_{s1,i}} + \frac{1}{k_{a1,i}} + \frac{1}{k_{b2,i}} + \frac{1}{k_{s2,i}} + \frac{1}{k_{a2,i}}} \quad (4.26)$$

When two teeth of pinion are in contact with two teeth of gear, for the first tooth pair $i = 1$ must be used, and for second tooth pair $i = 2$ must be used. Where $i = 1, 2$ and $k_{b1,i}, k_{s1,i}, k_{a1,i}, k_{b2,i}, k_{s2,i},$ and $k_{a2,i}$ can be calculated as

$$\frac{1}{k_{b1,i}} = \int_{-\alpha_1}^{\alpha_2} \frac{3\{1 + \cos\alpha_{1,i}[(\alpha_2 - \alpha)\sin\alpha - \cos\alpha]\}^2 (\alpha_2 - \alpha)\cos\alpha}{2EB[\sin\alpha + (\alpha_2 - \alpha)\cos\alpha]^3} d\alpha \quad (4.27)$$

$$\frac{1}{k_{s1,i}} = \int_{-\alpha_{1,i}}^{\alpha_2} \frac{1.2(1 + \vartheta)(\alpha_2 - \alpha)\cos\alpha \cos^2\alpha_{1,i}}{EB[\sin\alpha + (\alpha_2 - \alpha)\cos\alpha]} d\alpha \quad (4.28)$$

$$\frac{1}{k_{a1,i}} = \int_{-\alpha_{1,i}}^{\alpha_2} \frac{(\alpha_2 - \alpha)\cos\alpha \sin^2\alpha_{1,i}}{2EB[\sin\alpha + (\alpha_2 - \alpha)\cos\alpha]} d\alpha \quad (4.29)$$

$$\frac{1}{k_{b2,i}} = \int_{-\alpha'_{1,i}}^{\alpha'_2} \frac{3\{1 + \cos\alpha'_{1,i}[(\alpha'_2 - \alpha)\sin\alpha - \cos\alpha]\}^2 (\alpha'_2 - \alpha)\cos\alpha}{2EB[\sin\alpha + (\alpha'_2 - \alpha)\cos\alpha]^3} d\alpha \quad (4.30)$$

$$\frac{1}{k_{s2,i}} = \int_{-\alpha'_{1,i}}^{\alpha'_2} \frac{1.2(1 + \vartheta)(\alpha'_2 - \alpha)\cos\alpha \cos^2\alpha'_{1,i}}{EB[\sin\alpha + (\alpha'_2 - \alpha)\cos\alpha]} d\alpha \quad (4.31)$$

$$\frac{1}{k_{a1,i}} = \int_{-\alpha'_{1,i}}^{\alpha'_2} \frac{(\alpha'_2 - \alpha)\cos\alpha \sin^2\alpha'_{1,i}}{2EB[\sin\alpha + (\alpha'_2 - \alpha)\cos\alpha]} d\alpha \quad (4.32)$$

Where α_0 is pressure angle, α_2 is the base tooth angle half of pinion, α'_2 is the base tooth angle half, $\alpha_{1,i}$, and $\alpha'_{1,i}$, is shown in Figure 4.22. Finally, total meshing stiffness of single/double-teeth pair contact can be expressed by

$$k_t = k_{t,1} + k_{t,2} = \sum_{i=1}^2 \frac{1}{\frac{1}{k_h} + \frac{1}{k_{b1,i}} + \frac{1}{k_{s1,i}} + \frac{1}{k_{a1,i}} + \frac{1}{k_{b2,i}} + \frac{1}{k_{s2,i}} + \frac{1}{k_{a2,i}}} \quad (4.33)$$

For a pair gear for which contact ratio changes between 1 and 2, the duration of two teeth and single tooth must be calculated.

4.4. Conclusion: Comparison of the Results of Analytic Method and that of Numerical Method (Finite Element Method)

Analytic mesh stiffness of the mating gear pairs were computed. The gear pair parameters are given in Table 4.2. Mesh stiffness diagram for case studies given in Table 4.2 are shown in Figure 4.26- 4.35.

A comparison of mesh stiffness which is calculated by analytical methods and finite element, shows that; in analytical methods, teeth is assumed as a cantilever beam and the body is considered as a rigid object. So, the deformation of gear body is ignored. That means, in the analysis, the teeth as well as the gear body contributes to the elasticity, and the angular deformation is computed about gear axis and it is

defined by degree or radian unit. So, the stiffness unit in finite element is Nm/Rad, and in analytical method it is N/m.

In both method, the mesh stiffness in two-teeth-contact regions higher than one teeth involved. Stiffness curves in both cases are almost like a square wave, but in finite element curves this similarity is more pronounced. In both cases, as soon as the second gear is involved the stiffness value instantly changes. In both cases, you can easily evaluate relationship between stiffness variations during teeth involvement with transmission errors and gearing system noise. By changing the units and putting stiffness graph in a figure, the results are shown as Figure 4.36 and Figure 4.45.

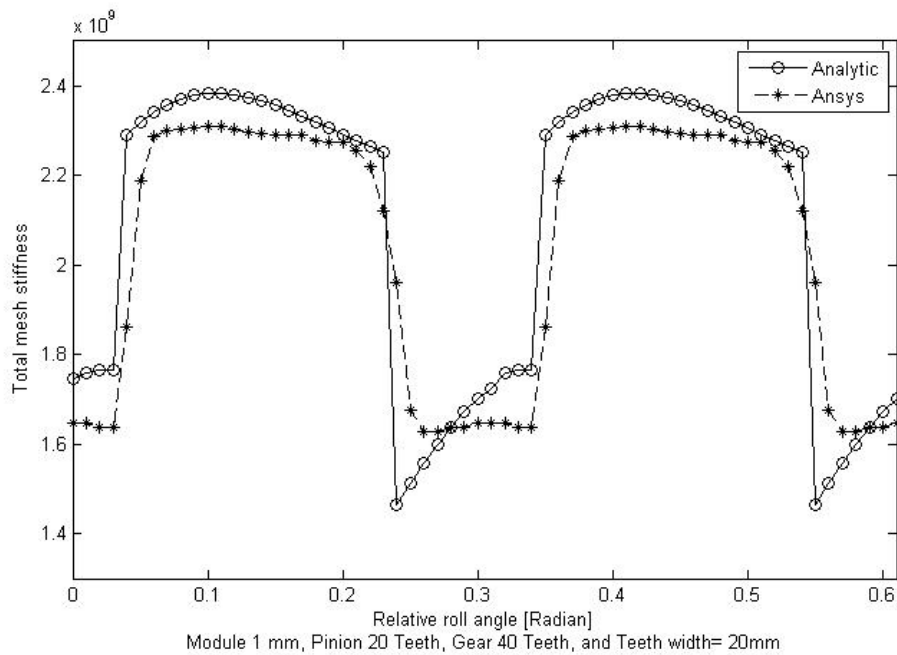


Figure 4.16. Comparison of Total Mesh Stiffness Between Analytic Method and Numerical Method Evaluations of Gear Pair Case 1.

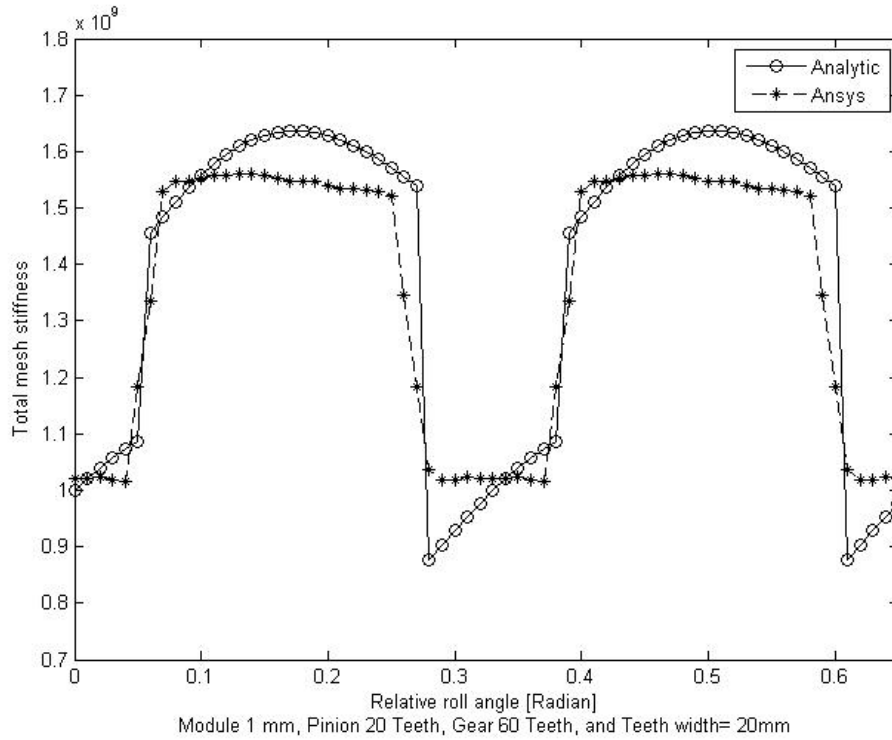


Figure 4.17. Comparison of Total Mesh Stiffness Between Analytic Method and Numerical Method Evaluations of Gear Pair Case 2.

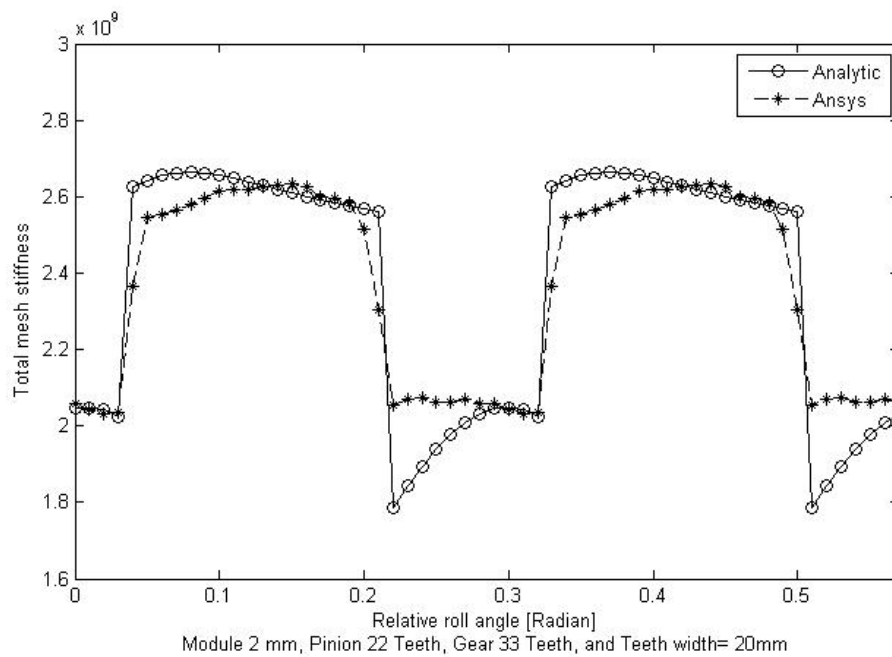


Figure 4.18. Comparison of Total Mesh Stiffness Between Analytic Method and Numerical Method Evaluations of Gear Pair Case 3.

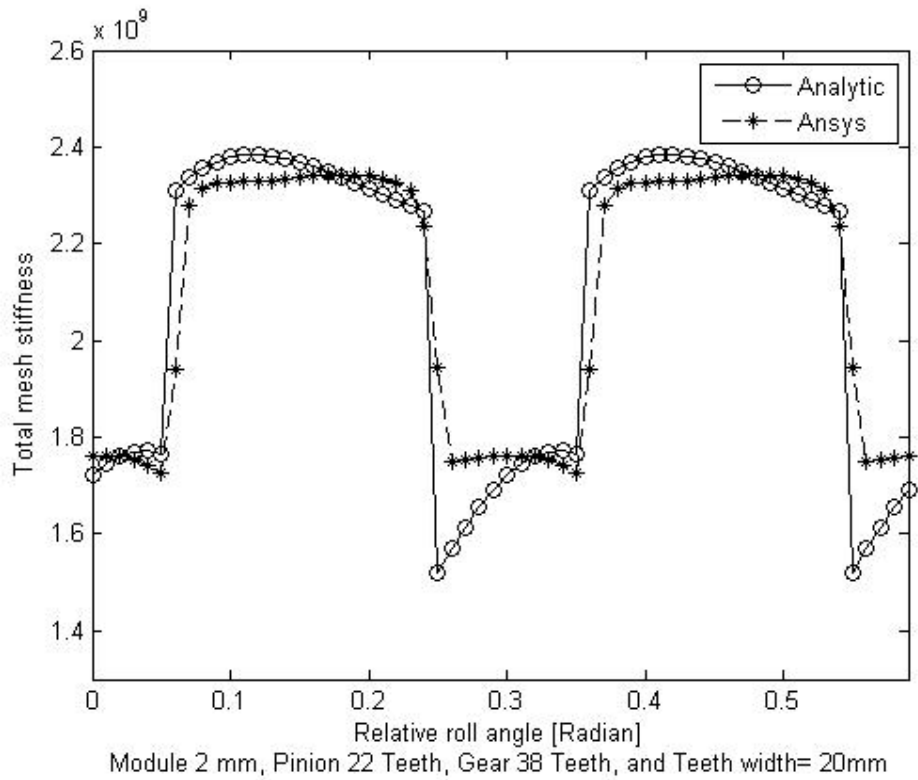


Figure 4.19. Comparison of Total Mesh Stiffness Between Analytic Method and Numerical Method Evaluations of Gear Pair Case 4.

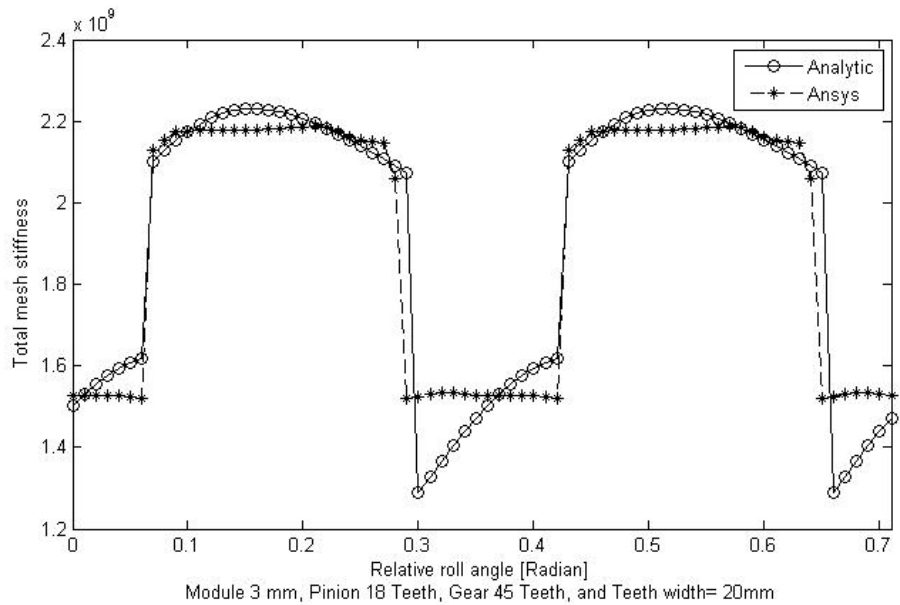


Figure 4.20. Comparison of Total Mesh Stiffness Between Analytic Method and Numerical Method Evaluations of Gear Pair Case 5.

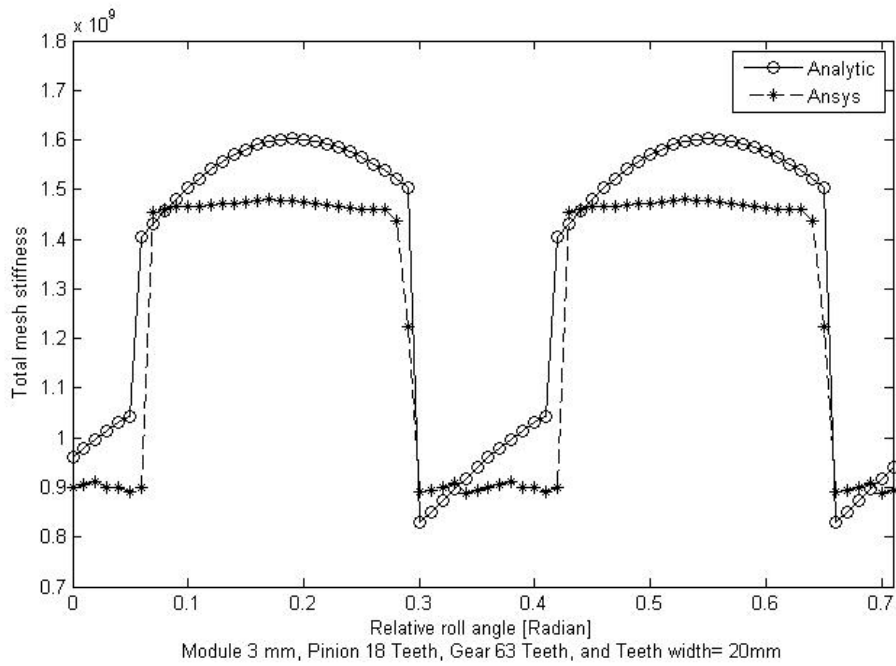


Figure 4.21. Comparison of Total Mesh Stiffness Between Analytic Method and Numerical Method Evaluations of Gear Pair Case 6.

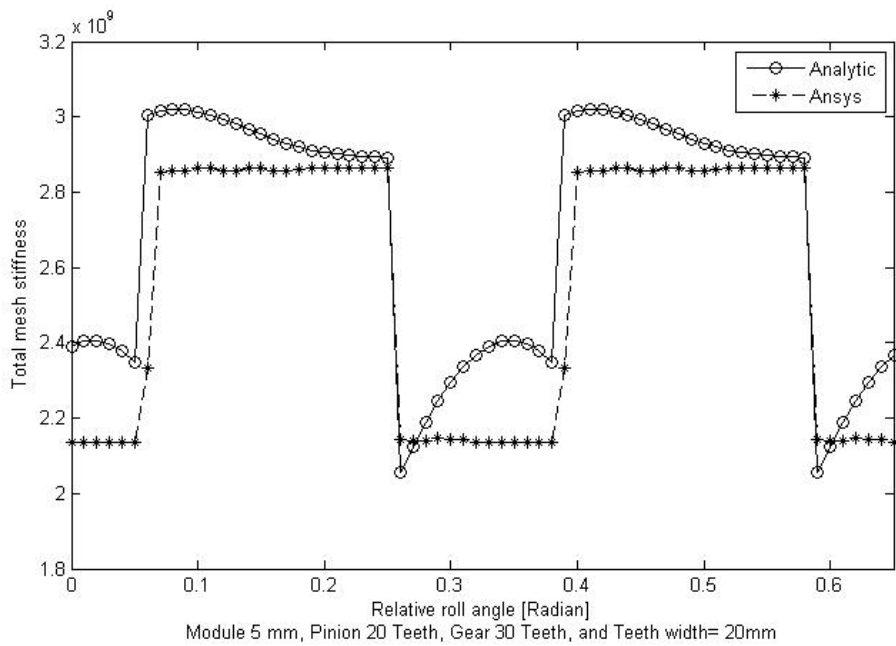


Figure 4.22. Comparison of Total Mesh Stiffness Between Analytic Method and Numerical Method Evaluations of Gear Pair Case 7.

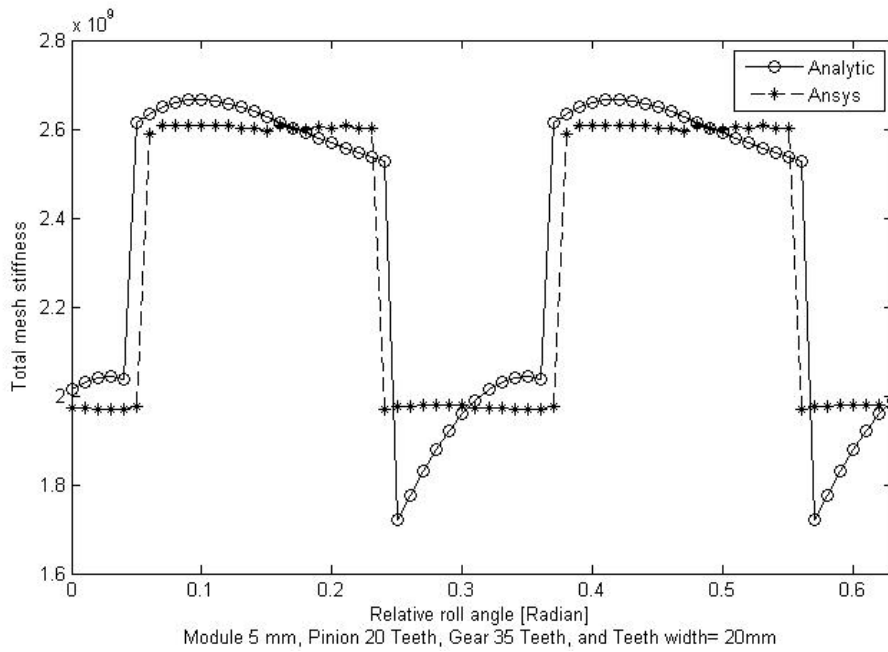


Figure 4.23. Comparison of Total Mesh Stiffness Between Analytic Method and Numerical Method Evaluations of Gear Pair Case 8.

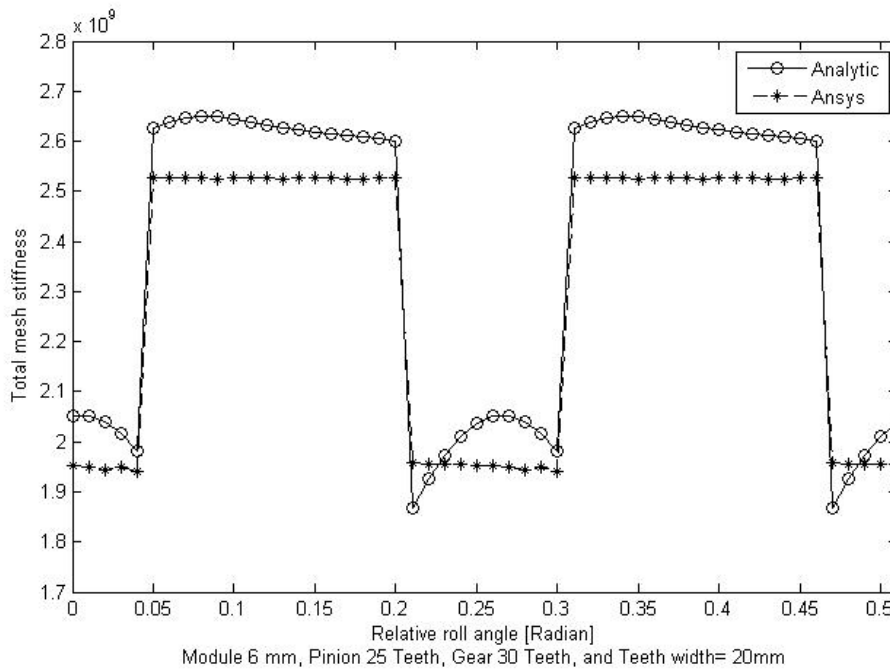


Figure 4.24. Comparison of Total Mesh Stiffness Between Analytic Method and Numerical Method Evaluations of Gear Pair Case 9.

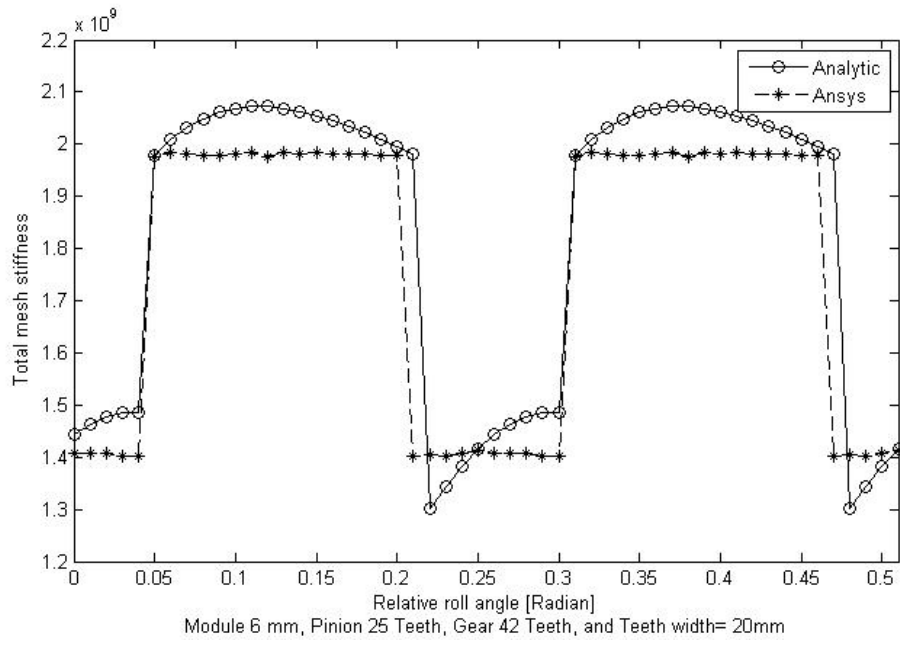


Figure 4.25. Comparison of Total Mesh Stiffness Between Analytic Method and Numerical Method Evaluations of Gear Pair Case 10.

CHAPTER 5

Spur Gear Pairs Transmission Error Regulation

5.1. Introduction

This chapter is devoted to developing a nonlinear controller which supervises a nonlinear spur gear pair. The non-linearity stems from the so-called mesh stiffness which changes periodically as the number of teeth come into contact, changes. When a controller is designed to regulate the speed of a spur gear pair, the following facts must be accounted for: i) the system has an inherent non-linearity which is owed to the geometry of involute profile, ii) the spur gear pair mathematical model is semi-definite, and the last but the most important one is that iii) when the elastic modes of motion is taken into account, the system is said to be an underactuated multibody system. When these facts are considered, it is seen that this simple looking mechanism that has been used in many machinery as a power transmitter between parallel shafts and/or as a torque/velocity amplifier poses itself as a challenge in control engineering practice.

In this chapter, a top-down approach is assumed. That is to say, it is started from the most general flexible multibody system which provides a theoretic base for the spur gear pair control, in subsequent subsection. Firstly, it is discussed what types of flexible multibody systems are fully actuated and what types of flexible multibody systems can be classified as underactuated flexible multibody systems. This discussion will lead to a definite problem statement which relates to the servo control of a spur gear pair. Then, it is started to write the dynamic equations that describe the time-dependent response of a spur gear pair to both input torque acting on pinion and disturbances that act on gear. In the general sense, it will be started from 6-DOF nonlinear dynamic model which includes many elements i.e. shaft, bearing elasticity and non-linearity due to backlash and terms that represent profile and manufacturing errors. Next, it will be stated assumptions explicitly and simplify the dynamic model to make it easy to solve. In the final part of this section, it will be attempted to develop a nonlinear controller which regulates the output shaft speed of a spur gear pair under loading disturbances. This problem is formulated as a velocity profile tracking problem. In the next chapter, these theoretical information will be used to develop a MATLAB Simulink model which integrates the FE analysis

result, the nonlinear mesh stiffness model, to the Simulink model as a nonlinear spring and simulation results will be discussed.

5.2. Trajectory Tracking of Multibody Systems

In this section trajectory tracking of multibody systems are discussed. Both underactuated and fully actuated systems are examined. Although a spur gear pair with elastic modes is naturally an underactuated system, the surface of fully actuated system analysis method will be scratched to show the distinction between fully actuated multibody systems and underactuated multibody systems. Apart from this use, the subsection where fully actuated systems are studied, is out of the scope of this work. Readers who are interested in underactuated multibody systems, may skip this section and start with the section 5.2.2 where underactuated flexible multibody systems are studied.

5.2.1. Fully Actuated Multibody Systems (FAMS)

FAMS's have as many control inputs and outputs as DOF. For trajectory tracking control of fully actuated multiply systems the inverse dynamics method which is called computed torque, is the most useful. FAMS with f DOF and m inputs (where $m = f$), are defined by motion equation,

$$M(q)\ddot{q} + k(q, \dot{q}) = g(q, \dot{q}) + \bar{B}(q)u \quad (5.1)$$

and the m outputs

$$y = h(q) \quad (5.2)$$

The fully actuated system's trajectory tracking by inverse dynamics is performed in two ways. First one is schema that tracks the desired trajectories of the generalized coordinates $y = q$. However, often one is more interested in tracking an output in the form of $y = h(q)$. This is performed with inverse dynamics for the output $y = h(q)$ directly.

After this introductory discussion about fully actuated flexible multibody systems, we will move on to underactuated systems. The next subsection, underactuated multibody dynamics, will lay out the theoretical background of this work. A thorough comprehension of that subsection is a prerequisite to study gear dynamics and it is a prerequisite to understand the Simulink model.

5.2.2. Underactuated Multibody Dynamics

If the control forces and torques is smaller than the number of degrees of freedom $f > m$ of the system, this multibody system is underactuated. Further, it is assumed that the number of inputs and output coincides ($y \in \mathbb{R}^m$).

5.2.2.1. Underactuated Multibody Systems Analysis

The systems with f DOF featuring the generalized coordinates $q \in \mathbb{R}^f$ and $m < f$ inputs $u \in \mathbb{R}^m$ and outputs $y \in \mathbb{R}^m$ are considered. The motion equation is

$$M(q)\ddot{q} + k(q, \dot{q}) = g(q, \dot{q}) + \bar{B}(q)u \quad (5.3)$$

with the output of system

$$y = h(q) \quad (5.4)$$

is partitioned into two parts

$$\begin{bmatrix} M_{aa}(q) & M_{au}(q) \\ M_{au}^T(q) & M_{uu}(q) \end{bmatrix} \begin{bmatrix} \ddot{q}_a \\ \ddot{q}_u \end{bmatrix} + \begin{bmatrix} k_a(q, \dot{q}) \\ k_u(q, \dot{q}) \end{bmatrix} = \begin{bmatrix} g_a(q, \dot{q}) \\ g_u(q, \dot{q}) \end{bmatrix} + \begin{bmatrix} \bar{B}_a(q) \\ \bar{B}_u(q) \end{bmatrix} u \quad (5.5)$$

The first f_a rows of the partitioned equation of motion of actuated part, the remaining f_u rows are unactuated. In the end, the equation of motion simply reads

$$\begin{bmatrix} M_{aa}(q) & M_{au}(q) \\ M_{au}^T(q) & M_{uu}(q) \end{bmatrix} \begin{bmatrix} \ddot{q}_a \\ \ddot{q}_u \end{bmatrix} + \begin{bmatrix} k_a(q, \dot{q}) \\ k_u(q, \dot{q}) \end{bmatrix} = \begin{bmatrix} g_a(q, \dot{q}) \\ g_u(q, \dot{q}) \end{bmatrix} + \begin{bmatrix} u \\ 0 \end{bmatrix} \quad (5.6)$$

The internal dynamics issue will be touched in the sequel. When dynamics of a spur gear pair is studied, it will be shown that the internal dynamics is bounded which is a prerequisite for successful nonlinear controller. Thus the system, spur gear pair, is said to be stable under the guide of nonlinear controller.

5.2.3. Normal Form of Input-Output

The feedback linearization is based on normal form of input-output. This normal form is obtained by generalizing a coordinate transformation $z = \Phi(x)$ to the motion equation (5.3). In this case, the coordinate transformation is

$$z = \Phi(x) \text{ where } x = \begin{bmatrix} q_a \\ \dot{q}_a \\ q_u \\ \dot{q}_u \end{bmatrix} \text{ and } x = \begin{bmatrix} \xi_1 \\ \dot{\xi}_1 \\ \eta_1 \\ \dot{\eta}_1 \end{bmatrix} = \begin{bmatrix} h(q) \\ H(q)\dot{q} \\ q_u \\ \dot{q}_u \end{bmatrix} \quad (5.7)$$

equation of motion (5.3) yields

$$y = \xi_1 \quad (5.8)$$

$$\dot{\xi}_1 = \xi_2 \quad (5.9)$$

$$\dot{\xi}_2 = HM^{-1}\bar{B}_u + HM^{-1}[g - k] + \bar{h} = \alpha(\xi, \eta)u + \beta(\xi, \eta) \quad (5.10)$$

$$\dot{\eta} = \hat{q}(\xi, \eta)u + \hat{P}(\xi, \eta)u \quad (5.11)$$

Figure 5.1 shows the normal form of input-output schematically.

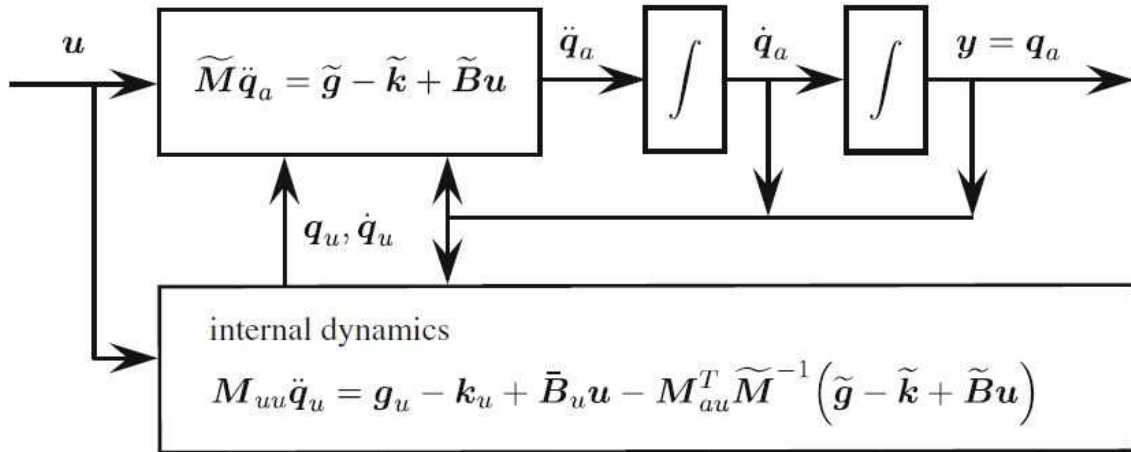


Figure 5.1: Graphical Representation of the Input-Output Normal Form of Underactuated Multibody Systems [26].

5.2.4. Linearization

Linearizing feedback control law that cancels the nonlinearities of the input-output normal form is given in (5.12)

$$u = \alpha^{-1}(\xi, \eta)(v - \beta(\xi, \eta)) \quad (5.12)$$

Where the new input is v . The input-output normal form (5.9)-(5.11) yields

$$y = \xi_1 \quad (5.13)$$

$$\dot{\xi}_1 = \xi_2 \quad (5.14)$$

$$\dot{\xi}_2 = v \quad (5.15)$$

$$\dot{\eta} = \hat{q}(\xi, \eta) + \hat{P}(\xi, \eta)\alpha^{-1}(\xi, \eta)(v - \beta(\xi, \eta)) \quad (5.16)$$

tracking control follows as

$$v = \ddot{y}_d + K_1(\dot{y}_d - \dot{y}) + K_0(y_d - y) \quad (5.17)$$

Introducing $e = y_d - y$ and inserting (5.17) in (5.13)-(5.16) yields

$$\ddot{e} + K_1\dot{e} + K_0e = 0 \quad (5.18)$$

This error dynamics can be controlled with K_0, K_1 to place the eigenvalues of the response at desired locations.

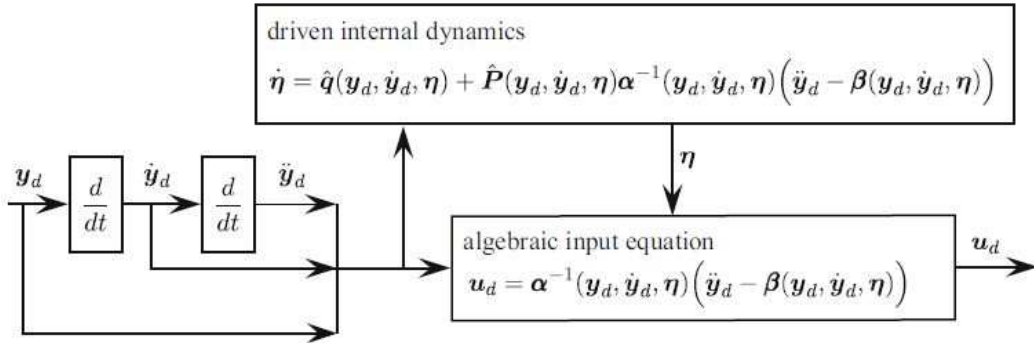


Figure 5.2: Graphical Representation of Feedforward Control of Underactuated Multibody Systems [26].

5.2.5. Model Inversion and Feedforward Control

For feedforward control an inverse model is derived from (5.8)-(5.11). The desired trajectory is given as $\xi_1 = y_d, \xi_2 = \dot{y}_d, \dot{\xi}_2 = \ddot{y}_d$. Then, the input u_d follows from (5.12) as

$$u_d = \alpha^{-1}(y_d, \dot{y}_d, \eta)(\ddot{y}_d - \beta(y_d, \dot{y}_d, \eta)) \quad (5.19)$$

The computation of u_d depends on the $y_d, \dot{y}_d, \ddot{y}_d$ and the states of the internal dynamics η . These latter ones are the solution of Equation (5.11) which are driven

by y_d, \dot{y}_d and u_d . Replacing u_d in the internal dynamics (5.11) by Equation (5.19) yields for the η coordinates the differential equation

$$\dot{\eta} = \hat{q}(y_d, \dot{y}_d, \eta) + \hat{P}(y_d, \dot{y}_d, \eta) \alpha^{-1}(y_d, \dot{y}_d, \eta) (\ddot{y}_d - \beta(y_d, \dot{y}_d, \eta)) \quad (5.20)$$

Inverse model is shown in Figure 5.2.

5.2.6. Systems with Collocated Output

The collocated output

$$y = q_a \quad (5.21)$$

are the actuated generalized coordinates q_a .

5.2.6.1. Input-Output Normal Form

For the system given in (5.1) with collocated output (5.21) the input-output normal form the coordinates are given by

$$z = \begin{bmatrix} \xi \\ \eta \end{bmatrix} \quad \text{with} \quad \xi = \begin{bmatrix} \xi_1 \\ \xi_2 \end{bmatrix} = \begin{bmatrix} y \\ \dot{y} \end{bmatrix} = \begin{bmatrix} q_a \\ \dot{q}_a \end{bmatrix}, \quad \eta = \begin{bmatrix} \eta_1 \\ \eta_2 \end{bmatrix} = \begin{bmatrix} q_u \\ \dot{q}_u \end{bmatrix} \quad (5.22)$$

These equations given in (5.6) are reordered to establish the input-output normal form

$$M_{aa} \ddot{q}_a = g_a - k_a + \bar{B}_a u - M_{au} \ddot{q}_u \quad (5.23)$$

$$M_{uu} \ddot{q}_u = g_u - k_u + \bar{B}_u u - M_{au}^T \ddot{q}_a \quad (5.24)$$

The sub-matrix M_{aa} is the upper left block of the mass matrix M and M_{uu} is the lower left sub-matrix. Thus, Equation (5.24) for \ddot{q}_u yields

$$\ddot{q}_u = M_{uu}^{-1} (g_u - k_u + \bar{B}_u u - M_{au}^T \ddot{q}_a) \quad (5.25)$$

Inserting this in Equation (5.23) yields

$$\begin{aligned} & (M_{aa} - M_{au} M_{uu}^{-1} M_{au}^T) \ddot{q}_a \\ & = g_a - M_{au} M_{uu}^{-1} g_u - k_a + M_{au} M_{uu}^{-1} k_u + \bar{B}_u u - M_{au} M_{uu}^{-1} \bar{B}_u u \end{aligned} \quad (5.26)$$

or in compact form

$$\tilde{M}\ddot{q}_a = \tilde{g} - \tilde{k} + \tilde{B}u \quad (5.27)$$

terms that appear in (5.27) are summarized as:

$$\tilde{M} = M_{aa} - M_{au}M_{uu}^{-1}M_{au}^T \quad (5.28)$$

$$\tilde{g} = g_a - M_{au}M_{uu}^{-1}g_u \quad (5.29)$$

$$\tilde{k} = k_a - M_{au}M_{uu}^{-1}k_u \quad (5.30)$$

$$\tilde{B} = \bar{B}_a - M_{au}M_{uu}^{-1}\bar{B}_u \quad (5.31)$$

Matrix \tilde{M} can be solved for \ddot{q}_a and then it can be replaced in Equation (5.24). Differential equation of motion can be summarized as:

$$\tilde{M}(q)\ddot{q}_a = \tilde{g}(q, \dot{q}) - \tilde{k}(q, \dot{q}) + \tilde{B}(q)u \quad (5.32)$$

$$\begin{aligned} M_{uu}(q)\ddot{q}_a &= g_u(q, \dot{q}) - k_u(q) + \bar{B}_u(q)u - M_{au}^T(q)\tilde{M}^{-1}(q)(\tilde{g}(q, \dot{q}) \\ &\quad - \tilde{k}(q, \dot{q}) + \tilde{B}(q)u) \end{aligned} \quad (5.33)$$

Equations (5.32) and (5.33) represent the input-output normal form of (5.5) with the collocated output $y = q_a = \xi_1$.

$$y = \xi_1 \quad (5.34)$$

$$\dot{\xi}_1 = \xi_2 \quad (5.35)$$

$$\dot{\xi}_2 = \tilde{M}^{-1}(\xi, \eta)(\tilde{g}(\xi, \eta) - \tilde{k}(\xi, \eta) + \tilde{B}(\xi_1, \eta_1)u) \quad (5.36)$$

$$\dot{\eta}_1 = \eta_2 \quad (5.37)$$

$$\begin{aligned} \dot{\eta}_2 &= M_{uu}^{-1}(\xi, \eta)(g_u(\xi, \eta) - k_u(\xi, \eta) + \bar{B}_u(\xi_1, \eta_1)u \\ &\quad - M_{au}^T(\xi, \eta)\tilde{M}^{-1}(\xi, \eta)[\tilde{g}(\xi, \eta) - \tilde{k}(\xi, \eta) + \tilde{B}(\xi_1, \eta_1)u]) \end{aligned} \quad (5.38)$$

The decoupling matrix is given by

$$\alpha(q) = \alpha(\xi_1, \eta_1) = \tilde{M}^{-1}(q)\tilde{B}(q) \quad (5.39)$$

5.2.6.2. Linearization

The linearizing feedback law is then

$$u = \tilde{B}^{-1}(\tilde{M}v + \tilde{k} - \tilde{g}) \quad (5.40)$$

where v is a new input. Applying feedback law in state space yields

$$y = \xi_1 \quad (5.41)$$

$$\dot{\xi}_1 = \xi_2 \quad (5.42)$$

$$\dot{\xi}_2 = v \quad (5.43)$$

$$\dot{\eta}_1 = \eta_2 \quad (5.44)$$

$$\dot{\eta}_2 = M_{uu}^{-1}(g_u - k_u + \bar{B}_u \tilde{B}^{-1}(\tilde{M}v + \tilde{k} - \tilde{g}) - M_{au}^T v) \quad (5.45)$$

The internal dynamics is given by Equation (5.45). In the case of bounded internal dynamics, the linearizing feedback law (5.40) can be used for stabilization of the output.

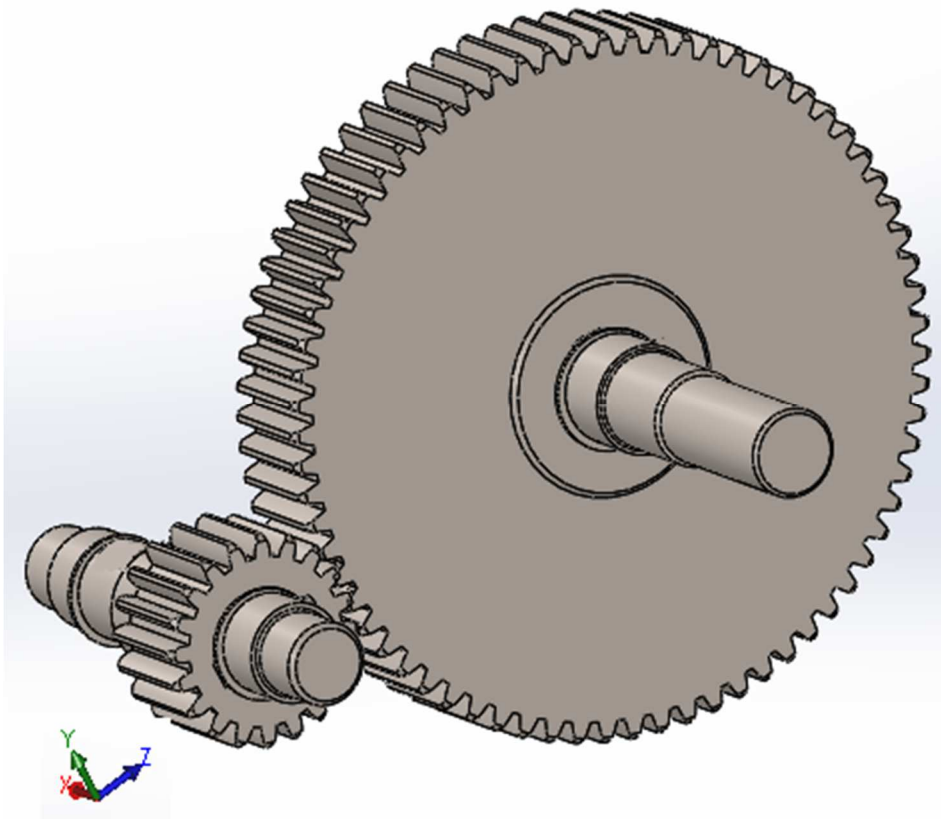


Figure 5.3: Spur Gear Pair's CAD Model.

5.2.6.3. Model Inversion and Feedforward Control

The input required to exactly reproduce the desired output $y_d = q_{a,d}$, can be written as

$$u_d = \tilde{B}^{-1}(y_d, q_u) \left(\tilde{M}(y_d, q_u) \ddot{y}_d + \tilde{k}(y_d, q_u, \dot{y}_d, \dot{q}_u) - \tilde{g}(y_d, q_u, \dot{y}_d, \dot{q}_u) \right) \quad (5.46)$$

The desired output trajectory provides the values y_d and \dot{y}_d . However, the states q_u, \dot{q}_u which are associated with the unactuated DOF, are required.

$$\begin{aligned} M_{uu}(y_d, q_u) \ddot{q}_a &= g_u(y_d, q_u, \dot{y}_d, \dot{q}_u) - k_u(y_d, q_u, \dot{y}_d, \dot{q}_u) + \bar{B}_u(y_d, q_u) u_d \\ &\quad - M_{au}^T(y_d, q_u) \tilde{M}^{-1}(y_d, q_u) [\tilde{g}(y_d, q_u, \dot{y}_d, \dot{q}_u) \\ &\quad - \tilde{k}(y_d, q_u, \dot{y}_d, \dot{q}_u) + \bar{B}_u(y_d, q_u) u_d] \end{aligned} \quad (5.47)$$

The internal dynamics are driven by the desired trajectory, i.e. y_d, \dot{y}_d and the desired input u_d which is given by Equation (5.46). Eliminating the desired input u_d by inserting (5.46) in Equation (5.47) the internal dynamics of driven read in compact form

$$M_{uu} \ddot{q}_u = g_u - k_u + \bar{B}_u \tilde{B}^{-1} (\tilde{M} \dot{y}_d + \tilde{k} - \tilde{g}) - M_{au}^T \dot{y}_d \quad (5.48)$$

5.3. Spur Gear Pair Dynamic Model

In this section, the dynamic model given in [12] is reviewed and then using some crude assumptions this model is simplified. This simplification makes the control problem easier. The original 6 DOF model proposed in [12] is versatile one which includes many elements and effects: nonlinearity due to backlash, profile and manufacturing errors and the effect of many supporting machine elements can be included in this 6 DOF model as a discrete elements, such as the elasticity and damping characteristics of shafts and bearings. However, it is convenient to simplify this 6 DOF model and reduce it to 2 DOF model, in our first attempt to solve the nonlinear control problem. Next, it will be started with the original dynamic model given in [12].

5.3.1. A Spur Gear Pair Dynamic Model Supported by Elastic Shafts and Bearing: Model with Friction, Backlash and Manufacturing Error

The lumped-parameter dynamic model will be considered. You can find it in Figure 5.4. will be considered in this study. In this model, gears are represented by rigid wheels that are connected to each other along the line-of-action (LOA) through a number of elements, these wheels are connected to each other. These elements are known to exhibit backlash type nonlinearity, flexibility, backlash and the geometric deviations of the gear mesh. The time-varying gear mesh stiffness $k_m(t)$ is the first element. A viscous damper c_m is the second element which is considered to simulate power losses at the gear mesh. A displacement function which defined

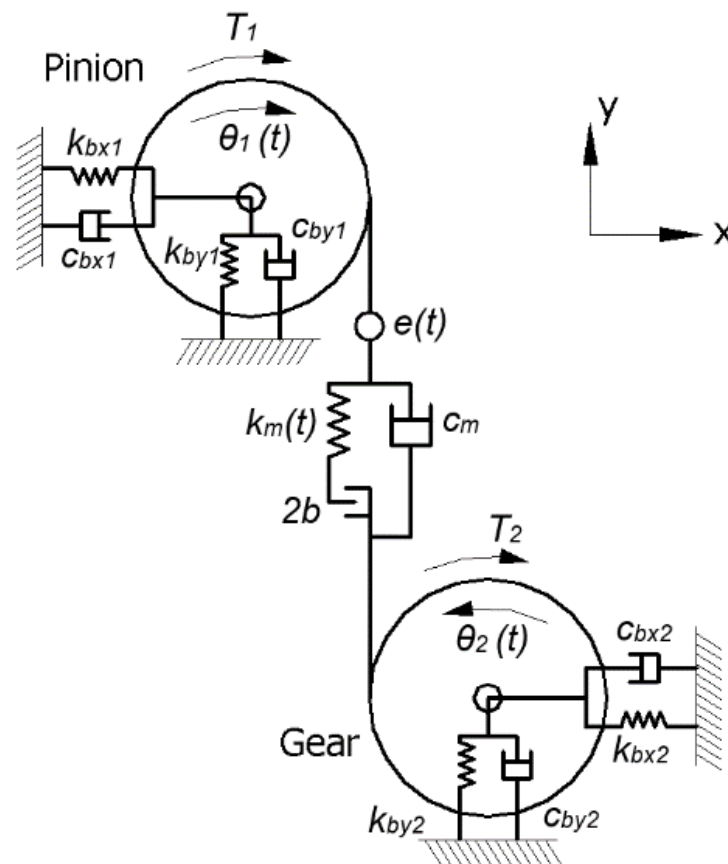


Figure 5.4: The Lumped-Parameter Dynamic Model of a Spur Gear.

by $e(t)$ is represented at the LOA to model manufacturing errors, tooth surface wear or tooth profile modifications applied for noise or load distribution aims.

Considering x_i and y_i as linear coordinate translations and θ_i as the rotational displacement of gear i , the equations of motion of the 6-DOF model represented in Figure 5.4 are given as

$$\begin{aligned}
J_1 \ddot{\theta}_1(t) + r_1 c_m \left(r_1 \dot{\theta}_1(t) - r_2 \dot{\theta}_2(t) + \dot{y}_1(t) - \dot{y}_2(t) - \dot{e}(t) \right) \\
+ r_1 k_m(t) g [r_1 \theta_1(t) - r_2 \theta_2(t) + y_1(t) - y_2(t) - e(t)] \\
= T_1 - \sum_k \mu_k N_k(t) R_{1k}
\end{aligned} \tag{5.49}$$

$$\begin{aligned}
J_2 \ddot{\theta}_2(t) - r_2 c_m \left(r_1 \dot{\theta}_1(t) - r_2 \dot{\theta}_2(t) + \dot{y}_1(t) - \dot{y}_2(t) - \dot{e}(t) \right) \\
- r_2 k_m(t) g [r_1 \theta_1(t) - r_2 \theta_2(t) + y_1(t) - y_2(t) - e(t)] \\
= -T_2 - \sum_k \mu_k N_k(t) R_{2k}
\end{aligned} \tag{5.50}$$

$$\begin{aligned}
m_1 \ddot{y}_1 + c_m \left(r_1 \dot{\theta}_1(t) - r_2 \dot{\theta}_2(t) + \dot{y}_1(t) - \dot{y}_2(t) - \dot{e}(t) \right) \\
+ k_m(t) g [r_1 \theta_1(t) - r_2 \theta_2(t) + y_1(t) - y_2(t) - e(t)] \\
+ c_{by1} \dot{y}_1(t) + k_{by1} y_1(t) = 0
\end{aligned} \tag{5.51}$$

$$\begin{aligned}
m_2 \ddot{y}_2 + c_m \left(r_1 \dot{\theta}_1(t) - r_2 \dot{\theta}_2(t) + \dot{y}_1(t) - \dot{y}_2(t) - \dot{e}(t) \right) \\
- k_m(t) g [r_1 \theta_1(t) - r_2 \theta_2(t) + y_1(t) - y_2(t) - e(t)] \\
+ c_{by2} \dot{y}_2(t) + k_{by2} y_2(t) = 0
\end{aligned} \tag{5.52}$$

$$m_1 \ddot{x}_1 + c_{bx1} \dot{x}_1(t) + k_{bx1} x_1(t) = \sum_k \mu_k N_k(t) \tag{5.53}$$

$$m_2 \ddot{x}_2 + c_{bx2} \dot{x}_2(t) + k_{bx2} x_2(t) = - \sum_k \mu_k N_k(t) \tag{5.54}$$

5.3.2. Simplification of 6 DOF Model and Assumptions

The dynamic model employs a number of assumptions. First of all, gear wheels are assumed to rigid with only flexibility coming from the gear mesh. This assumption would be tested if the gears have thin rims. Other gear motions, namely rotations about x and y and translations in the axial directions, were excluded from this model for the sake of simplicity. This assumes that the support conditions in both sides of the gear pair in axial direction are symmetric. Finally, simplified damping elements described earlier are used, primarily due to the lack of knowledge in modeling gear pair damping. Such damping models were shown to be reasonably accurate. Further, it is assumed that the elasticity and damping characteristics of shafts and

bearings can be ignored. $e(t)$ which represents the profile and manufacturing errors, is dropped off the equation. Backlash which is an inherent characteristics of every gear assembly is ignored. Because, if the backlash had been considered, it would have been made the analysis more complicated. Assembly error such as eccentricity of center distance errors, the geometric constraint of shafts, shafts are assumed to be in perfect parallel conditions. These assumption simplifies the problem in great deal. When the results of this work is examined, these assumptions must always be kept in mind.

5.3.3. Dynamic Model of a Spur Gear Pair: Model without Friction, Backlash, Elastic Shafts and Bearing and Profile Error Free

When the assumptions made in previous subsection are applied to the 6 DOF model given in subsection 5.3.1, the simplified model given below is obtained

$$J_1\ddot{\theta}_1(t) + r_1c_m (r_1\dot{\theta}_1(t) - r_2\dot{\theta}_2(t)) + r_1k_m(t)[r_1\theta_1(t) - r_2\theta_2(t)] = T_1 \quad (5.56)$$

$$J_2\ddot{\theta}_2(t) - r_2c_m (r_1\dot{\theta}_1(t) - r_2\dot{\theta}_2(t)) - r_2k_m(t)[r_1\theta_1(t) - r_2\theta_2(t)] = T_2 \quad (5.57)$$

This is a 2 DOF dynamic model of a spur gear pair with nonlinear stiffness term which changes with the angular position of the gear pair periodically. This periodic nonlinear mesh stiffness was studied by analytical method and FE method in chapter (4). In the Simulink model this dynamic model is simulated and controlled. In the dynamic equation given above, T_1 is the control torque and T_2 is load. It is presumed that the control Torque T_1 can be adjusted, but load torque T_2 is determined by the operational condition. The mesh stiffness is a function of time, however a close examination of this term reveals that actually it is a function of the pinion and gear absolute angular position. Thus the argument of mesh stiffness can be expressed in two different way. First it is as a function of time. Mesh stiffness can be written as the mean stiffness term plus an uncertain part which changes with position.

$$k_m(t) = k_{ma}(t) + \Delta k_m(t) \quad (5.58)$$

Where $k_m(t)$ is the mean stiffness and $\Delta k_m(t)$ is the alternating component of the mesh stiffness. In a second approach, variable mesh stiffness $k_m(t)$ can be written

as a nonlinear function of the angular position of pinion with a phase angle which relates the absolute angular position of pinion and gear at the start up position of simulation. It can be written as

$$k_m(t) = k_m(\theta_1(t), \phi_1) \quad (5.59)$$

where $\theta_1(t)$ is the angular position of pinion and ϕ_1 denotes the relative angular position of pinion with respect to an absolute starting position. Note that this is a nonlinear relationship between the stiffness term and the angular position. Hence any gear pair having a variable mesh stiffness which is a nonlinear function of pinion angular position is definitely a nonlinear differential equation.

5.3.4. Spur Gear Pair's Nonlinear Dynamic Model with Variable Mesh Stiffness Changing with Position

In this subsection, the spur pair's dynamic model in true form is given, both as a coupled nonlinear differential equation and in matrix form. Here, that the nonlinear mesh stiffness depends on pinion angular position is expressed explicitly. A typical nonlinear periodic mesh stiffness which was computed previously and given in chapter 4, is repeated here to underline the typical characteristics of this nonlinearity i.e. the changing number of teeth in contact and due to this the abrupt change in stiffness function. The equation of motion is given as differential equation below

$$\begin{aligned} J_1 \ddot{\theta}_1(t) + r_1 c_m (r_1 \dot{\theta}_1(t) - r_2 \dot{\theta}_2(t)) + r_1 k_m(\theta_1(t), \phi_1) [r_1 \theta_1(t) - r_2 \theta_2(t)] \\ = T_1 \end{aligned} \quad (5.60)$$

$$\begin{aligned} J_2 \ddot{\theta}_2(t) - r_2 c_m (r_1 \dot{\theta}_1(t) - r_2 \dot{\theta}_2(t)) - r_2 k_m(\theta_1(t), \phi_1) [r_1 \theta_1(t) - r_2 \theta_2(t)] \\ = T_2(t) \end{aligned} \quad (5.61)$$

The matrix form of motion is given below

$$\begin{aligned} \begin{bmatrix} J_1 & 0 \\ 0 & J_2 \end{bmatrix} \begin{Bmatrix} \ddot{\theta}_1 \\ \ddot{\theta}_2 \end{Bmatrix} + k_m(\theta_1(t), \phi_1) \begin{bmatrix} r_1^2 & -r_1 r_2 \\ -r_1 r_2 & r_2^2 \end{bmatrix} \begin{Bmatrix} \theta_1 \\ \theta_2 \end{Bmatrix} + c_m \begin{bmatrix} r_1^2 & -r_1 r_2 \\ -r_1 r_2 & r_2^2 \end{bmatrix} \begin{Bmatrix} \dot{\theta}_1 \\ \dot{\theta}_2 \end{Bmatrix} \\ = \begin{Bmatrix} T_1 \\ T_2(t) \end{Bmatrix} \end{aligned} \quad (5.62)$$

Here, the nonlinearity and coupling terms can be identified easily.

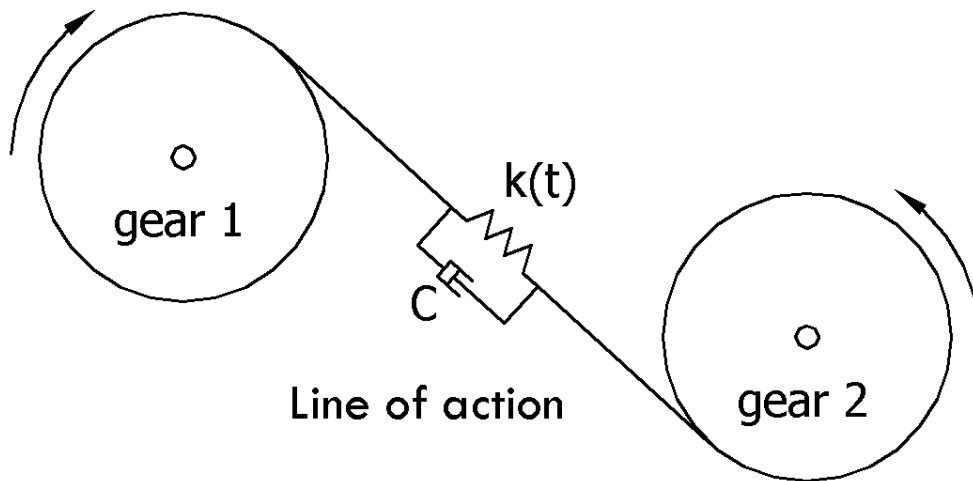


Figure 5.5: Simplified 2-DOF Spur gear pair model.

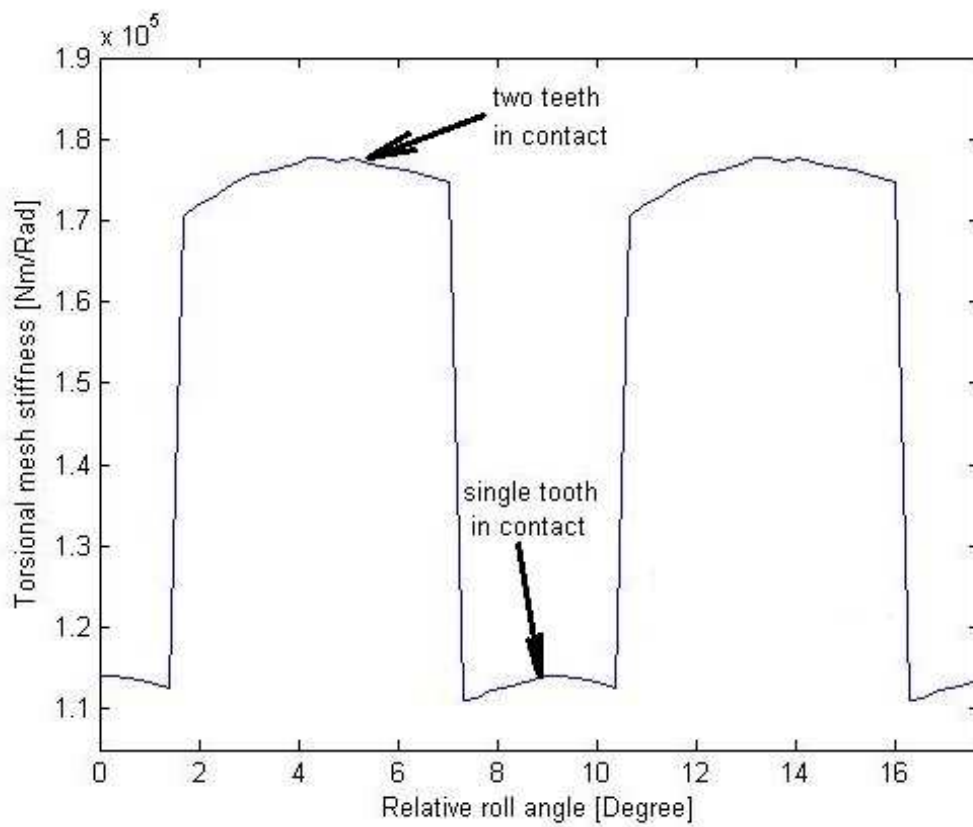


Figure 5.6: A typical mesh stiffness element: Nonlinearity due to change in the number of teeth in contact.

5.4. Analysis of Underactuated Multibody Systems: Servo Control of a Spur Gear Pair

This section is the core part of this chapter where it is used all the subjects discussed so far; the nonlinear dynamic model and the general approach to the control of nonlinear underactuated multibody systems. In this section it will be frequently refer to previous subsection and refer to those equations. It is obvious that a 2 DOF dynamic model where the torque acting on the pinion is controlled, is an underactuated multibody systems. Because the number of input is less than the number of the DOF of the system. If it is referred to [12] and examine the summary of [12] given in section 5.2 of this chapter, it can be concluded that system with collocated output is the most suitable form which use to design a controller. It can be used to suppress the high frequency oscillations in pinion and gear motion. This approach is straightforward, however, there is a critical issue that must be addressed before such a controller is implemented: it must be shown that the remaining internal dynamics and the nonlinear differential equation that represents that internal dynamic is stable i.e. the response that is computed by using internal dynamics is at least bounded. Next, we will start with the system with collocated output which is specially tailored for the problem at hand, i.e. 2 DOF spur gear pair's dynamic model.

5.4.1. Systems with Collocated Output: 2 DOF Model of Spur Gear Pair

The motion equation of an underactuated spur gear pair system which is given in Equation (5.60-62) can be written in compact form as

$$M(q)\ddot{q} + k(q, \dot{q}) = \bar{B}(q)u \quad (5.63)$$

with the angular position of the pinion as system output

$$y = q_a = h(q) = Hq \quad (5.64)$$

$$M(q) = M = \begin{bmatrix} J_1 & 0 \\ 0 & J_2 \end{bmatrix} \quad (5.65)$$

$$k(q, \dot{q}) = k_m(\theta_1(t), \phi_1) \underbrace{\begin{bmatrix} r_1^2 & -r_1 r_2 \\ -r_1 r_2 & r_2^2 \end{bmatrix}}_{G_r} \{q\} + c_m \underbrace{\begin{bmatrix} r_1^2 & -r_1 r_2 \\ -r_1 r_2 & r_2^2 \end{bmatrix}}_{G_r} \{\dot{q}\} \quad (5.66)$$

$$H = [1 \quad 0] \quad (5.67)$$

$$\bar{B} = \begin{bmatrix} 1 & 0 \\ 0 & 0 \end{bmatrix} \quad (5.68)$$

$$u = \begin{bmatrix} T_1 \\ T_2 \end{bmatrix} \quad (5.69)$$

$$q = \begin{bmatrix} \theta_1 \\ \theta_2 \end{bmatrix} \quad (5.70)$$

Then Equation (5.63) can be written

$$M \cdot \ddot{q} + k_m \cdot G_r \cdot q + c_m \cdot G_r \cdot \dot{q} = \bar{B} \cdot u \quad (5.71)$$

The above equation is partitioned into two parts

$$\begin{aligned} \begin{bmatrix} M_{aa} & M_{au} \\ M_{au}^T & M_{uu} \end{bmatrix} \begin{Bmatrix} \ddot{q}_a \\ \ddot{q}_u \end{Bmatrix} + k_m \cdot \begin{bmatrix} G_{raa} & G_{rau} \\ G_{rau}^T & G_{ruu} \end{bmatrix} \begin{Bmatrix} q_a \\ q_u \end{Bmatrix} + c_m \cdot \begin{bmatrix} G_{raa} & G_{rau} \\ G_{rau}^T & G_{ruu} \end{bmatrix} \begin{Bmatrix} \dot{q}_a \\ \dot{q}_u \end{Bmatrix} \\ = \begin{bmatrix} \bar{B}_{aa} & \bar{B}_{au} \\ \bar{B}_{au}^T & \bar{B}_{uu} \end{bmatrix} \begin{Bmatrix} u_a \\ u_u \end{Bmatrix} \end{aligned} \quad (5.72)$$

Thus, when Equation (5.72) is expanded, we obtain

$$\begin{aligned} \begin{bmatrix} M_{aa} & 0 \\ 0 & M_{uu} \end{bmatrix} \begin{Bmatrix} \ddot{q}_a \\ \ddot{q}_u \end{Bmatrix} + k_m \cdot \begin{bmatrix} G_{raa} & G_{rau} \\ G_{rau}^T & G_{ruu} \end{bmatrix} \begin{Bmatrix} q_a \\ q_u \end{Bmatrix} + c_m \cdot \begin{bmatrix} G_{raa} & G_{rau} \\ G_{rau}^T & G_{ruu} \end{bmatrix} \begin{Bmatrix} \dot{q}_a \\ \dot{q}_u \end{Bmatrix} \\ = \begin{bmatrix} \bar{B}_{aa} & 0 \\ 0 & 0 \end{bmatrix} \begin{Bmatrix} u_a \\ u_u \end{Bmatrix} \end{aligned} \quad (5.73)$$

5.4.2. Input-Output Normal Form

For system given in (5.73) the coordinates of the input/output normal form are given by

$$z = \begin{bmatrix} \xi \\ \eta \end{bmatrix} \quad \text{with} \quad \xi = \begin{bmatrix} \xi_1 \\ \xi_2 \end{bmatrix} = \begin{bmatrix} y \\ \dot{y} \end{bmatrix} = \begin{bmatrix} q_a \\ \dot{q}_a \end{bmatrix}, \quad \eta = \begin{bmatrix} \eta_1 \\ \eta_2 \end{bmatrix} = \begin{bmatrix} q_u \\ \dot{q}_u \end{bmatrix} \quad (5.74)$$

equation of motion is reordered as

$$M_{aa}\ddot{q}_a = -k_m \cdot \{G_r\}_1 \cdot \{q\} - c_m \cdot \{G_r\}_1 \cdot \{\dot{q}\} + \bar{B}_{aa}u_u \quad (5.75)$$

$$M_{uu}\ddot{q}_u = -k_m \cdot \{G_r\}_2 \cdot \{q\} - c_m \cdot \{G_r\}_2 \cdot \{\dot{q}\} + \bar{B}_{aa}u_u \quad (5.76)$$

When Equation (5.75) is expanded, we have

$$M_{aa}\ddot{q}_a = -k_m[G_r]_{11} \cdot q_a - k_m[G_r]_{12} \cdot q_u - c_m[G_r]_{11} \cdot \dot{q}_a - c_m[G_r]_{12} \cdot \dot{q}_u + \bar{B}_{aa}u_u \quad (5.77)$$

Above $\{G_r\}_i$ is the i th row of G_r and $[G_r]_{ij}$ is the element of G_r on the i th row and j th column. This yields

$$y = \xi_1 \quad (5.78)$$

$$\dot{\xi}_1 = \xi_2 \quad (5.79)$$

$$\dot{\xi}_2 = H \cdot M^{-1} \cdot \bar{B} \cdot u + H \cdot M^{-1} \cdot [M_{KC}] + \bar{h} = \alpha(\xi, \eta) \cdot u + \beta(\xi, \eta) \quad (5.80)$$

$$\dot{\eta} = -\hat{q}(\xi, \eta)u + \hat{P}(\xi, \eta) \cdot u \quad (5.81)$$

$$\alpha(\xi, \eta) = H \cdot M_{aa}^{-1} \cdot \bar{B}_{aa} \quad (5.82)$$

$$\beta(\xi, \eta) = M_{aa}^{-1} \{-k_m[G_r]_{11} \cdot \xi_1 - k_m[G_r]_{12} \cdot \eta_1 - c_m[G_r]_{11} \cdot \xi_2 - c_m[G_r]_{12} \cdot \eta_2\} \quad (5.83)$$

$$\hat{P}(\xi, \eta) = M_{uu}^{-1} \cdot B_{uu} \quad (5.84)$$

$$\hat{q}(\xi, \eta) = M_{uu}^{-1} \{-k_m[G_r]_{21} \cdot \xi_1 - k_m[G_r]_{22} \cdot \eta_1 - c_m[G_r]_{21} \cdot \xi_2 - c_m[G_r]_{22} \cdot \eta_2\} \quad (5.85)$$

5.4.3. Input-Output Linearization

The linearizing feedback law is given by

$$u = \alpha^{-1}(\xi, \eta)(v - \beta(\xi, \eta)) \quad (5.86)$$

where v is a new input. $\alpha^{-1}(\xi, \eta)$ and $\beta(\xi, \eta)$ are defined as

$$\alpha(\xi, \eta) = M_{aa}^{-1} \cdot \bar{B}_{aa} \quad (5.87)$$

And

$$\beta(\xi, \eta) = M_{aa}^{-1} \{-k_m[G_r]_{11} \cdot \xi_1 - k_m[G_r]_{12} \cdot \eta_1\}$$

$$-c_m[G_r]_{11} \cdot \xi_2 - c_m[G_r]_{12} \cdot \eta_2 \quad (5.88)$$

Applying (5.86) on the input-output normal form in state space yields

$$y = \xi_1 \quad (5.89)$$

$$\dot{\xi}_1 = \xi_2 \quad (5.90)$$

$$\dot{\xi}_2 = v \quad (5.91)$$

$$\dot{\eta} = -\hat{q}(\xi, \eta)u + \hat{P}(\xi, \eta) \cdot \alpha^{-1}(\xi, \eta)(v - \beta(\xi, \eta)) \quad (5.92)$$

$\hat{q}(\xi, \eta)$ and $\hat{P}(\xi, \eta)$ are defined as:

$$\hat{P}(\xi, \eta) = M_{uu}^{-1} \cdot B_{uu} \quad (5.93)$$

$$\begin{aligned} \hat{q}(\xi, \eta) = M_{uu}^{-1} \{ & -k_m[G_r]_{21} \cdot \xi_1 - k_m[G_r]_{22} \cdot \eta_1 \\ & -c_m[G_r]_{21} \cdot \xi_2 - c_m[G_r]_{22} \cdot \eta_2 \} \end{aligned} \quad (5.94)$$

Thus, a linear input-output behavior is achieved consisting of m chains of two integrators. The linearizing feedback law (5.12) in combination with eigenvalue assignment can be used for stabilization and asymptotic output tracking.

$$v = \dot{y}_d + K_1(\dot{y}_d - \dot{y}) + K_0(y_d - y) \quad (5.95)$$

applying control law (5.95) to the linearized subsystem yields the linear error dynamics

$$\ddot{e} = K_1\dot{e} + K_0e = 0 \quad (5.96)$$

5.4.4. Model Inversion and Feedforward Control

The input required in order to exactly reproduce the desired output $y_d = q_{a,d}$, follows from Equation (5.80) of the input-output normal form as

$$u_d = \alpha^{-1}(y_d, \dot{y}_d, \eta)(\ddot{y}_d - \beta(y_d, \dot{y}_d, \eta)) \quad (5.97)$$

The desired output trajectory provides the values y_d and \dot{y}_d , where

$$\alpha(y_d, \dot{y}_d, \eta) = H \cdot M_{aa}^{-1} \cdot \bar{B}_{aa} \quad (5.98)$$

$$\begin{aligned} \beta(y_d, \dot{y}_d, \eta) = M_{aa}^{-1} \{ & -k_m[G_r]_{11} \cdot y_d - k_m[G_r]_{12} \cdot \eta_1 - c_m[G_r]_{11} \cdot \dot{y}_d \\ & - c_m[G_r]_{12} \cdot \dot{\eta}_2 \} \end{aligned} \quad (5.99)$$

However, the states q_u, \dot{q}_u which associated with the unactuated degrees of freedom are required and must be computed from the differential equation (5.81) of the internal dynamics

$$\dot{\eta} = -\hat{q}(\xi, \eta)u + \hat{P}(\xi, \eta) \cdot u \quad (5.100)$$

The internal dynamics are driven by the desired trajectory, i.e. y_d, \dot{y}_d and the desired input u_d which is given by Equation (5.97). Eliminating the desired input u_d by inserting (5.97) in Equation (5.98) the driven internal dynamics read in compact form

$$\dot{\eta} = -\hat{q}(y_d, \dot{y}_d, \eta) + \hat{P}(y_d, \dot{y}_d, \eta) \cdot \alpha^{-1}(y_d, \dot{y}_d, \eta)(y_d - \beta(\dot{y}_d, \dot{y}_d, \eta)) \quad (5.101)$$

where

$$\begin{aligned} \hat{q}(y_d, \dot{y}_d, \eta) = M_{uu}^{-1} \{ & -k_m[G_r]_{21} \cdot y_d - k_m[G_r]_{22} \cdot \eta_1 - c_m[G_r]_{21} \\ & \cdot \dot{y}_d - c_m[G_r]_{22} \cdot \dot{\eta}_2 \} \end{aligned} \quad (5.102)$$

$$\hat{P}(y_d, \dot{y}_d, \eta) = M_{uu}^{-1} \cdot B_{uu} \quad (5.103)$$

$$\alpha(y_d, \dot{y}_d, \eta) = H \cdot M_{aa}^{-1} \cdot \bar{B}_{aa} \quad (5.104)$$

$$\begin{aligned} \beta(y_d, \dot{y}_d, \eta) = M_{aa}^{-1} \{ & -k_m[G_r]_{11} \cdot y_d - k_m[G_r]_{12} \cdot \eta_1 - c_m[G_r]_{11} \cdot \dot{y}_d \\ & - c_m[G_r]_{12} \cdot \dot{\eta}_2 \} \end{aligned} \quad (5.105)$$

Wrap Up: Underactuated Gear System Controlled by a Nonlinear Controller

The general block diagram of a gear system controlled by a nonlinear controller is given in Fig. 5.7. The pinion reference signal and the measured gear states are sent to the inverse model. Inverse model block calculates the necessary torque that drives the pinion at the desired speed. This torque drives the system, thus the desired acceleration, velocity and position of the pinion can be tracked accurately. However, the nonlinearity that stems from the gear mesh stiffness may deteriorate the system and the ideal conditions may cease to exist. Therefore, to make the

system robust against the uncertainties in the system, a second feedback PI system monitors the error state of the pinion and force the error in pinion state to zero. In the overall, the system has two cascaded feedback loop and full state measurement, i.e. gear and pinion states are measured, are used in these feedback loops. It is the duty of the inverse model to cancel the nonlinearity and it is the duty of the PI controller to ensure that error dynamics of the pinion is stable.

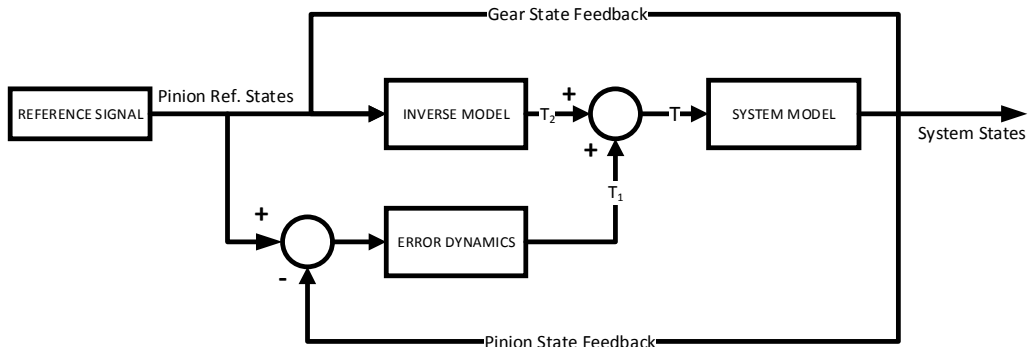


Figure 5.7 Block diagram of the controller and the gear system

5.5. Pole Placement: Error Dynamics

In this section, an analysis of error dynamics is made and examined the ramification of PI controller gains on error dynamics. To this end, a batch of run was made where these PI gains can be changed. The periodic mesh stiffness results in unwanted periodic forces which act on the gear teeth, it also causes transmission error between pinion and gear. To suppress these unwanted dynamics resulting from the gear involute profile, a controller has been proposed to eliminate these periodic mesh stiffness and tried to achieve almost a constant mesh stiffness. However, in practice, it is almost impossible to eliminate these side effects, so there will always be some periodic forces which results from the remaining mesh stiffness term which changes with a constant period. This remaining periodic mesh stiffness term will result in periodic forces acting on gear teeth. To improve the performance of PI controller when the system is subject to periodic forces, the Bode diagram of the error dynamics is plotted and tried to understand the behavior of error dynamics in high frequency and low frequency region. It is clear that there will always be a remaining periodic mesh stiffness term. The error dynamics is analyzed when the reference input velocity is a unit impulse function. It is convenient to plot 3D surfaces to understand the error dynamics under different conditions. These things are illustrated and studied in this section.

5.5.1. Transfer Function of a Single Unit Mass System with PID controller

5.5.1.1. Error Dynamics

Here, a servo system is considered as an example of a second-order system. The equation for the load element is

$$\ddot{\theta} = \ddot{\theta}_d \quad (5.106)$$

When the above equations is applied to error dynamics it can be seen that the dynamic equation of the system controlled by a PI controller is

$$\ddot{\theta} - \ddot{\theta}_d = K_P(\dot{\theta}_d - \dot{\theta}) + K_I(\theta_d - \theta) \quad (5.107)$$

The final form of the error dynamics is written as

$$\ddot{\theta}_e + K_P\dot{\theta}_e + K_I\theta_e = 0 \quad (5.108)$$

The Transfer Function Between Reference Position Input and Error in Angular Position. When taken the Laplace transform of error dynamics it is the algebraic equation in s-domain

$$\theta_e \cdot [s^2 + K_P s + K_I] = u(s) \quad (5.109)$$

Then the transfer function between error in angular position and reference angular position can be written as

$$\frac{\theta_e}{u(s)} = \frac{1}{[s^2 + K_P s + K_I]} \quad (5.110)$$

5.5.1.2. Parametric Study on PI Gains: The Effect of K_p on Error Dynamics

Here, the effect of proportional gain on the error dynamics is studied. If the error dynamics transfer function is examined and compared it with a mass-spring-damper system, K_p appears as parameter simulating damping coefficient. As it is expected increasing K_p has the effect of suppressing oscillations, maximum over shoot and the time needed to reach an envelope around steady-state value which is achieved asymptotically. Hence it is concluded that if only a single parameter is to be varied,

then K_p should be increased to improve the tracking characteristics of the error dynamics. The practical value of this PI gain, e.g. proportional gain K_p , will be discussed later.

If the frequency characteristics are examined, the following observations can be made: the system can suppress low frequency disturbances, however it almost transmits the high frequency oscillations. This is not desirable, but increasing K_p has a positive effect on high frequency oscillations. It improves the disturbance rejection capacity of the error dynamics. However, it cannot be said that it brings the performance of the error dynamics to a desirable region.

5.5.1.3. Parametric Study on PI Gains: The Effect of K_I on Error Dynamics

Here, the effect of integral gain on the error dynamics is studied. If the error dynamics transfer function is examined and compared it with a mass-spring-damper system, K_I appears as parameter simulating spring coefficient. As it is expected increasing K_I has the effect of increasing the frequency of oscillations in the error dynamics.

If the frequency characteristics are examined, the following observations can be made: the system can suppress low frequency disturbances, however it almost transmits high frequency oscillations. This is not desirable and increasing K_I does not have a significant effect on high frequency oscillations. But it improves the disturbance rejection capacity of the error dynamics in low frequency regions.

5.5.1.4. Rule of Thumb to Select PI Gains

In the light of these observation, the following observation was made that it can be used for the selection of PI gains

Proportional gain of PI controller K_p must be set to a high value.

Integral gain of PI controller K_I must be set to a low value.

5.5.1.5. Desired PI Controller Gains: K_p , K_I

If the unit impulse response of the error dynamics and graphs of 3D surfaces (see Figure 5.10) is examined it is seen that when $K_p > 30$ and $K_I < 5 K_p$ and K_I has a less influence on the maximum error.

Parametric study of error dynamics is made when unit impulse input is given to the system. Here, it is suggested that $K_I < 5$ and $K_p \gg 20$. Considering the above upper and lower limits for K_p, K_I the conclusion has been reached that the limits given below can be used when PI gains are determined.

Table 5.1. Determined PI Gains

| Reference Input | K_p | K_I |
|-----------------|-------|-------|
| Unit impulse | >20 | <5 |

5.5.1.6. Selected PI Controller Gains

Finally, the following PI controller gains have been selected, examining the parametric plots and general trends there. A single simulation was made by using these gains and the output are plotted in Figure 5.11. The results are quite satisfactory. Especially, Bode diagram is designed such that it is able to reject disturbances in low frequency regions as well as high frequency regions. That the error dynamics is able reject disturbance at high frequencies is vital for error dynamics. These gains selected on purpose, will definitely suppress these unwanted oscillations in finite time and make the whole system stable and run smoothly in silence.

Table 5.2. PID Gains

| K_p | K_I |
|-------|-------|
| 40 | 4 |

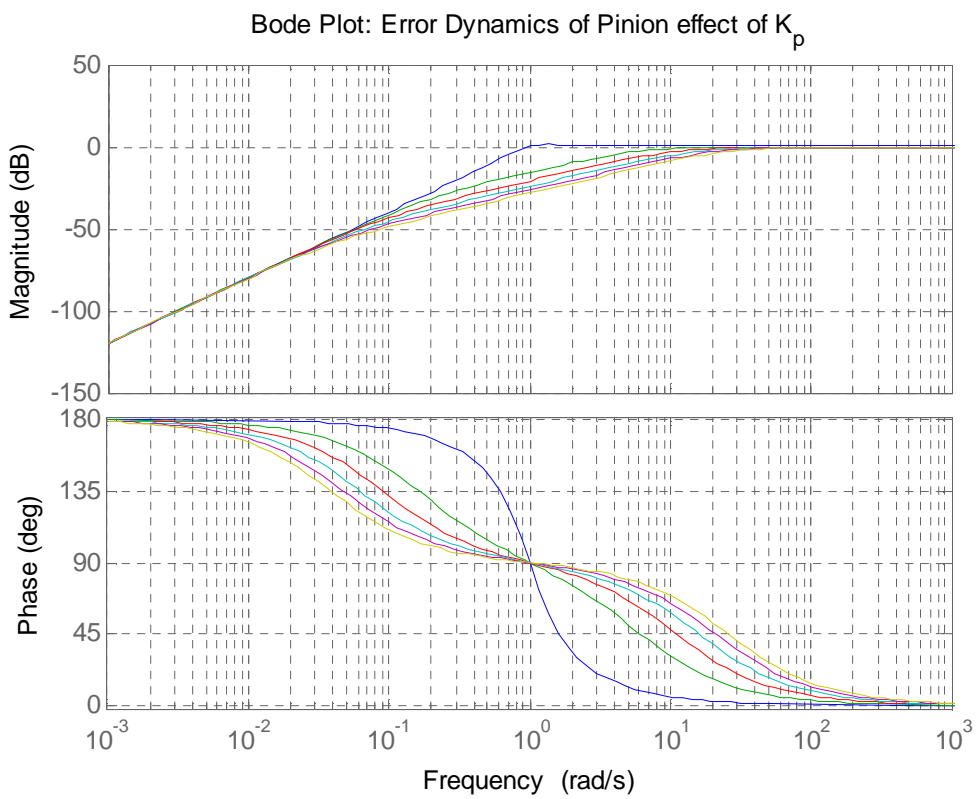
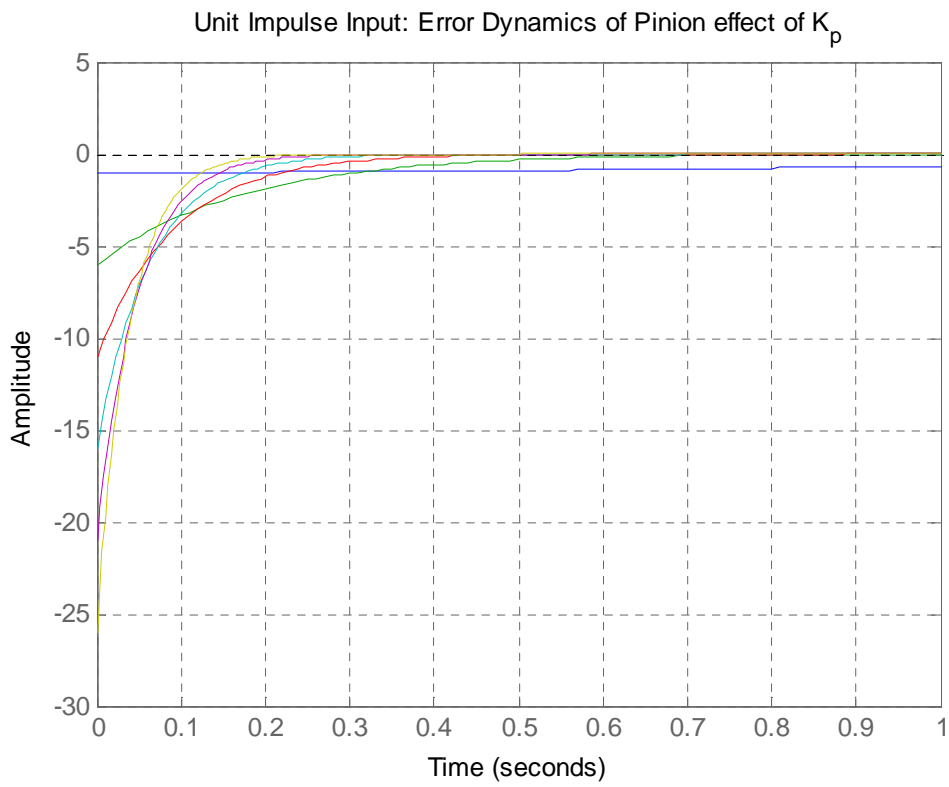


Figure 5.8: Error Dynamics Response to Unit Impulse Input: Effect of K_p .

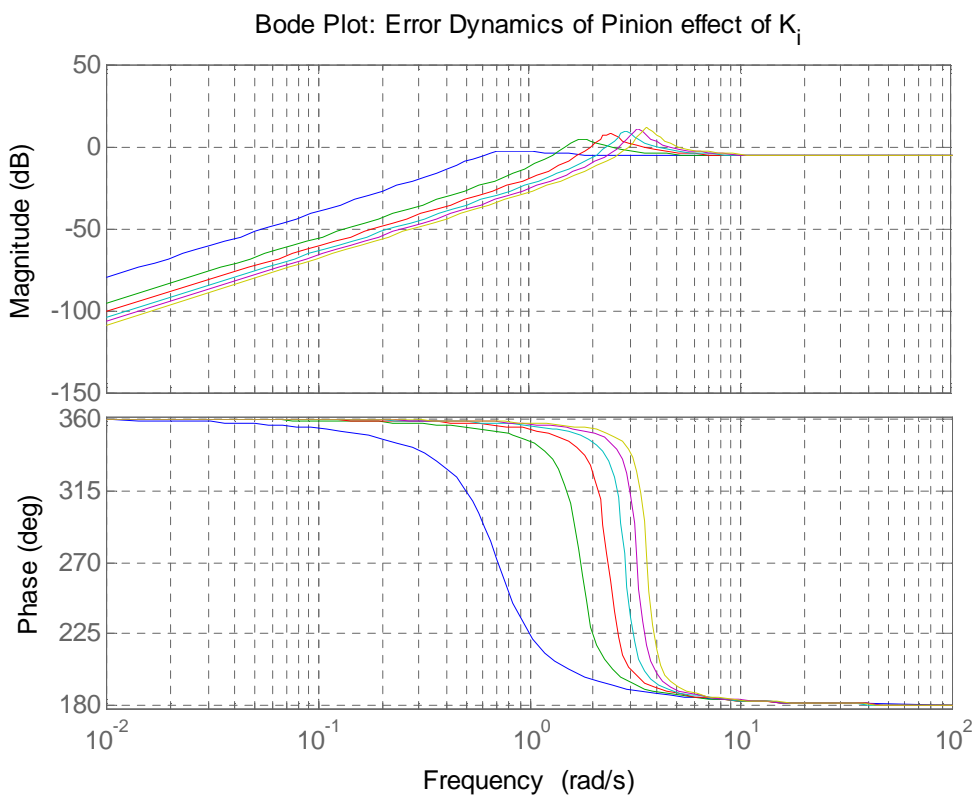
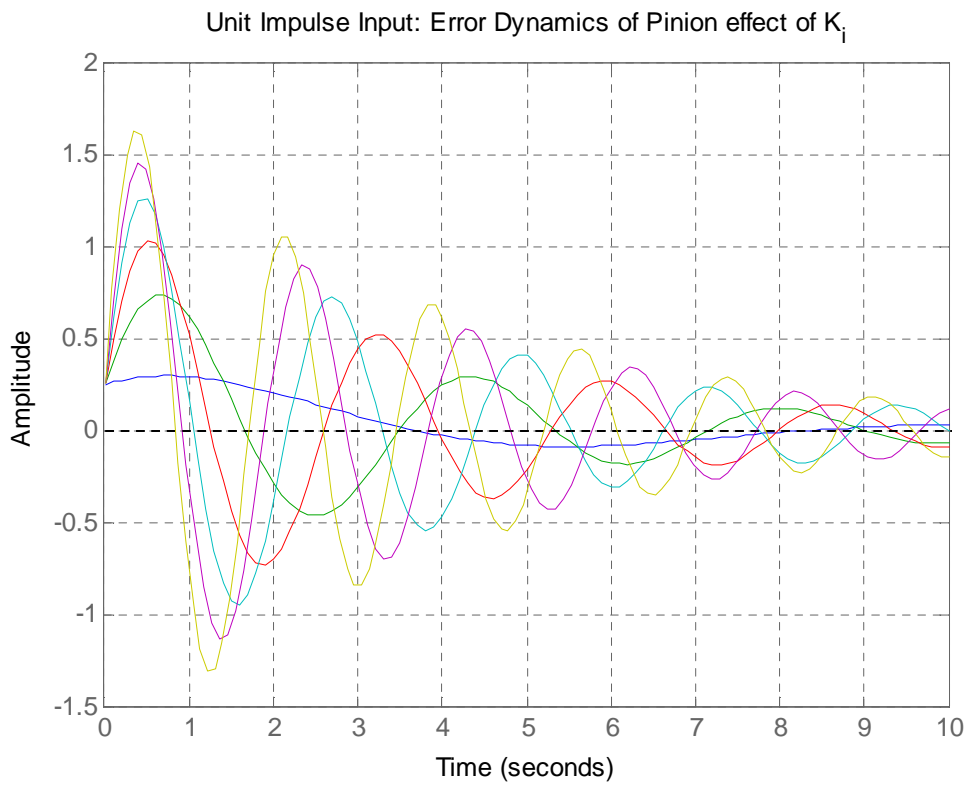
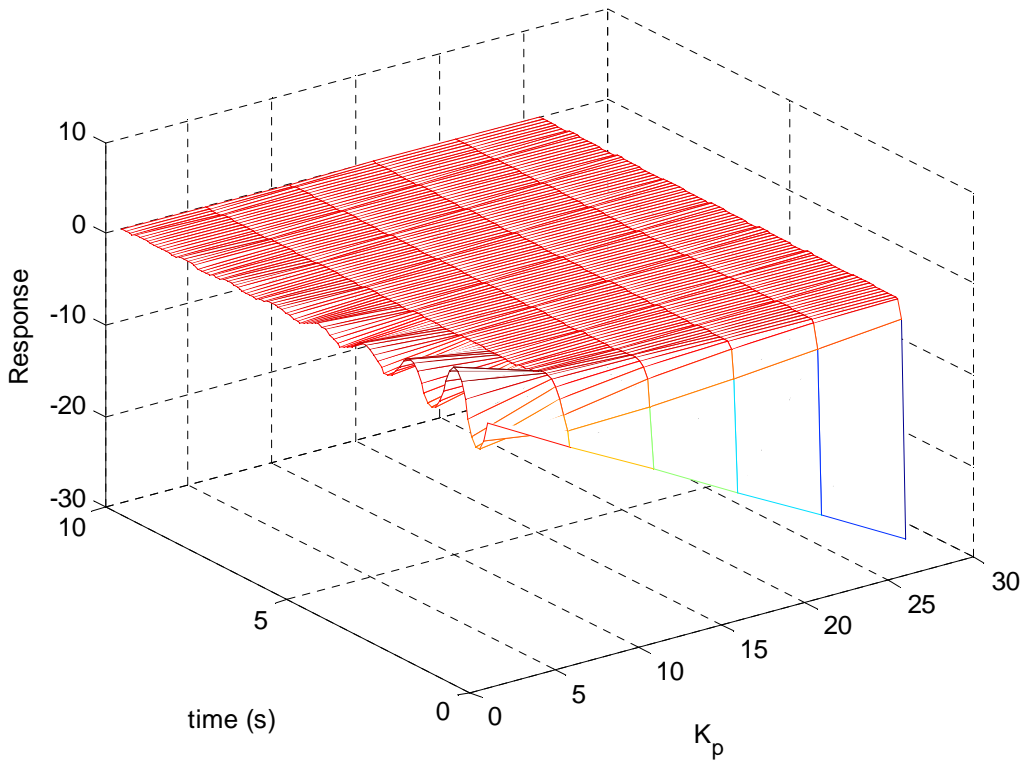


Figure 5.9: Error Dynamics Response to Unit Impulse Input: Effect of K_i .

Impulse Input Control surface: Error Dynamics v.s. proportional control gain K_p



Impulse Input Control surface: Error Dynamics v.s. integral control gain K_i

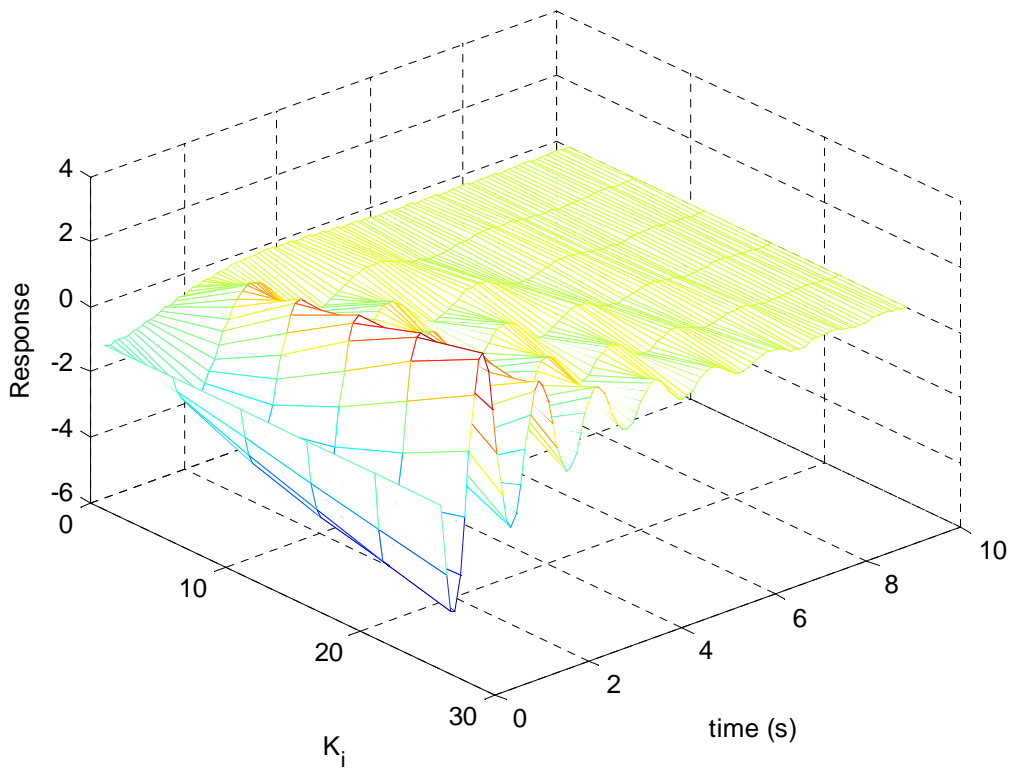


Figure 5.10: Unit impulse Input Control Surface.

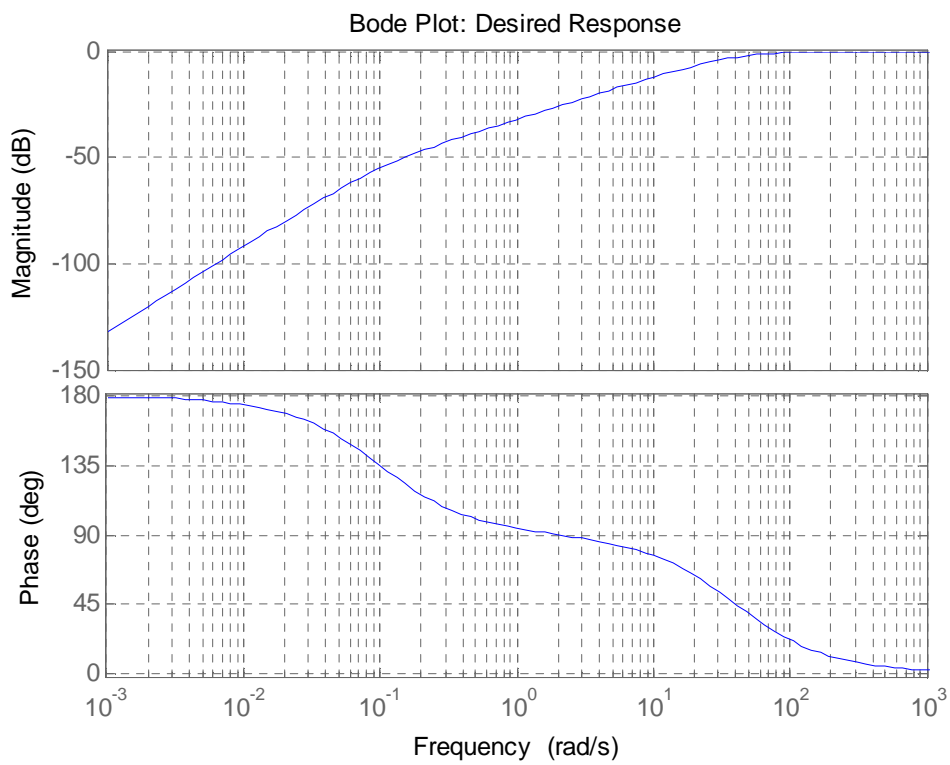
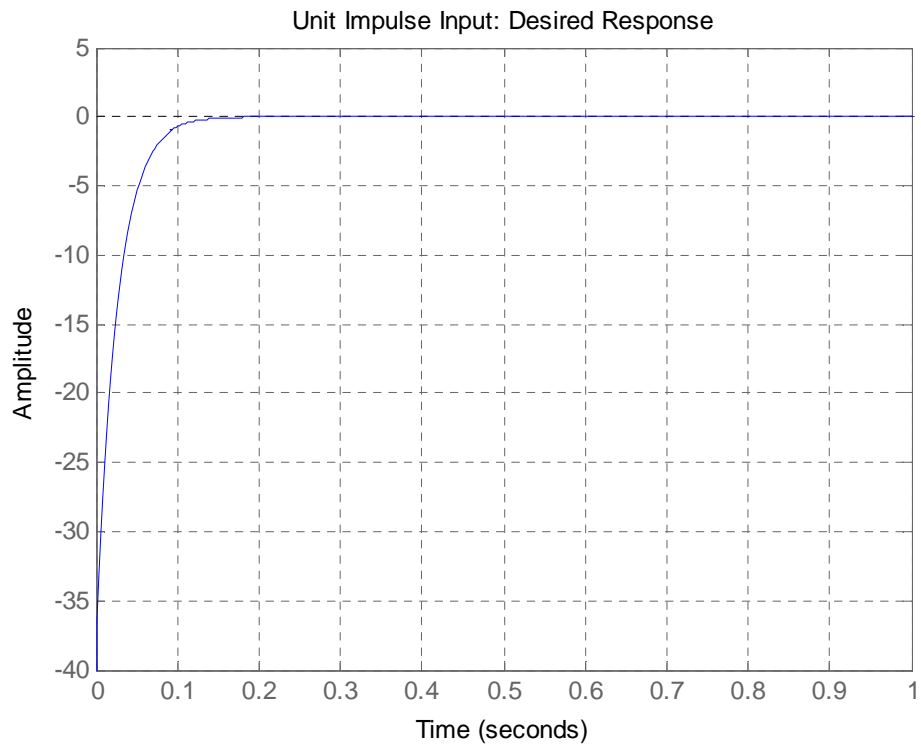


Figure 5.11: Desired Error Dynamics Response to Unit Impulse Input: $K_p = 40$, $K_I = 4$.

5.6. Conclusion

The 6-degrees of freedom dynamic model of the simulation of gear pairs was presented in this chapter. The simplified version of model was also derived. This model was analyzed by using the methods of underactuated multibody systems. Using those methods, mathematical relations related to system simulation and the desired control law were studied.

CHAPTER 6

Simulation Model: MATLAB Simulink Model of a Spur Gear Pair

6.1. Introduction

Here, a MATLAB Simulink model is constructed using the mathematical model developed in previous chapter i.e. Theory chapter. Various items of the Simulink model is explained by referring to the mathematical equations. The reader must note that a modular model approach was taken when the Simulink model was developed. These models are

1. Nonlinear gear dynamics model
2. Inverse dynamic model of a spur gear model
3. Error dynamics that helps the nonlinear controller reduce the tracking error to zero exponentially

One of the critical elements of the nonlinear spur gear model is the nonlinear spring element that models the interaction between gear teeth. Note that this nonlinear spring element was computed with the help ANSYS finite element program. In this chapter, it is exclusively shown that how to integrate the finite element model to the MATLAB Simulink model of a spur gear.

This contain: in section one, a quick review of the critical elements of the MATLAB Simulink model is made. In section two, a close look is taken at the content of these basic elements i.e. i) Nonlinear gear dynamics model, ii) Inverse dynamic model of a spur gear model iii) Error dynamics that helps the nonlinear controller reduce the tracking error exponentially. In section three, the spur gear pair's MATLAB Simulink model is compared which is controlled by a nonlinear controller and match various items of the model with the terms appearing in mathematical equations. Finally, conclusions and discussion section concludes this chapter.

6.2. An Overview of MATLAB Simulink Model

The outlook of MATLAB Simulink model is shown in Fig 6.1. In this figure several major blocks can be identified. These are:

1. Reference velocity profile
2. Inverse kinematic model

3. Inverse dynamic model
4. Nonlinear spur gear dynamic model
5. Error dynamics that take care the remaining error in gear dynamics

These items are described briefly below:

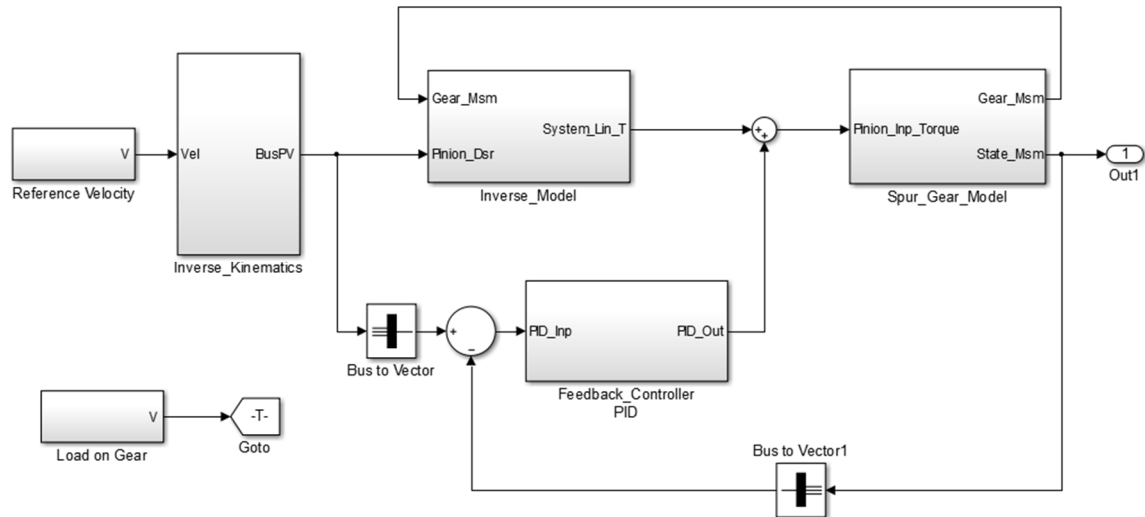


Figure 6.1: General Outlook of MATLAB Simulink Model of a Spur Gear Pair.

Reference velocity profile. In this module, reference velocity profile is defined. This velocity profile is the desired velocity profile of pinion

Inverse kinematics model. In this model using the reference velocity profile of pinion, reference velocity of pinion and gear are calculated

Inverse dynamic model. This dynamic model is designed such that it generates the nonlinear forces in the dynamic model of nonlinear spur gear pair model. Later, these nonlinear forces are used to cancel the non-linearity the nonlinear gear dynamics. This block assumes that there is a full access to exact mode of gear dynamics.

Nonlinear spur gear dynamic model. This is a model of the real system that is controlled by the nonlinear controller. It is designed according to the nonlinear 2-DOF model of a spur pair.

Error dynamics. Once the nonlinear terms are canceled by the nonlinear forces generated by the inverse dynamic model, the remaining linear model is controlled in this block to make the error in tracking decay to zero exponentially. Here, a standard PI controller is used.

Note that this model requires full knowledge of the exact mathematical model of the physical system i.e. spur gear pair.

If the mathematical model is inaccurate, there will be nonlinear forces which deteriorates the performance of the nonlinear controller. Especially, one cannot guarantee that PI controller works perfectly. Thus, the error dynamics will not decrease to zero exponentially and indeed it will be forced by the dynamic model which is excited by periodic forces.

Next chapter, starts with a detailed description of these models which are identified above. A detailed representation of the inside of those major blocks will be provided.

6.3. Inside the MATLAB Simulink Model: Simulink Model of a Spur Gear Pair

This section provides an in depth analysis of the inside of the major blocks which have been identified in previous section. These are guide the flow of text.

1. Reference velocity profile
2. Inverse kinematic model
3. Inverse dynamic model
4. Nonlinear spur gear dynamic model
5. Error dynamics

First, it will be started with the reference velocity profile:

6.3.1. Reference Velocity Profile

In order to specify the reference velocity that is to be tracked by the pinion, the angular acceleration profile of pinion is designed at first. This guarantees that the second order dynamics of spur gear is at least piece-wise continuous in acceleration. It also implies that reference velocity profile is continuous and smooth as well. For this purpose, the signal builder block of MATLAB Simulink program is used. In Figure 6.2, the manual switches to connect and disconnect different acceleration profiles to the system is used. After the manual switch, there is a gain block to scale the acceleration signal, thus an acceleration profile may have the same shape but with a different scaled magnitude of the original signal. Finally, the integrator block to compute the corresponding velocity profile is used, desired for the pinion.

6.3.2. Inverse Kinematic Model

Inverse kinematic model computes the angular position and velocity when the pinion is driven at the reference velocity. It uses the simple kinematic relationships for a pair of spur gear. This block is illustrated in Figure 6.4. Finally, bus blocks are used to rearrange the output of this block.

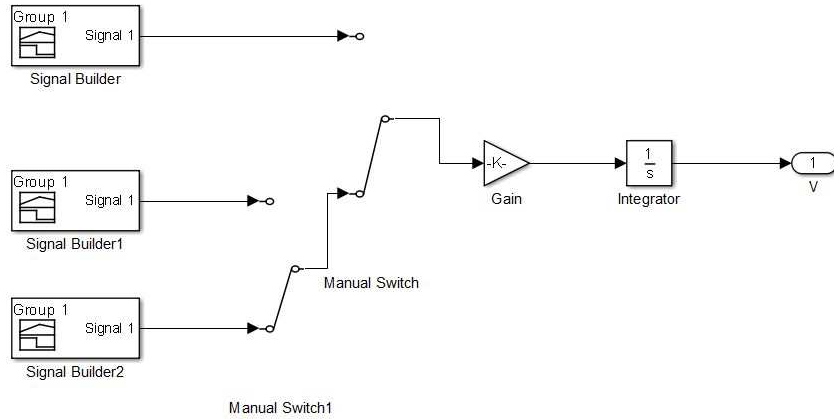


Figure 6.2: Reference Velocity Profile Block.

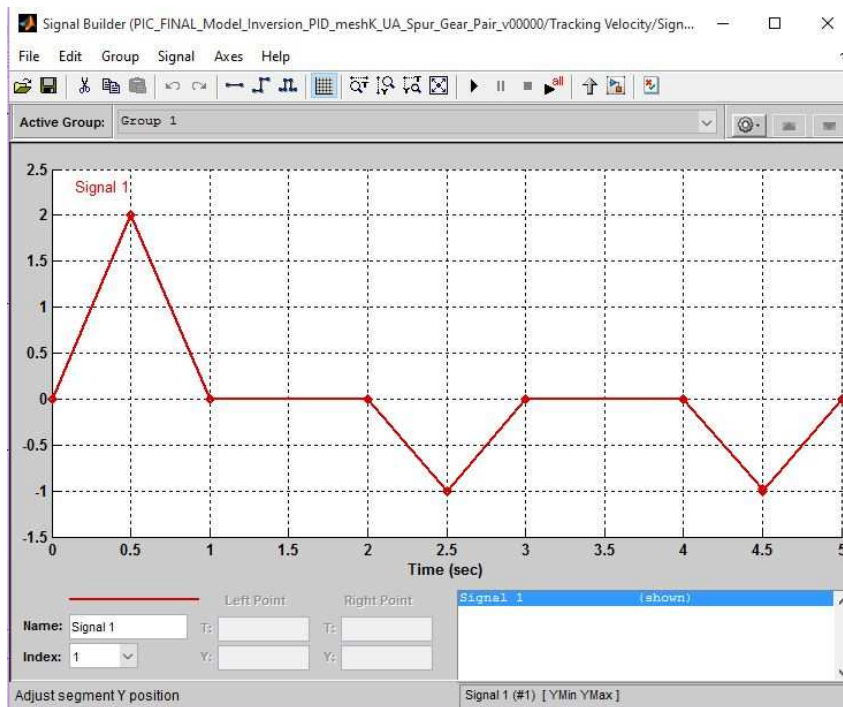


Figure 6.3: Signal Builder for Acceleration.

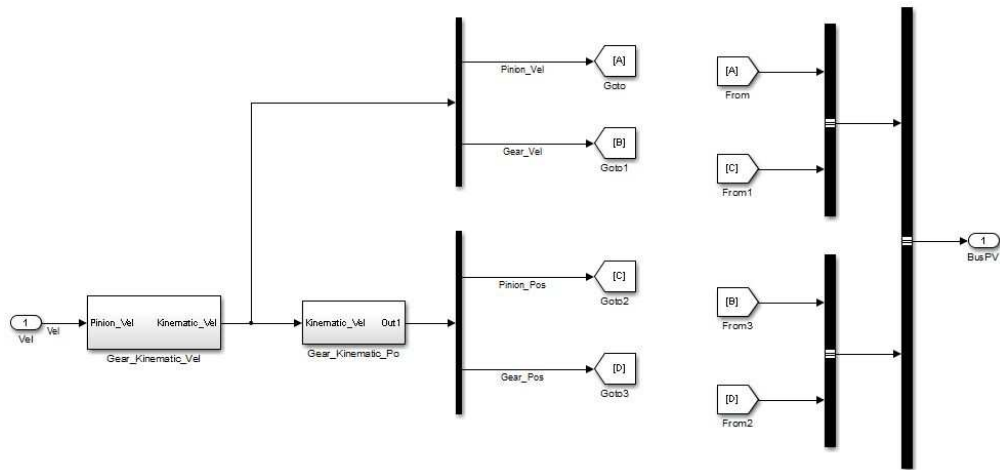


Figure 6.4: Inverse Kinematic Model.

6.3.3. Inverse Dynamic Model

Inverse dynamic model computes the nonlinear forces developed in the model and cancels these nonlinear forces. This inverse dynamic model requires that an exact mathematical model of the real mechanical system is known. Once these nonlinear terms are canceled, the remaining dynamics is linear, so it can be controlled with standard PI controller.

Inverse dynamic model of the system computes the torque that is to be applied on the pinion so that the pinion tracks the reference velocity profile designed for it. This reference velocity is computed in the inverse kinematics block. To facilitate this dynamic behavior, the reference velocity and reference position of the pinion is input to the system and the corresponding underactuated dynamics of gear body which is a function of the so-called desired behavior of pinion i.e. reference velocity and reference position and the gear velocity and position are computed. Thus, output of this block i.e. inverse dynamics block outputs the necessary torque that drives the system as desired.

This inverse dynamics has two subsystems which models the pinion and gear dynamics which are exactly the same copy the real physical system. Hence it may be reasoned that an exact knowledge of the system properties are essential when such a model is developed. This is especially important when it comes to the nonlinear term i.e. the nonlinear mesh stiffness function. Beside these two subsystem an additional subsystem models the sensor system that measures the acceleration, velocity, and position of the gear body.

The first subsystem is the dynamic model of the gear body. This subsystem is shown in Figure 6.6. The dynamic model of gear is composed of two sub blocks which model the damping e of gear teeth and the so-called mesh stiffness of gear teeth. The reader should note that mesh stiffness is calculated with ANSYS finite element program and the details of the finite element model is discussed in relevant chapter. Here, the results of that finite element model is just used in the discrete nonlinear spring constant model. Besides, these two blocks, additional external loads can enter the dynamic model of gear body via the manual switch included in the Simulink model. Note that in inverse dynamic model of the gear body, the pinion velocity and position are taken from the reference velocity profile which is determined at the start of simulation. This is a major difference between the inverse dynamic model and the real system model where the pinion acceleration, velocity and position are the result of the solution of nonlinear coupled differential equation set. This will be discussed later.

In Figure 6.7, the sub models of the gear dynamics are shown, the damping model is generated according to the relevant part of the gear dynamics equation given below inside rectangle:

$$J_1 \ddot{\theta}_1(t) + r_1 c_m (r_1 \dot{\theta}_1(t) - r_2 \dot{\theta}_2(t)) + r_1 k_m(t) [r_1 \theta_1(t) - r_2 \theta_2(t)] = T_1 \quad (6.1)$$

$$J_2 \ddot{\theta}_2(t) - \boxed{r_2 c_m (r_1 \dot{\theta}_1(t) - r_2 \dot{\theta}_2(t))} - r_2 k_m(t) [r_1 \theta_1(t) - r_2 \theta_2(t)] = T_2 \quad (6.2)$$

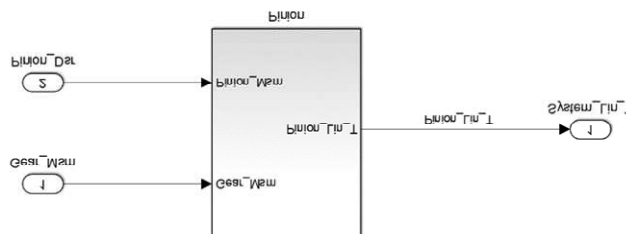


Figure 6.5: Inverse Dynamic Model.

The stiffness model, see Figure 6.7, is generated according to the relevant part of the gear dynamics equation given below:

$$J_1 \ddot{\theta}_1(t) + r_1 c_m (r_1 \dot{\theta}_1(t) - r_2 \dot{\theta}_2(t)) + r_1 k_m(t) [r_1 \theta_1(t) - r_2 \theta_2(t)] = T_1 \quad (6.3)$$

$$J_2\ddot{\theta}_2(t) - r_2c_m \left(r_1\dot{\theta}_1(t) - r_2\dot{\theta}_2(t) \right) - \boxed{r_2k_m(t)[r_1\theta_1(t) - r_2\theta_2(t)]} = T_2 \quad (6.4)$$

and the sensor model is developed by integration the acceleration of the gear body which is computed according to the formula given below. The acceleration model see Figure 6.6, is generated according to the relevant part of the gear dynamics equation given below:

$$J_1\ddot{\theta}_1(t) + r_1c_m \left(r_1\dot{\theta}_1(t) - r_2\dot{\theta}_2(t) \right) + r_1k_m(t)[r_1\theta_1(t) - r_2\theta_2(t)] = T_1 \quad (6.5)$$

$$\boxed{J_2\ddot{\theta}_2(t) - r_2c_m \left(r_1\dot{\theta}_1(t) - r_2\dot{\theta}_2(t) \right) - r_2k_m(t)[r_1\theta_1(t) - r_2\theta_2(t)]} = \boxed{T_2} \quad (6.6)$$

The second subsystem is the dynamic model of the pinion body. This subsystem is shown in Figure 6.8. The dynamic model of gear is composed of two sub blocks which model the damping effect of gear teeth and the so-called mesh stiffness of gear teeth.

In Figure 6.9, the sub models of the gear dynamics are shown, the damping model is generated according to the relevant part of gear dynamics equation given below inside rectangle:

$$J_1\ddot{\theta}_1(t) + \boxed{r_1c_m \left(r_1\dot{\theta}_1(t) - r_2\dot{\theta}_2(t) \right)} + r_1k_m(t)[r_1\theta_1(t) - r_2\theta_2(t)] = T_1 \quad (6.7)$$

$$J_2\ddot{\theta}_2(t) - r_2c_m \left(r_1\dot{\theta}_1(t) - r_2\dot{\theta}_2(t) \right) - r_2k_m(t)[r_1\theta_1(t) - r_2\theta_2(t)] = T_2 \quad (6.8)$$

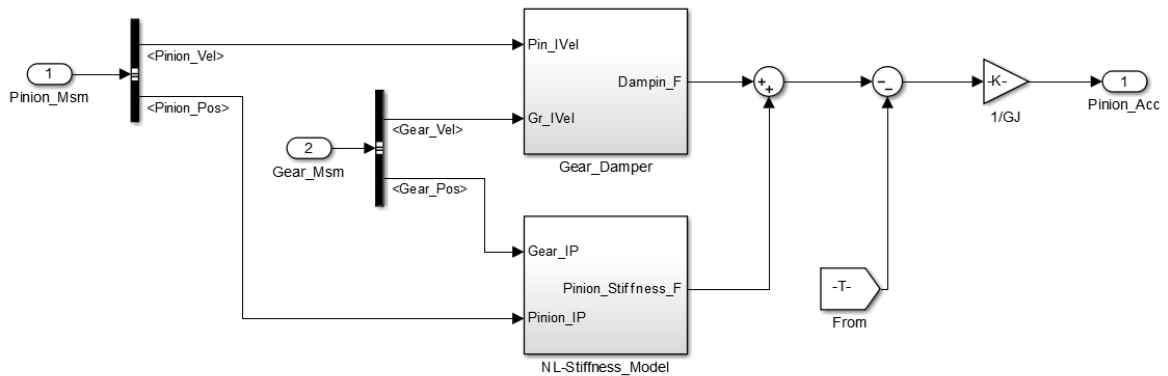


Figure 6.6: Inverse Dynamic Model: Gear Model.

The stiffness model, see Figure 6.9, is generated according to the relevant part of the gear dynamics equation given below inside rectangle:

$$J_1 \ddot{\theta}_1(t) + r_1 c_m (r_1 \dot{\theta}_1(t) - r_2 \dot{\theta}_2(t)) + \boxed{r_1 k_m(t) [r_1 \theta_1(t) - r_2 \theta_2(t)]} = T_1 \quad (6.9)$$

$$J_2 \ddot{\theta}_2(t) - r_2 c_m (r_1 \dot{\theta}_1(t) - r_2 \dot{\theta}_2(t)) - r_2 k_m(t) [r_1 \theta_1(t) - r_2 \theta_2(t)] = T_2 \quad (6.10)$$

and the sensor model is developed by integration the acceleration of the gear body which is computed according to the formula given below. The acceleration model see Figure 6.8, is generated according to the relevant part of the gear dynamics equation given below:

$$\boxed{J_1} \ddot{\theta}_1(t) + r_1 c_m (r_1 \dot{\theta}_1(t) - r_2 \dot{\theta}_2(t)) + r_1 k_m(t) [r_1 \theta_1(t) - r_2 \theta_2(t)] = \boxed{T_1} \quad (6.11)$$

$$J_2 \ddot{\theta}_2(t) - r_2 c_m (r_1 \dot{\theta}_1(t) - r_2 \dot{\theta}_2(t)) - r_2 k_m(t) [r_1 \theta_1(t) - r_2 \theta_2(t)] = T_2 \quad (6.12)$$

Note that input to the system has an extra term which is proportional to the desired acceleration term of the pinion.

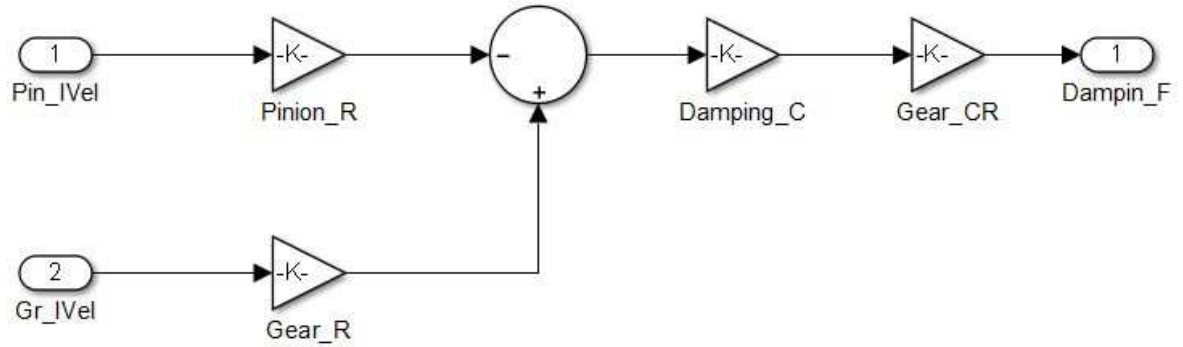
This additional torque will be in effect take place in the error dynamics and make the system to follow the reference velocity profile, the other part of the torque is computed such that it will cancel the nonlinearity in the real system model.

6.3.4. System Model: Nonlinear Spur Gear Pair Model

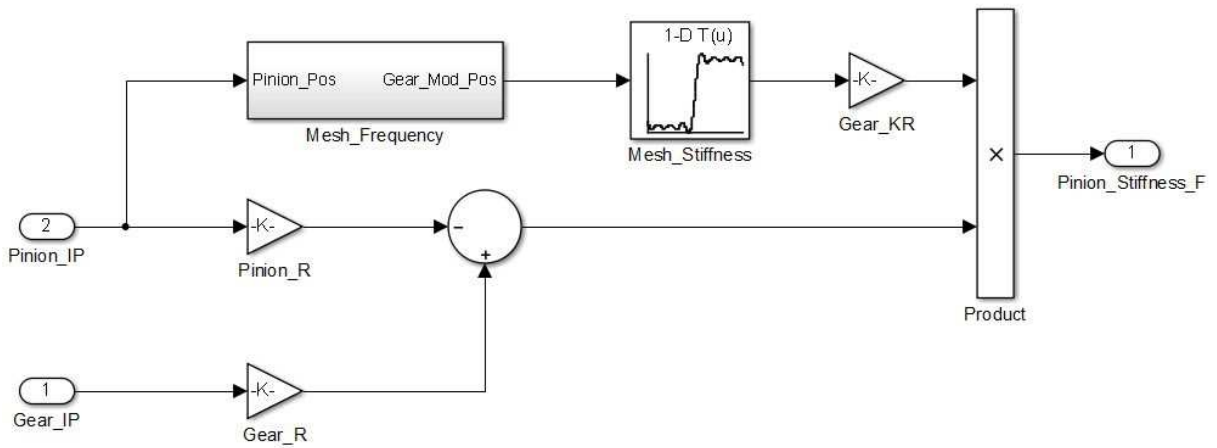
This system model, see Figure 6.10, represents the real physical system. The torque computed in previous steps is input to the system and it is expected that pinion will track the reference velocity profile and gear has a stable dynamic behavior at worst its response will be bounded. As the real system has two components which can be match with pinion and gear bodies. Since there is not any direct control on either pinion or gear acceleration, velocity and position. They will be the result of the solution of differential equation representing the real system model.

The first subsystem is the dynamic model of the pinion body. This subsystem is shown in Figure 6.11. The dynamic model of gear is composed of two sub blocks which model the damping effect of gear teeth and the so-called mesh stiffness of

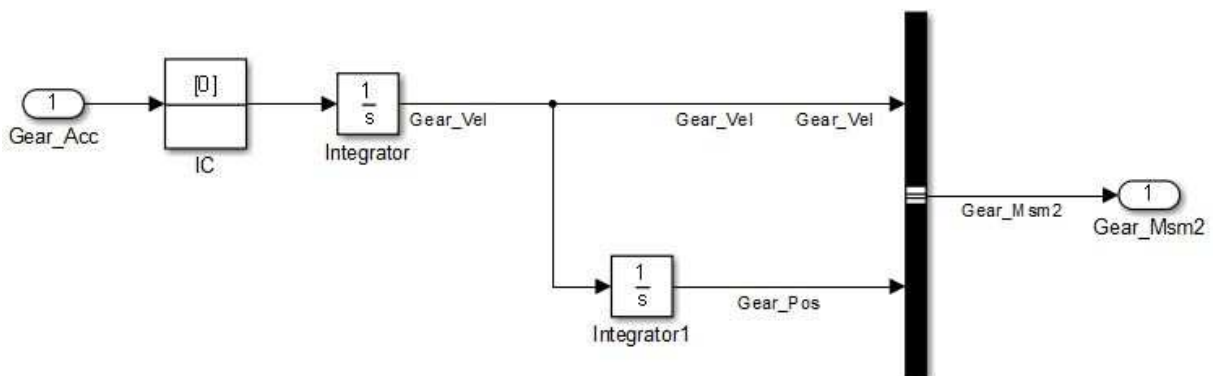
gear teeth. The reader should note that mesh stiffness is calculated with ANSYS finite element program and the details of the finite element model is discussed in relevant chapter.



Damper model



Nonlinear mesh stiffness model



Gear sensor model

Figure 6.7: Inverse Dynamic Model: Gear Damper/Stiffness Model.

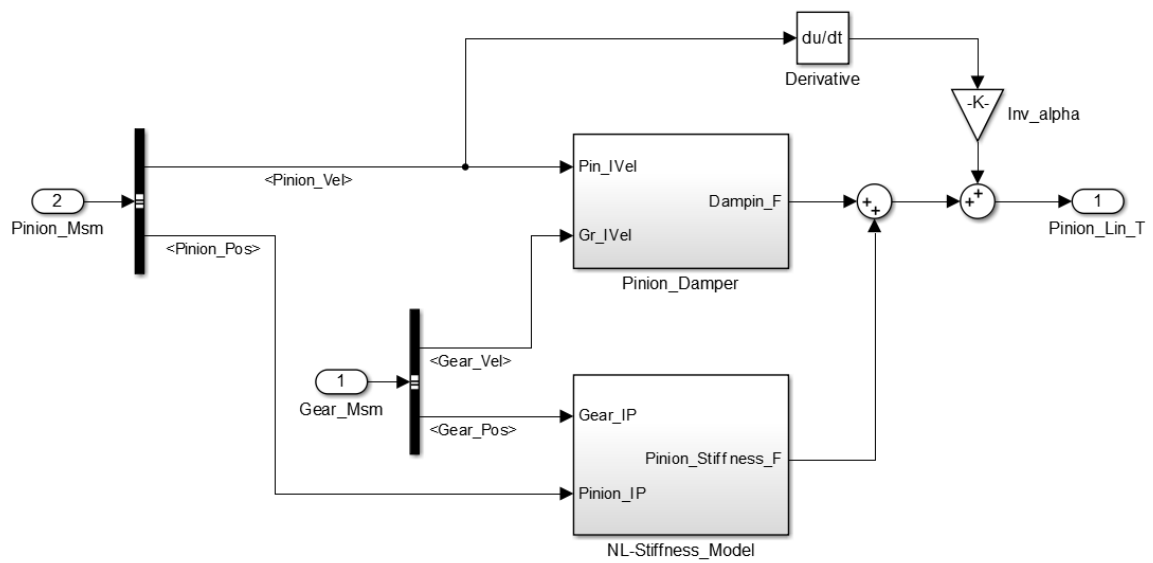


Figure 6.8: Inverse Dynamic Model: Pinion model.

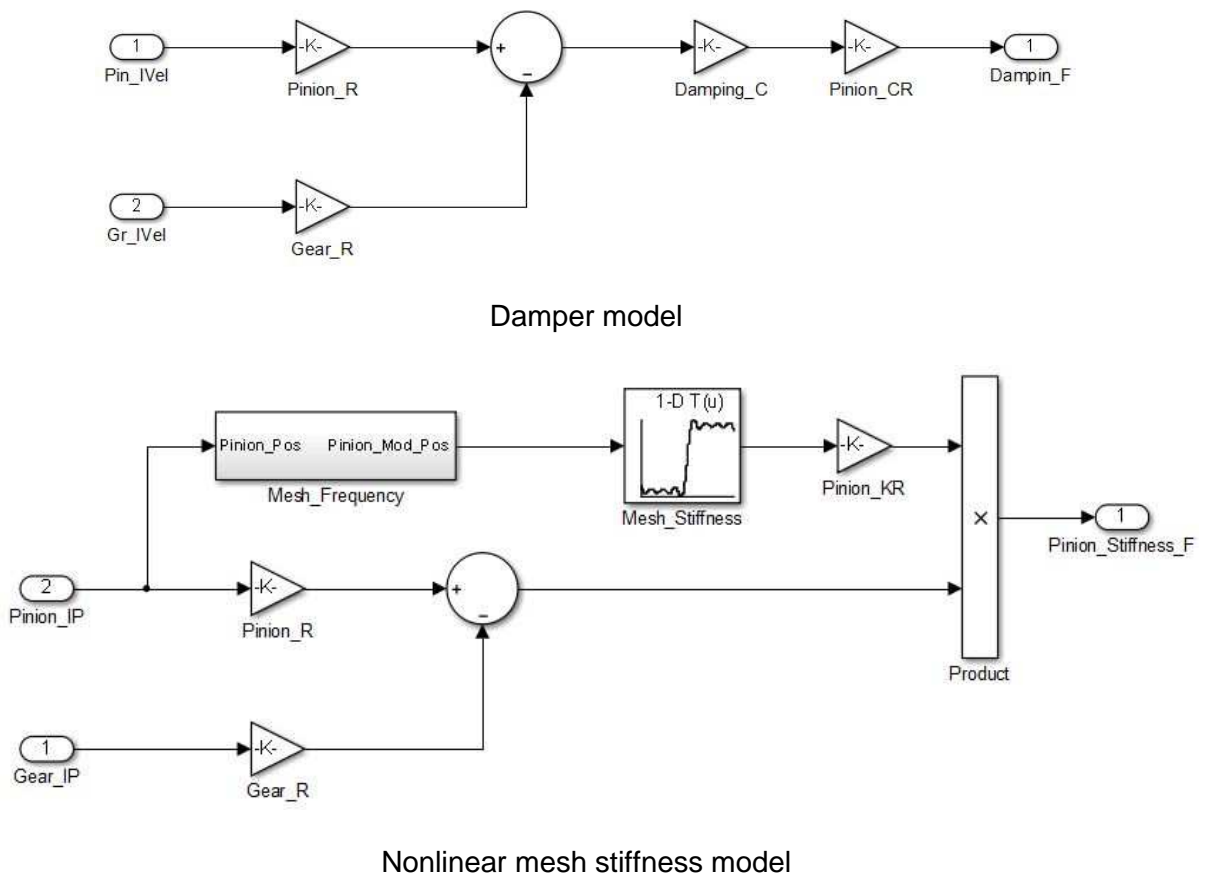


Figure 6.9: Inverse Dynamic Model: Pinion Damper/Stiffness Model.

In Figure 6.12, the sub models of the gear dynamics are shown, the damping model is generated according to the relevant part of the gear dynamics equation given below inside rectangle:

$$J_1 \ddot{\theta}_1(t) + \boxed{r_1 c_m (r_1 \dot{\theta}_1(t) - r_2 \dot{\theta}_2(t))} + r_1 k_m(t) [r_1 \theta_1(t) - r_2 \theta_2(t)] = T_1 \quad (6.13)$$

$$J_2 \ddot{\theta}_2(t) - r_2 c_m (r_1 \dot{\theta}_1(t) - r_2 \dot{\theta}_2(t)) - r_2 k_m(t) [r_1 \theta_1(t) - r_2 \theta_2(t)] = T_2 \quad (6.14)$$

The stiffness model, see Figure 6.12, is generated according to the relevant part of the gear dynamics equation given below:

$$J_1 \ddot{\theta}_1(t) + r_1 c_m (r_1 \dot{\theta}_1(t) - r_2 \dot{\theta}_2(t)) + \boxed{r_1 k_m(t) [r_1 \theta_1(t) - r_2 \theta_2(t)]} = T_1 \quad (6.15)$$

$$J_2 \ddot{\theta}_2(t) - r_2 c_m (r_1 \dot{\theta}_1(t) - r_2 \dot{\theta}_2(t)) - r_2 k_m(t) [r_1 \theta_1(t) - r_2 \theta_2(t)] = T_2 \quad (6.16)$$

and the sensor model is developed by integration the acceleration of the gear body which is computed according to the formula given below. The acceleration model see Figure 6.11, is generated according to the relevant part of the gear dynamics equation given below:

$$\boxed{J_1} \ddot{\theta}_1(t) + r_1 c_m (r_1 \dot{\theta}_1(t) - r_2 \dot{\theta}_2(t)) + r_1 k_m(t) [r_1 \theta_1(t) - r_2 \theta_2(t)] = \boxed{T_1} \quad (6.17)$$

$$J_2 \ddot{\theta}_2(t) - r_2 c_m (r_1 \dot{\theta}_1(t) - r_2 \dot{\theta}_2(t)) - r_2 k_m(t) [r_1 \theta_1(t) - r_2 \theta_2(t)] = T_2 \quad (6.18)$$

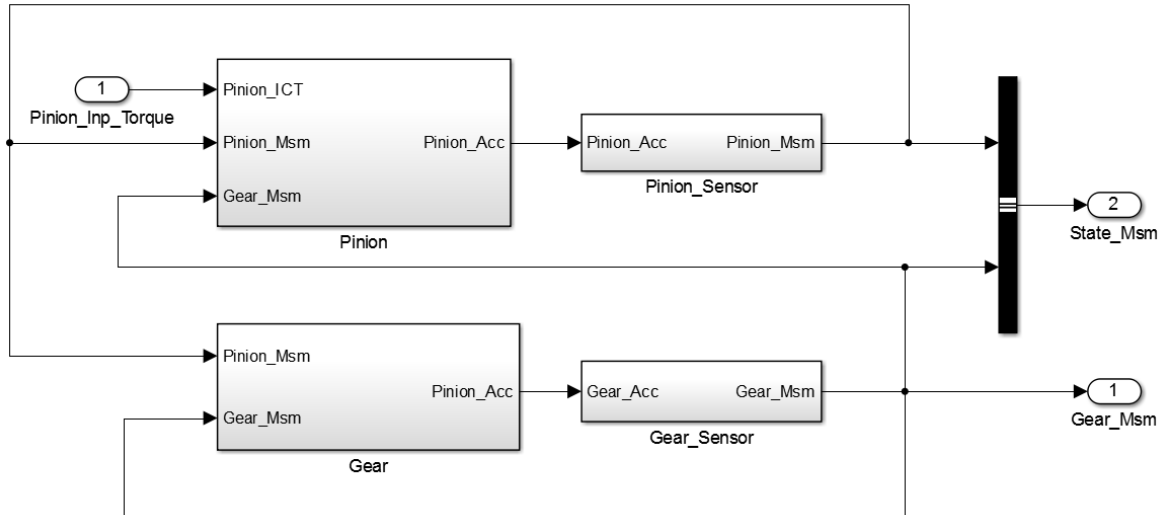


Figure 6.10: System Model.

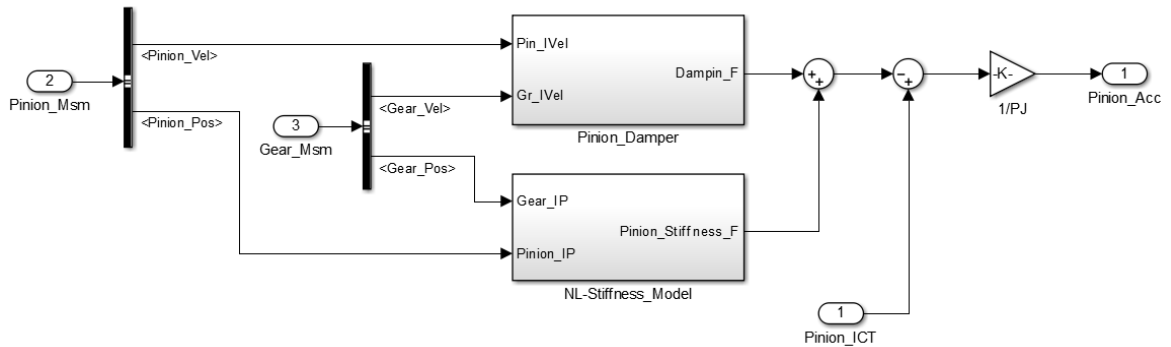


Figure 6.11: System Model: Pinion Model.

The second subsystem is the dynamic model of the gear body. This subsystem is shown in Figure 6.13. The dynamic model of gear is composed of two sub blocks which model the damping effect of gear teeth and the so-called mesh stiffness of gear teeth. In Figure 6.14, the sub models of the gear dynamics are shown, the damping model is generated according to the relevant part of the gear dynamics equation given below inside rectangle:

$$J_1 \ddot{\theta}_1(t) + r_1 c_m (r_1 \dot{\theta}_1(t) - r_2 \dot{\theta}_2(t)) + r_1 k_m(t) [r_1 \theta_1(t) - r_2 \theta_2(t)] = T_1 \quad (6.19)$$

$$J_2 \ddot{\theta}_2(t) - \boxed{r_2 c_m (r_1 \dot{\theta}_1(t) - r_2 \dot{\theta}_2(t))} - r_2 k_m(t) [r_1 \theta_1(t) - r_2 \theta_2(t)] = T_2 \quad (6.20)$$

The stiffness model, see Figure 6.14, is generated according to the relevant part of the gear dynamics equation given below inside rectangle:

$$J_1 \ddot{\theta}_1(t) + r_1 c_m (r_1 \dot{\theta}_1(t) - r_2 \dot{\theta}_2(t)) + r_1 k_m(t) [r_1 \theta_1(t) - r_2 \theta_2(t)] = T_1 \quad (6.21)$$

$$J_2 \ddot{\theta}_2(t) - r_2 c_m (r_1 \dot{\theta}_1(t) - r_2 \dot{\theta}_2(t)) - \boxed{r_2 k_m(t) [r_1 \theta_1(t) - r_2 \theta_2(t)]} = T_2 \quad (6.22)$$

and the sensor model is developed by integration the acceleration of the gear body which is computed according to the formula given below. The acceleration model see Figure 6.13, is generated according to the relevant part of the gear dynamics equation given below:

$$J_1 \ddot{\theta}_1(t) + r_1 c_m (r_1 \dot{\theta}_1(t) - r_2 \dot{\theta}_2(t)) + r_1 k_m(t) [r_1 \theta_1(t) - r_2 \theta_2(t)] = T_1 \quad (6.23)$$

$$\boxed{J_2} \ddot{\theta}_2(t) - r_2 c_m (r_1 \dot{\theta}_1(t) - r_2 \dot{\theta}_2(t)) - r_2 k_m(t) [r_1 \theta_1(t) - r_2 \theta_2(t)] = \boxed{T_2} \quad (6.24)$$

Gear and pinion sensor models are just the integration of the corresponding acceleration terms. These are given in Figure 6.12 and Figure 6.14

6.3.5. Error Dynamics: PI Controller

After the nonlinearity due to gear mesh stiffness is canceled by the inverse dynamics model, the resulting dynamics is linear in the state vector of the system model. Indeed, there is two uncoupled dynamics of mass systems. To control these two masses and force their response to approach zero exponentially the PI controller given in Figure 6.15 is used. This PI controller closes the feedback loop. The block that models the PI controller is given in Figure 6.16.

6.4. Conclusion

In this chapter, the MATLAB Simulink model is introduced and described. Relevant part of the Simulink model is associated with dynamic model of a spur gear pair which is discussed in the theory chapter. This MATLAB Simulink model is used to make several simulations and investigate the characteristics of the system under the guidance of the nonlinear controller. The reader should note that the system is underactuated and there is a control on the pinion, on the contrary there is no direct control on the gear dynamic. The gear dynamic can only be controlled by the second-order term i.e. acceleration of the pinion. It should be pointed to this fact: this complicates the problem in great deal. In addition, the nonlinear spring effect of

the gear teeth add up to this complexity. Finally, in all these models, it is assumed that the controller has full access to the system parameters and state vectors. In some situation this condition is considered to be quite severe.

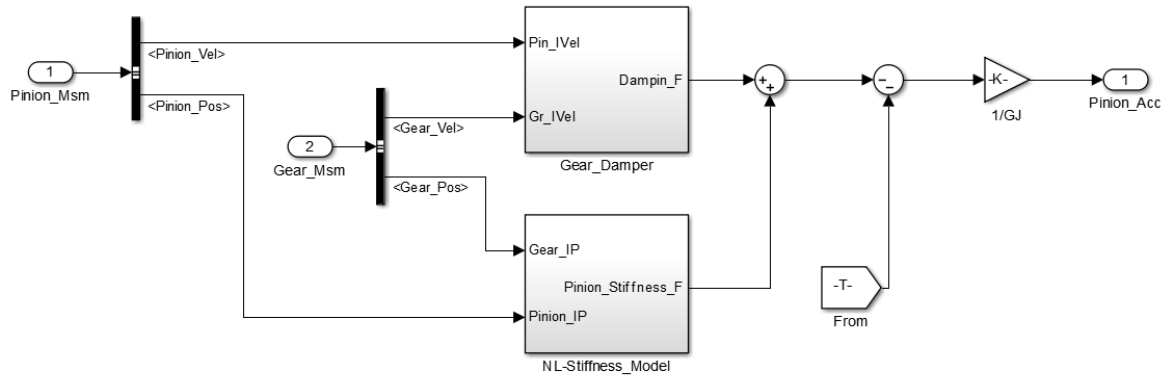
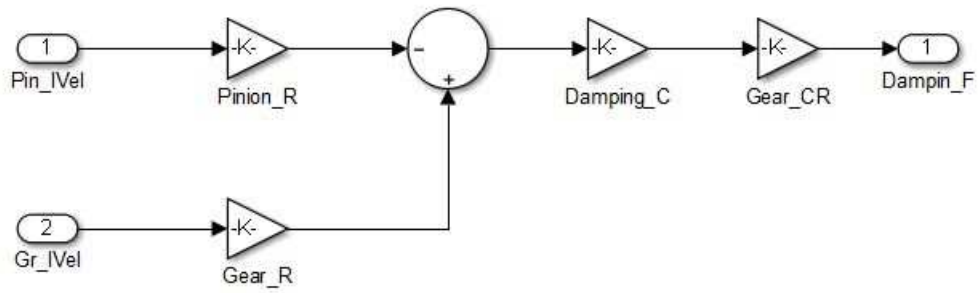
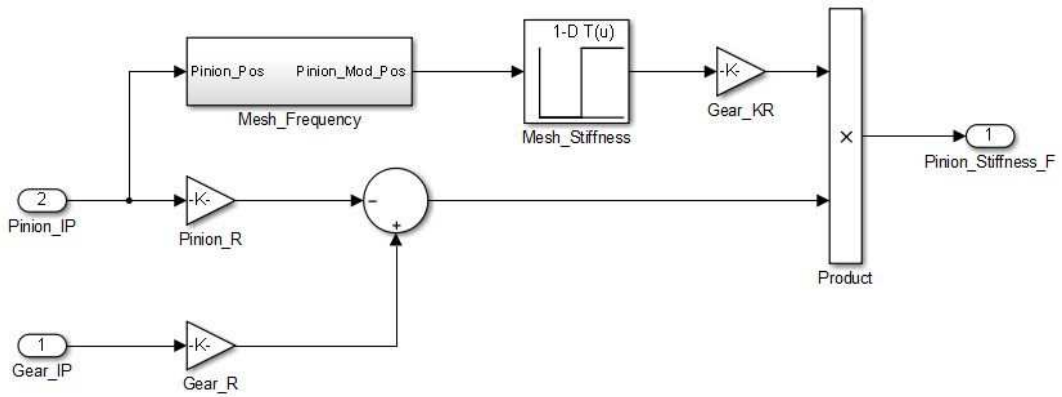


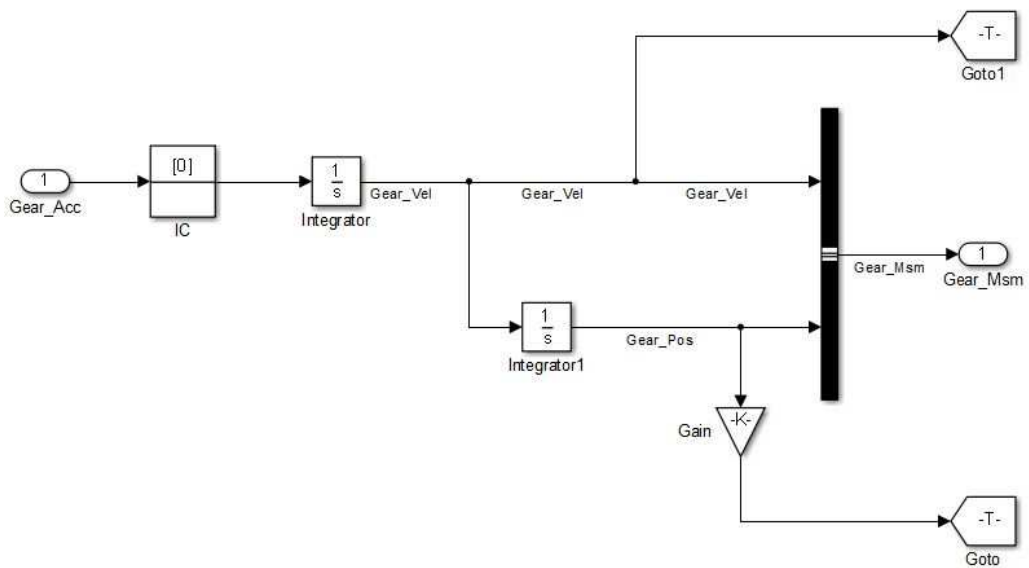
Figure 6.12: System Model: Gear Model.



Damper model



Mesh stiffness model



Gear sensor model

Figure 6.13: System Model: Gear Damper/Stiffness/Sensor Model.

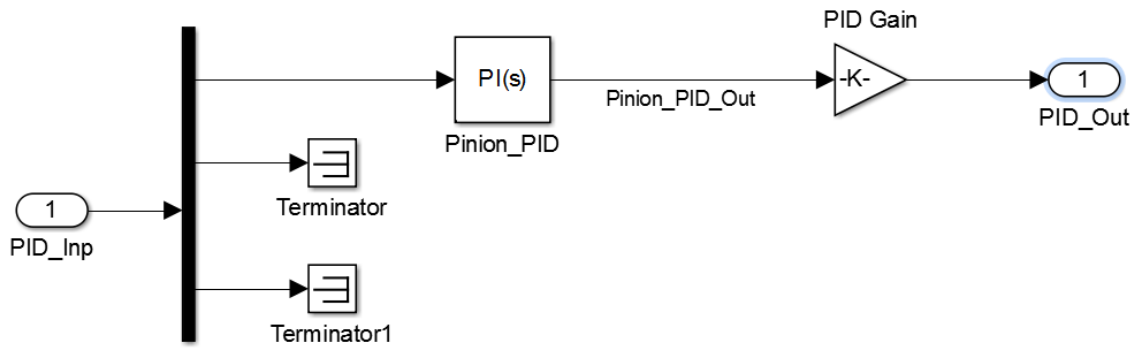


Figure 6.14: Error Dynamics.

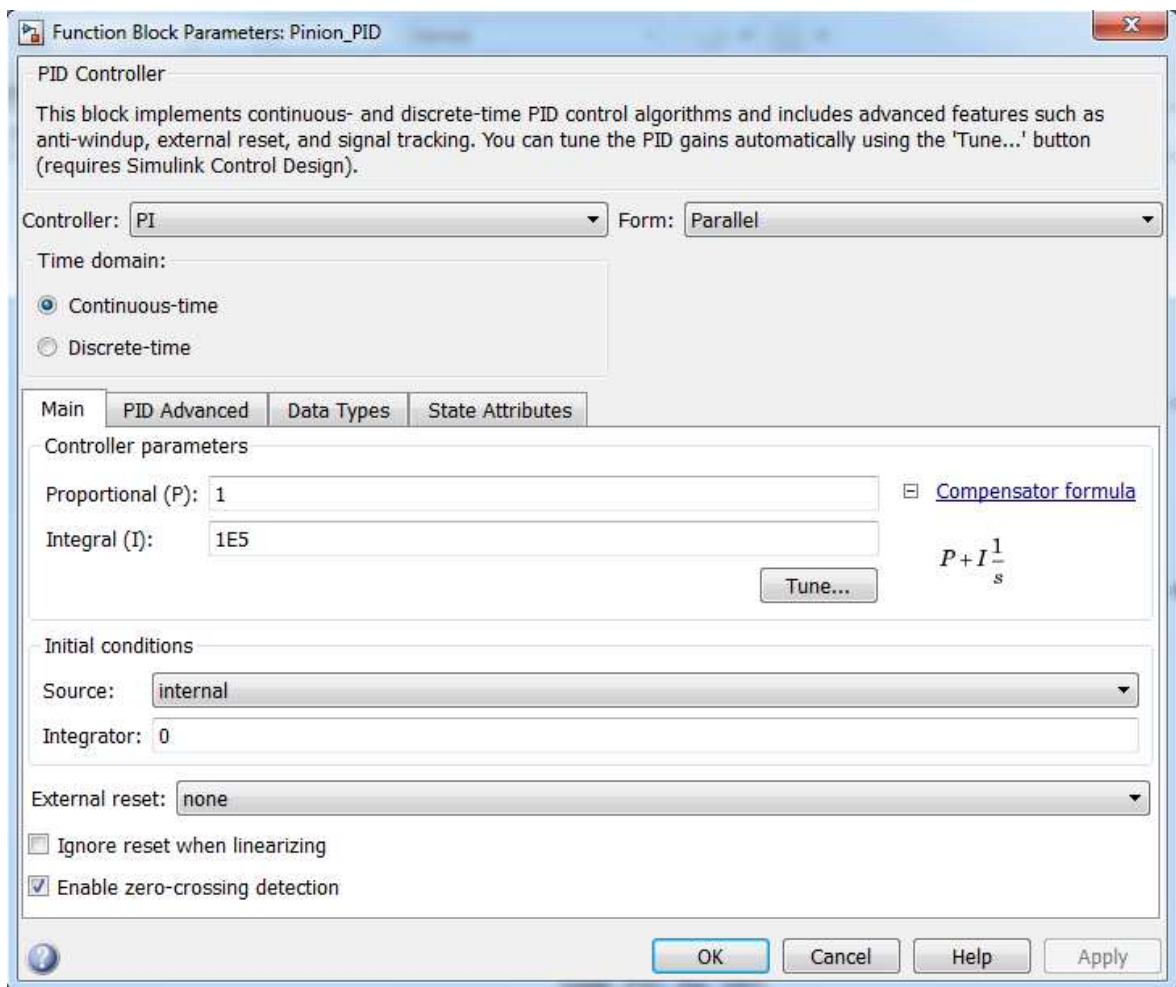


Figure 6.15: Error Dynamics: PI Controller.

CHAPTER 7

Results: Simulations

7.1. Introduction

In this chapter, MATLAB Simulink model that has been introduced previously, is used to simulate a pair of spur gear under the guidance of a nonlinear controller which has been designed for an underactuated system. This nonlinear controller makes use of an inverse model of the system and it uses this model to cancel the nonlinear terms of the differential equations of motions of a spur gear pair. It was made clear that this nonlinearity stems from the nonlinear mesh stiffness. This nonlinearity is due to the change in the number of that comes into contact as the gears rotate. This nonlinear stiffness term was computed by ANSYS finite element software and inserted into the Simulink model. It is obvious that the success rate this so-called nonlinear controller depends on the quality of the knowledge of this nonlinear stiffness term. Despite the fact that this is a hard constraint on the development of such a controller, it is not far from being realistic, because every gear pair can be analyzed by a software and furthermore the information pertaining the starting position of gears can be tracked easily for instance with an absolute encoders.

Under these premises, the main goal of this chapter is not only to validate the spur gear model and the success rate of the so-called nonlinear controller for an underactuated system, but also to investigate the robustness of such a controller under uncertain conditions e.g. uncertainty in the knowledge of the nonlinear stiffness term, unexpected loading conditions on the output shaft. These events has been simulated by a number of scenarios. The representation of the nonlinear mesh stiffness is also the subject of several simulations. In the first place the Fast Fourier Transform (FFT) of the nonlinear periodic mesh stiffness is computed to see the contributions of its harmonics. Then, many simulations are made to observe the effect of the number of harmonics on the control of a gear pair.

This chapter contain: In section one, an introduction to the chapter is made. In section two, a strategy is developed for the simulations. In section three, simulations are made and the results are presented in systematic way. In section four, a critical review of the simulation results is made and the downside of the method is exposed.

This critical review will shed light on the future works. In section five, conclusions are given and this marks the end of this chapter.

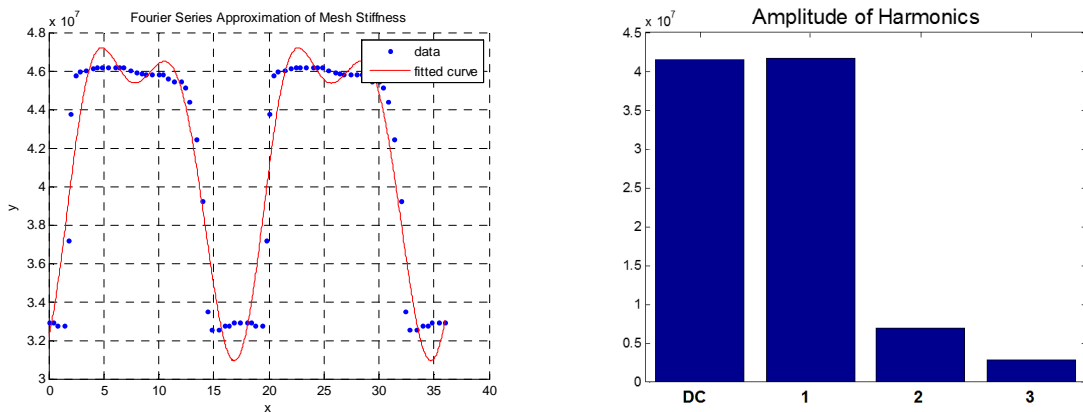


Figure 7.1. Mesh Stiffness Curve with Three FFT Harmonics.

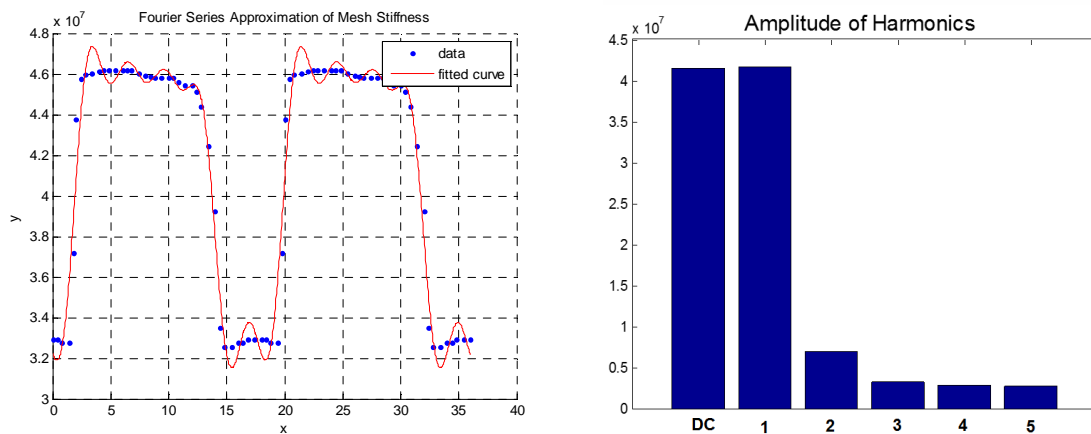


Figure 7.2. Mesh Stiffness Curve with Five FFT Harmonics.

7.2. A Strategy for Simulations

7.2.1. Case Study-1

In this case, a naive model is simulated and the success rate of nonlinear controller is investigated. Thus, nonlinear spring term takes a smooth shape and the sudden jump in the curve is less pronounced. Further velocity and acceleration curves, is investigated, in the first place. Below, in Table 7.1, parameters of such a system is given. Loading conditions and acceleration profile are given in Figure 7.3 and 7.4, respectively. The parameters of the gears can be found in Table 4.2, Case 1 and the associated mesh stiffness is given in Figures 4.12. Table 7.1 presents data

associated to the dynamics of MATLAB Simulink model like loading condition and acceleration curve that is to be followed by the pinion and gear.

Table 7.1. Data related to MATLAB Simulink Model-1

| | |
|--|--------------------------|
| MATLAB Simulink Model Identity | MI_PID_FFT_UA_SG_v00.slx |
| MATLAB Mesh Stiffness Data File Identity | DF_m1_N1_20_N2_40_Ansys |
| ANSYS Finite Element Model Identity | ANSYS- m1_N1-20_N2-40 |
| Geometry of Gears | See Table 4.2 (Case 1) |
| Gear Loading type | Constant load |
| Loading Curve | See Figure 7.3 |
| Acceleration Curve | See Figure 7.4 |
| Mesh Stiffness Curve | See Figure 4.12 |
| Mesh Stiffness Data (System Model) | Raw Data |
| Mesh Stiffness Data (Inverse Model) | Raw Data |
| Nonlinear Controller Type | Model Inversion |
| PID Setting (Kp, Ki,Kd) | (100,5,80) |
| Simulation Time Span | 15 sec |

In this simulations, it was assumed that the output gear is loaded with a constant torque of value 20 N/m (Figure 7.3) and the acceleration curve that is to be tracked by the pinion is given in Figure 7.4. Note that this acceleration curve is amplified by a constant of 200. Hence, the dynamic effects are quite effective and it is expected that it would have a major effect on the transmission error curve and the velocity curve of pinion and gear.

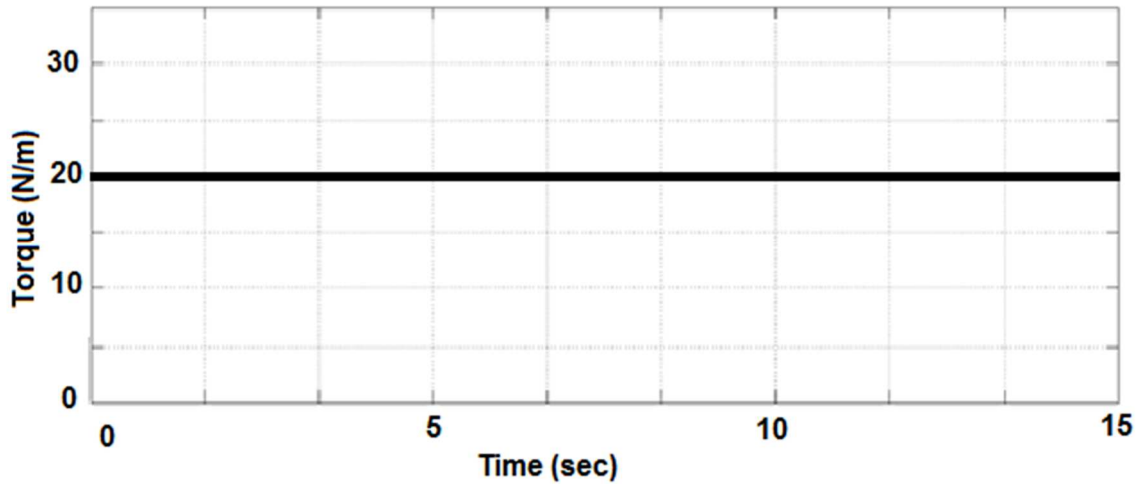


Figure 7.3. Loading Curve.

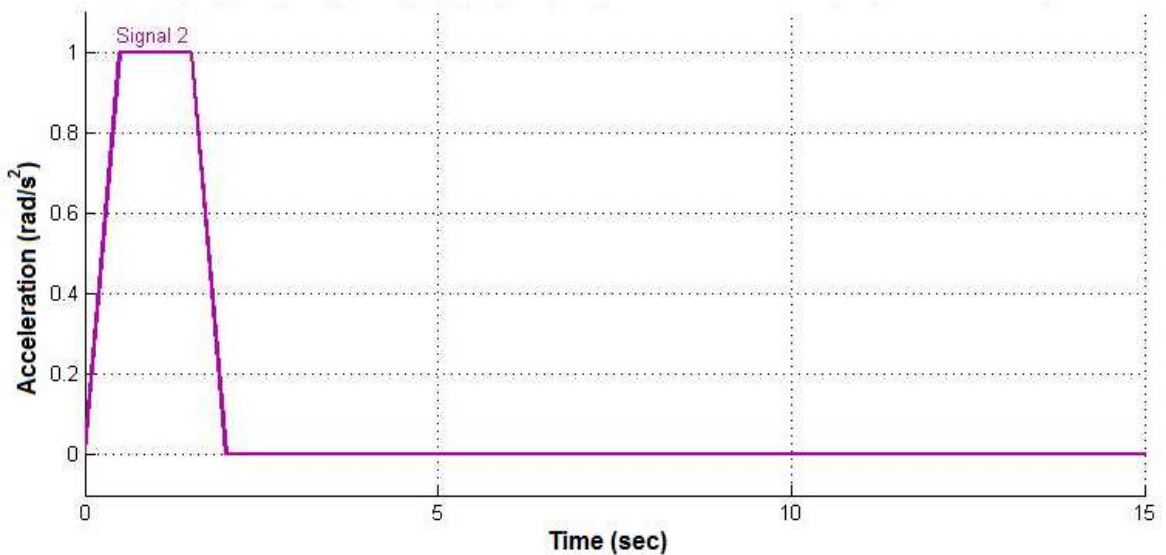


Figure 7.4. Acceleration Curve.

7.2.2. Case Study-2

Here, a naive model is simulated and the success rate of nonlinear controller is investigated. Thus, nonlinear spring term takes a smooth shape and the sudden jump in the curve is less pronounced. Further velocity and acceleration curves, is investigated, in the first place. Below, in Table 7.2, parameters of such a system is given. Loading conditions and Acceleration profile are given in Figure 7.5 and Figure 7.6, respectively. The output gear is loaded with a sinus wave function variable torque. The parameters of the gears can be found in Table 4.2, Cases 1 and the associated mesh stiffness is given in Figures 4.12. Table 7.2 presents data

associated to the dynamics of MATLAB Simulink model like loading condition and acceleration curve that is to be followed by the pinion and gear.

In this simulations, it was assumed that the output gear is loaded with a sinusoidal variable torque witch varies between 19 and 21 N/m (Figure 7.5), and the acceleration curve that is to be tracked by the pinion is given in Figure 7.6. Note that this acceleration curve is amplified by a constant of 200 too.

Table 7.2. Data related to MATLAB Simulink Model-2

| | |
|--|--------------------------------|
| MATLAB Simulink Model Identity | MI_PID_FFT_MeshK_UA_SG_v00.slx |
| MATLAB Mesh Stiffness Data File Identity | DF_m1_N1_20_N2_40_Ansys |
| ANSYS Finite Element Model Identity | ANSYS- m1_N1-20_N2-40 |
| Geometry of Gears | See Table 4.2 (Case 1) |
| Gear Loading type | Sinus wave function |
| Loading Curve | See Figure 7.5 |
| Acceleration Curve | See Figure 7.6 |
| Mesh Stiffness Curve | See Figure 4.12 |
| Mesh Stiffness Data (System Model) | Raw Data |
| Mesh Stiffness Data (Inverse Model) | Raw Data |
| Nonlinear Controller Type | Model Inversion |
| PID Setting (Kp, Ki, Kd) | (100,5,80) |
| Simulation Time Span | 15 sec |

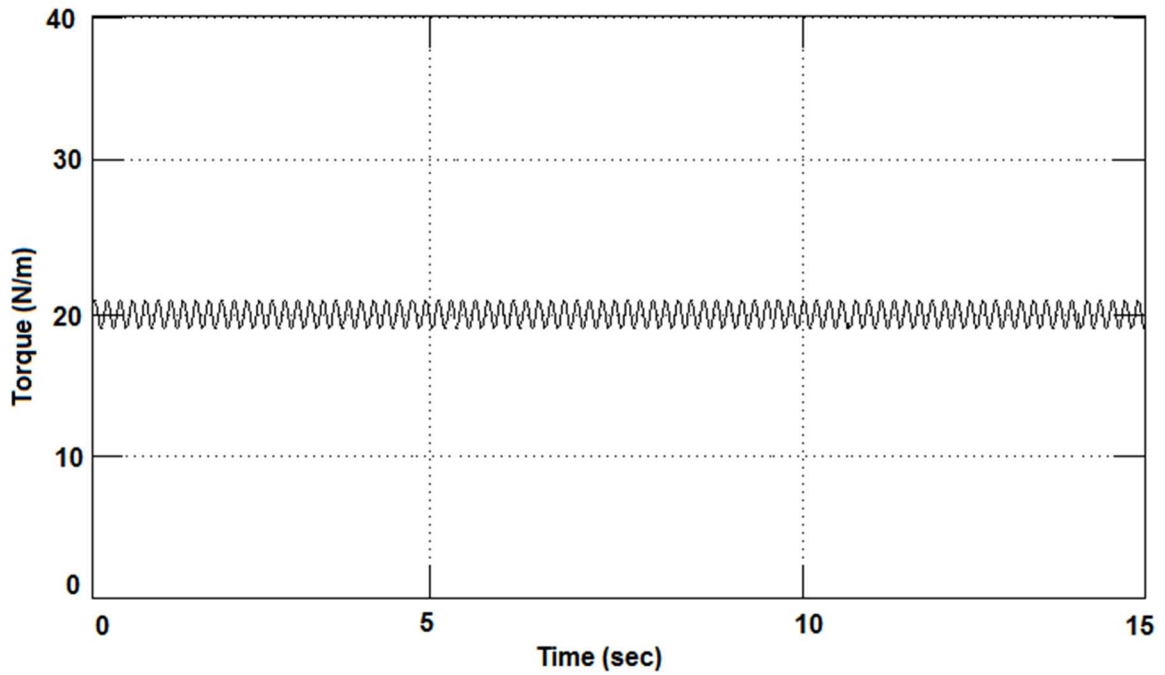


Figure 7.5. Loading Curve.

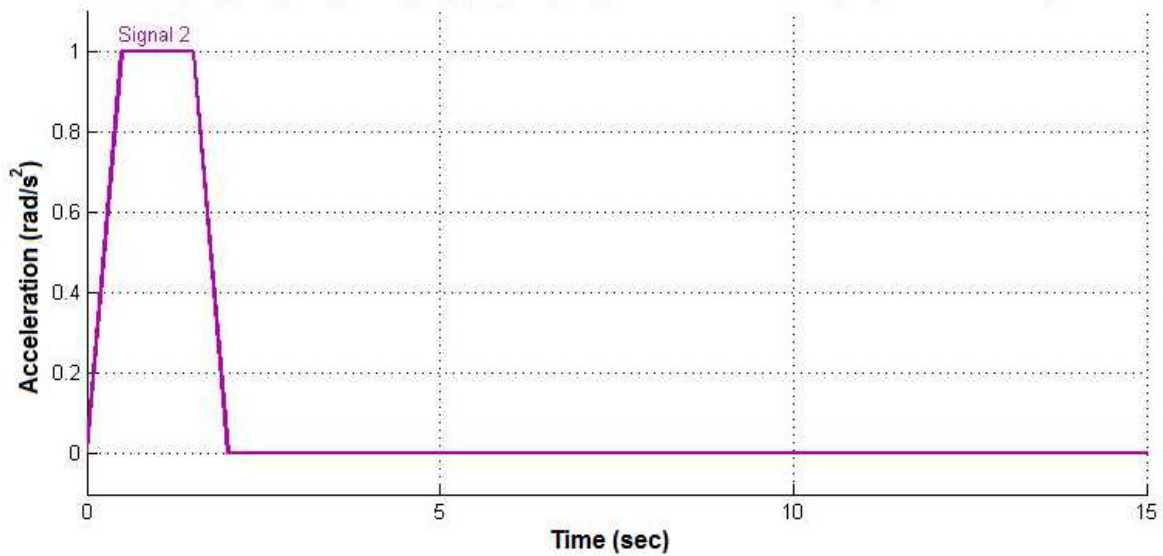


Figure 7.6. Acceleration Curve.

7.2.3. Case Study-3

In this case, a naive model is simulated and the success rate of nonlinear controller is investigated. Thus, nonlinear spring term takes a smooth shape and the sudden jump in the curve is less pronounced. Further velocity and acceleration curves, is investigated, in the first place. Below, in Table 7.3, parameters of such a system is given. Loading conditions and Acceleration profile are given in Figure 7.7 and Figure 7.8, respectively. The output gear is loaded with a random variable torque. The

parameters of the gears can be found in Table 4.2, Cases 1 and the associated mesh stiffness is given in Figures 4.12. Table 7.3 presents data associated to the dynamics of MATLAB Simulink model like loading condition and acceleration curve that is to be followed by the pinion and gear.

In this simulations, it was assumed that the output gear is loaded with random torque value witch varies between 19 and 21 N/m (Figure 7.7) and the acceleration curve that is to be tracked by the pinion is given in Figure 7.8. Note that this acceleration curve is amplified by a constant of 200 too.

Table 7.3. Data related to MATLAB Simulink Model-3

| | |
|--|----------------------------|
| MATLAB Simulink Model Identity | MI_PID_MeshK_UA_SG_v00.slx |
| MATLAB Mesh Stiffness Data File Identity | DF_m1_N1_20_N2_40_Ansys |
| ANSYS Finite Element Model Identity | ANSYS- m1_N1-20_N2-40 |
| Geometry of Gears | See Table 4.2 (Case 1) |
| Gear Loading type | Random value |
| Loading Curve | See Figure 7.7 |
| Acceleration Curve | See Figure 7.7 |
| Mesh Stiffness Curve | See Figure 4.12 |
| Mesh Stiffness Data (System Model) | Raw Data |
| Mesh Stiffness Data (Inverse Model) | Raw Data |
| Nonlinear Controller Type | Model Inversion |
| PID Setting (Kp, Ki,Kd) | (100,5,80) |
| Simulation Time Span | 15 sec |

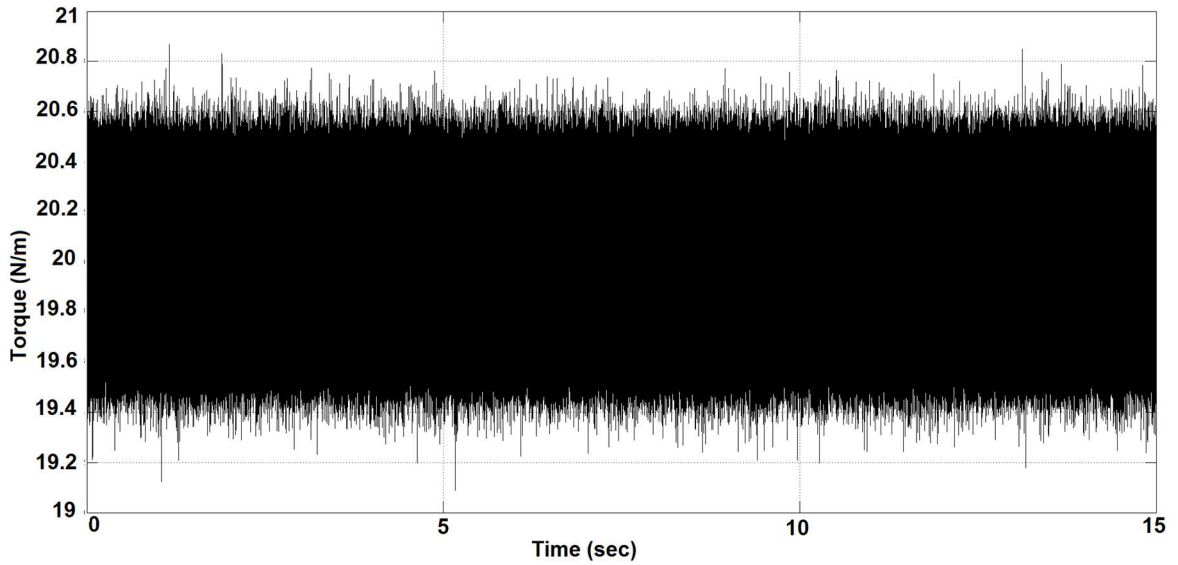


Figure 7.7. Loading Curve.

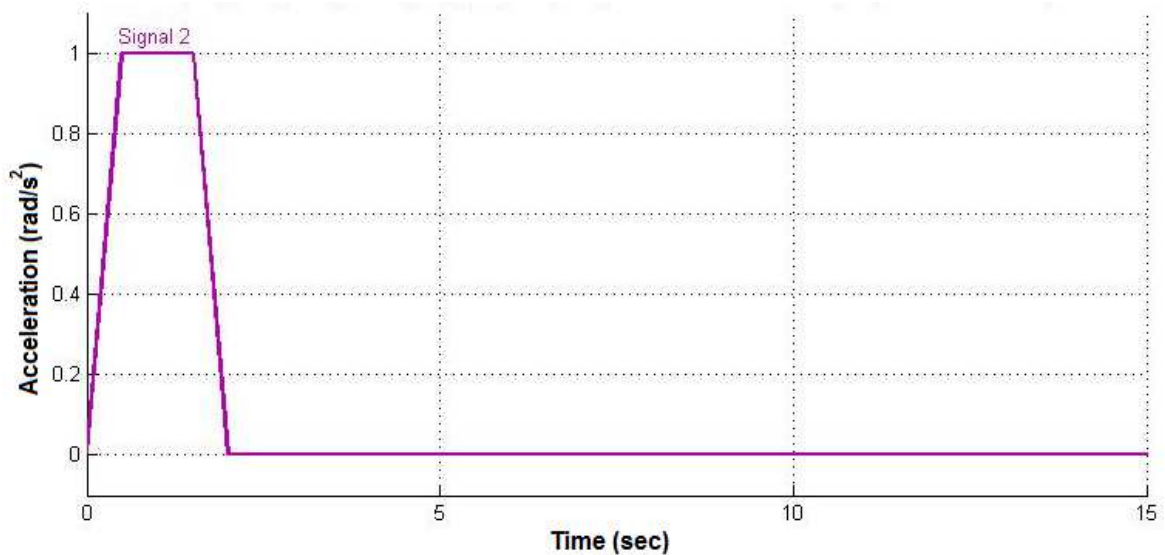


Figure 7.8. Acceleration Curve.

7.3. Simulation Results

At this stage of the work, transmission error which shown in Figure 7.9, 7.17 and 7.25 will be regulated. According to information of Table 7.1, 7.2 and 7.3, Mesh Stiffness Data System Model will enter controller as raw data. Also, Mesh Stiffness Data Inverse Model will enter controller as raw data. The result of this simulations can be seen in Figures 7.9- 7.32. It is seen that during acceleration period, transmission error curve is affected adversely. Then, it settles around a constant negative value and oscillates about that value. These high frequency oscillations are due to the change in mesh stiffness. Input torque, also has a special trend which

is due the acceleration curve imposed on the pinion speed. High frequency oscillations exist as the nonlinear controller tries to cancel nonlinear forces due to change in mesh stiffness, (see Figure 7.11, 7.19 and 7.27). Figure 7.11, 7.19 and 7.27 clearly displays the acceleration curve of pinion; Since acceleration curve has been tracked successfully, as it was expected, a smooth velocity curve of pinion has been obtained. These figures, (Figure 7.9, 7.17 and 7.25) show that nonlinear controller can control an underactuated power transmission systems after a few second, e.g. gear mechanism with elastic deformation.

For the problem at hand, since the torque applied on the pinion is controlled, only the states associated with pinion can be regulated. States which are associated with gear are the underactuated part of the dynamical system and their characteristics are determined by internal dynamics. At best, it is expected to have bounded-response is obtained, whereas Figure 7.14, 7.15, 7.22, 7.23, 7.30, and 7.31 demonstrates that velocity curve has been tracked accurately.

In general the following conclusions are drawn: in a typical underactuated mechanism, it is only possible that the states associated with the actuated part are controllable, dynamics of states associated with unactuated parts, are driven by internal dynamics. If nonlinear systems are compared, it can be said that actuated part of nonlinear system match with the controllable part of a linear system and unactuated part of nonlinear system with stable internal dynamics match with the uncontrollable but stabilizable part of linear systems. Therefore, in general, one expects that unactuated part of a nonlinear system having an internal dynamics at best have an asymptotically stable or bounded behavior. In the worst case, the unactuated part of a system has an unstable internal dynamics and states associated with unactuated part are uncontrollable e.g. states goes to infinity as time proceeds.

When a pair of spur gear is analyzed, it is seen that the internal dynamic is stable, however, acceleration curve is not asymptotically stable but has got bounded-response. On the other hand, states of pinion can be controlled precisely. This observation has already been confirmed by simulations.

To simulate these three case study the solver set to ode4 (Runge-Kutta) method, fixed-step size type, by size 1×10^{-6} second.

7.3.1. Result of Case Study-1

The result of simulation of case 1 can be seen in Figures 7.9 to 7.16. In Figure 7.9, it is seen that in the starting times of motion when Transmission error is about 0.4×10^{-4} radian and this value in 10th second is 0.005×10^{-4} radian and in 15th second is about 0.001×10^{-4} radian.

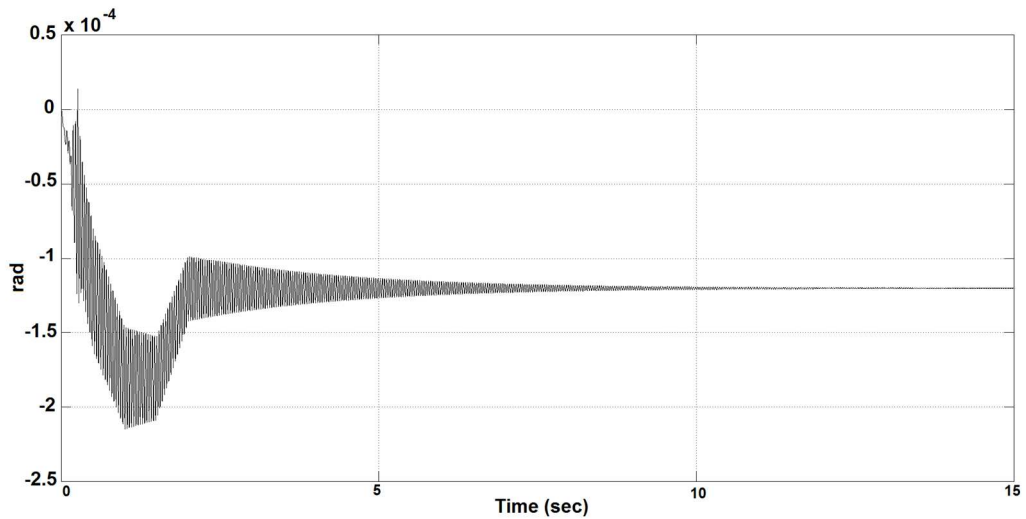


Figure 7.9. Transmission Error.

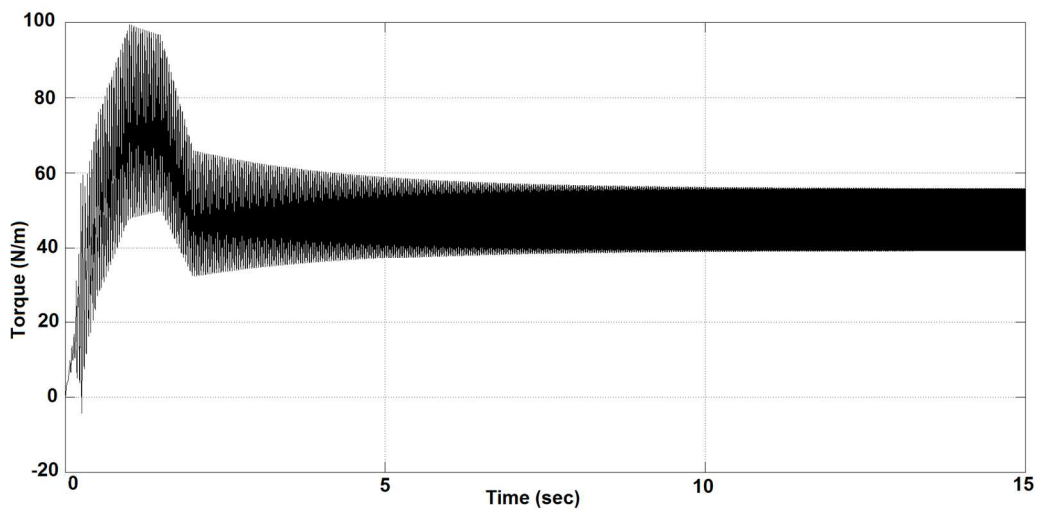


Figure 7.10. Input Torque.

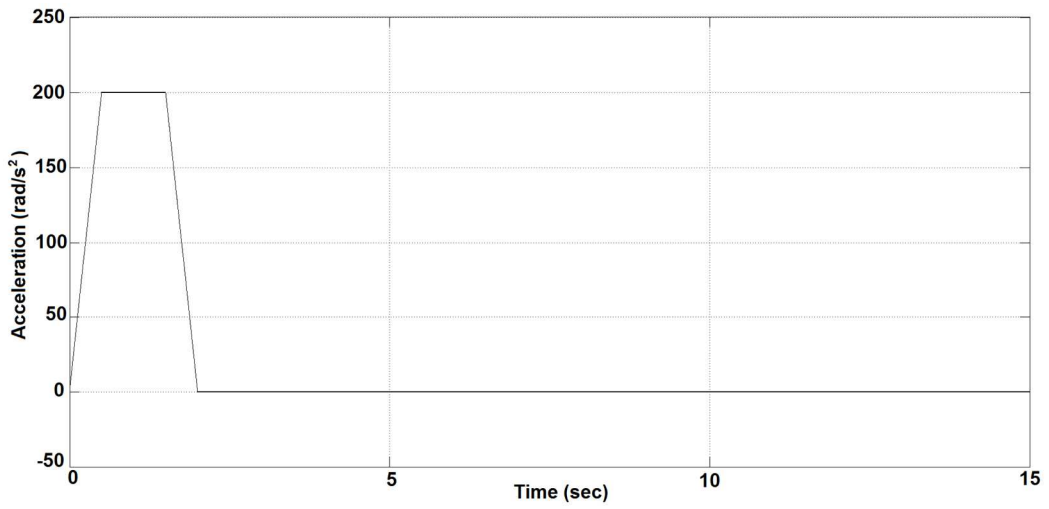


Figure 7.11. Acceleration Curve of Pinion.

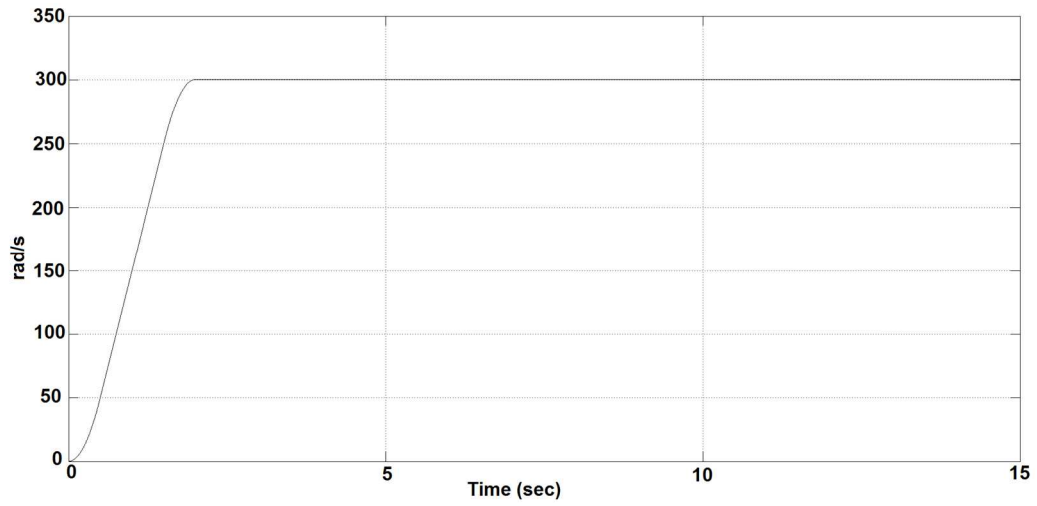


Figure 7.12. Velocity Curve of Pinion.

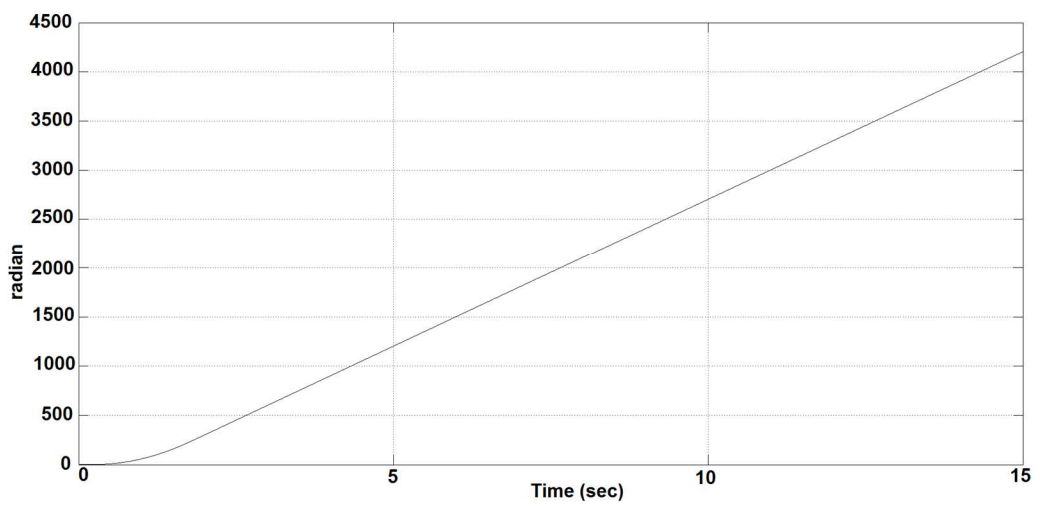


Figure 7.13. Position Curve of Pinion.

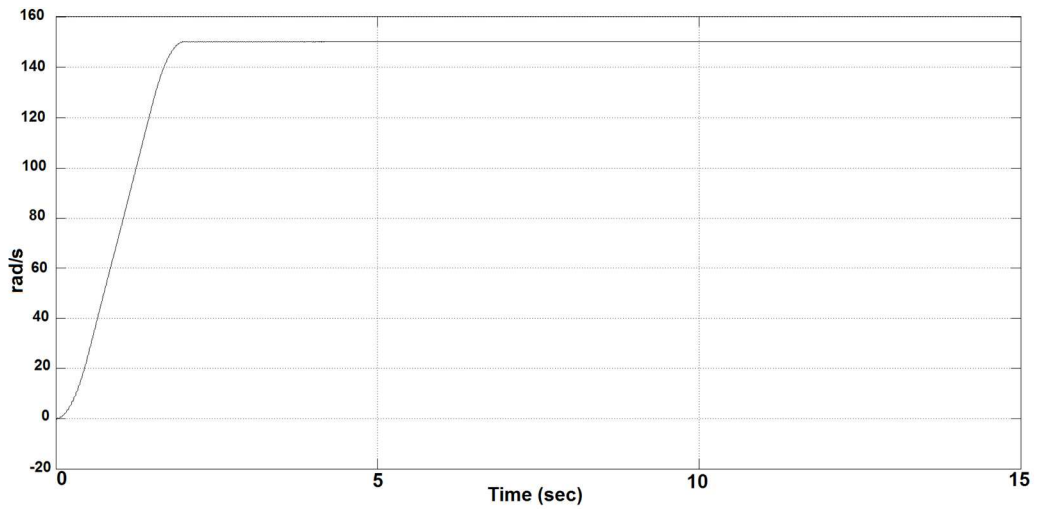


Figure 7.14. Velocity Curve of Gear.

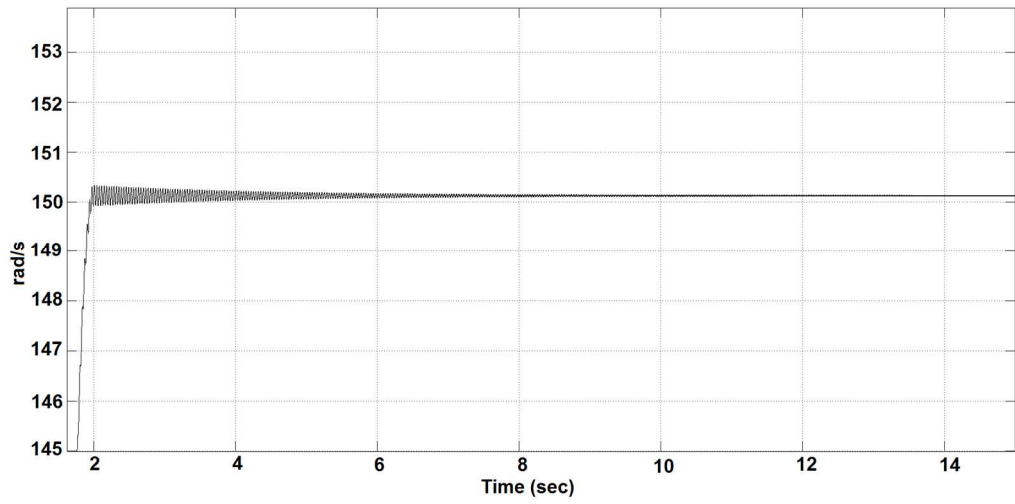


Figure 7.15. A Close Look at Velocity Curve of Gear.

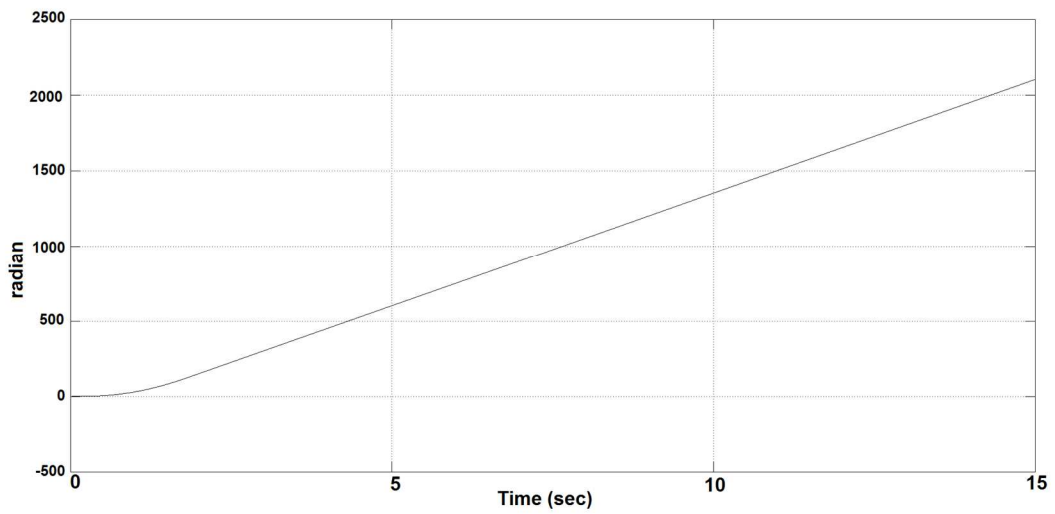


Figure 7.16. Position Curve of Gear.

7.3.2. Result of Case Study-2

The result of simulation of case 2 can be seen in Figures 7.17 to 7.24. In Figure 7.9, it is seen that in the starting times of motion when Transmission error is about 0.3×10^{-4} radian and this value in 10th second is 0.01×10^{-4} radian and in 15th second is about 0.002×10^{-4} radian.

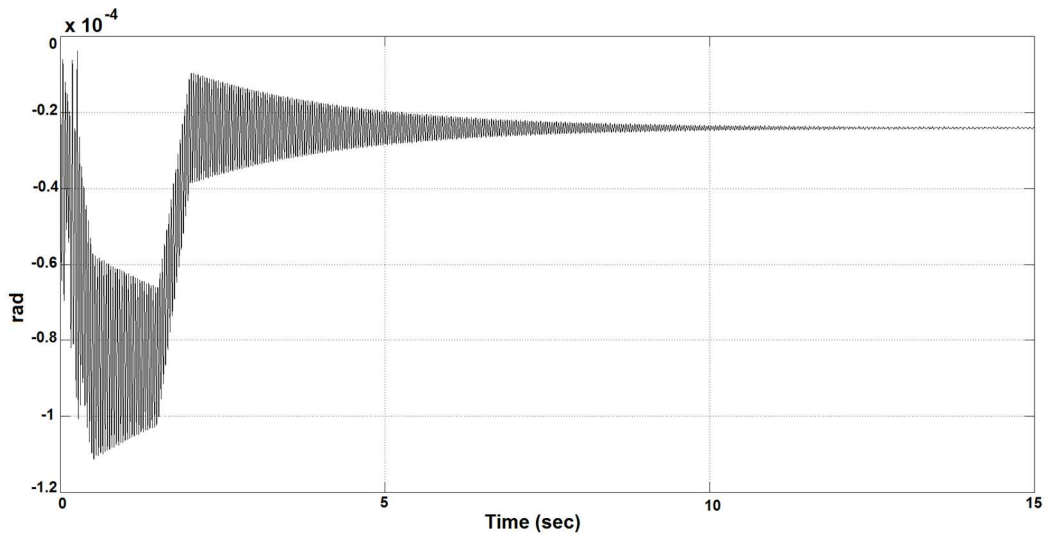


Figure 7.17. Transmission Error.

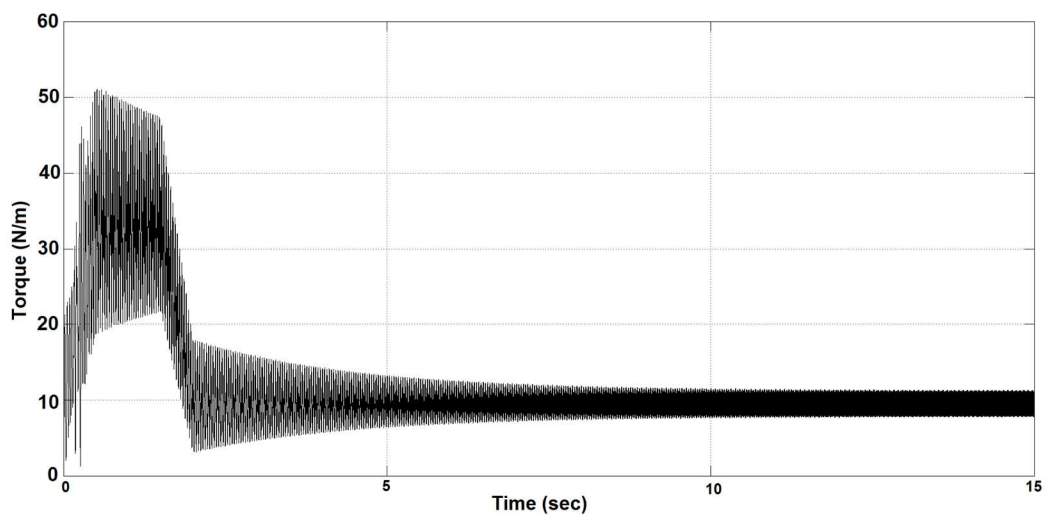


Figure 7.18. Input Torque.

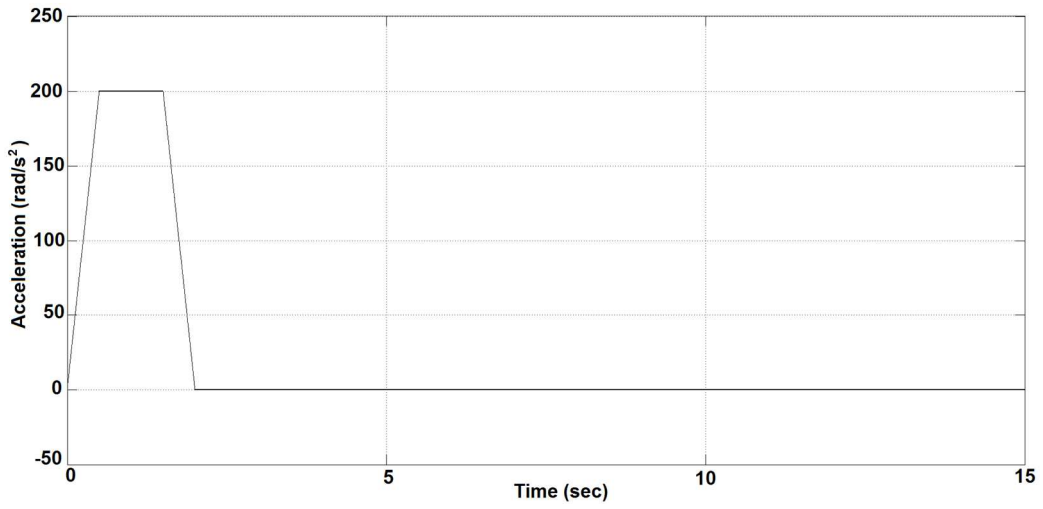


Figure 7.19. Acceleration Curve of Pinion.

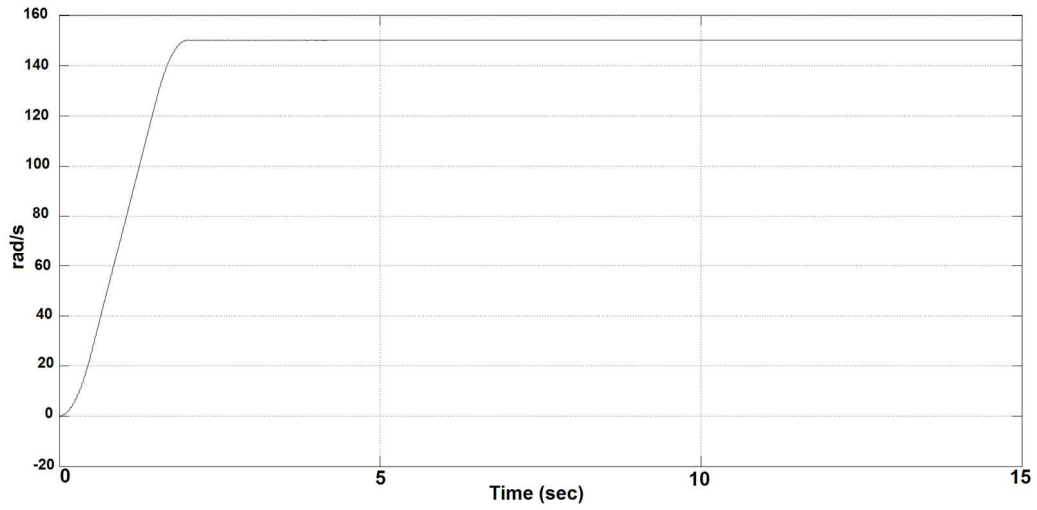


Figure 7.20. Velocity Curve of Pinion.

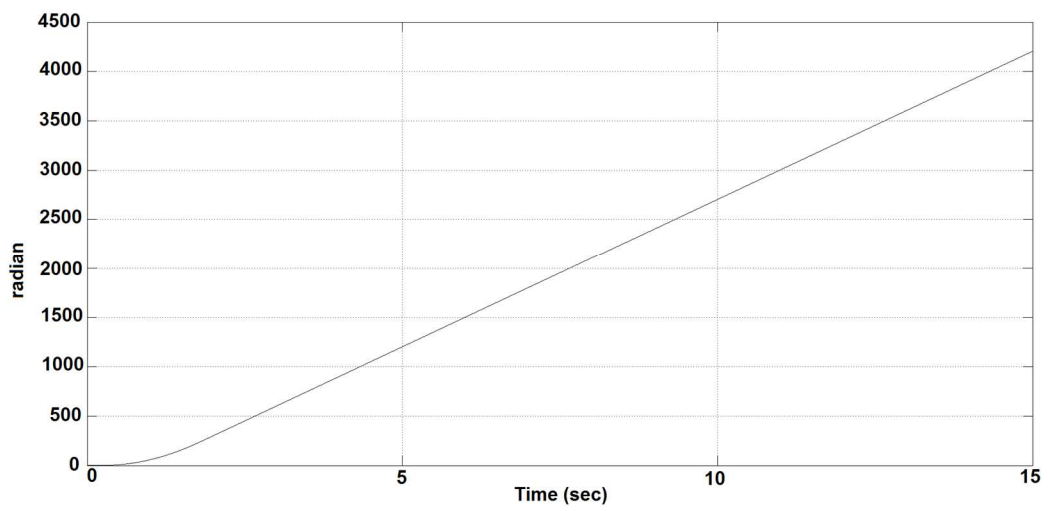


Figure 7.21. Position Curve of Pinion.

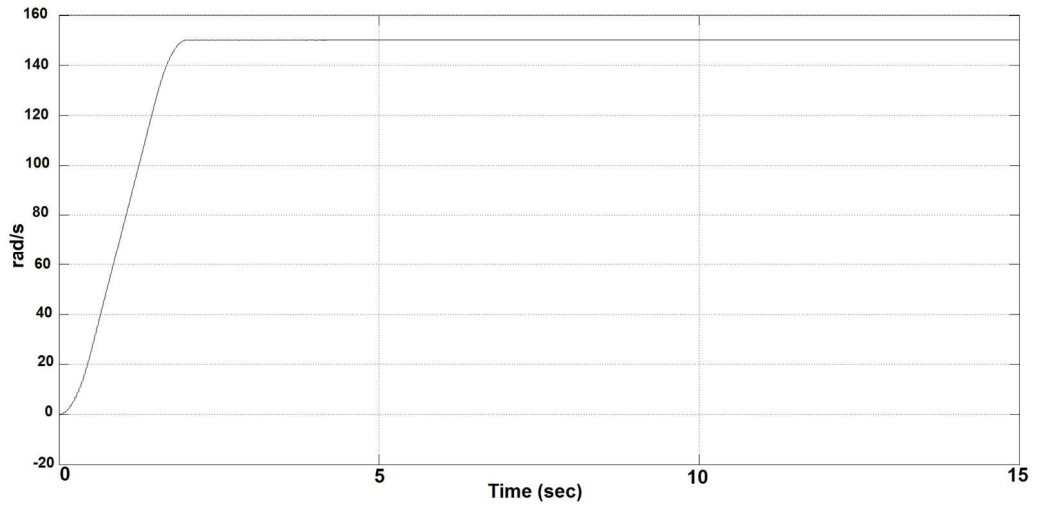


Figure 7.22. Velocity Curve of Gear.

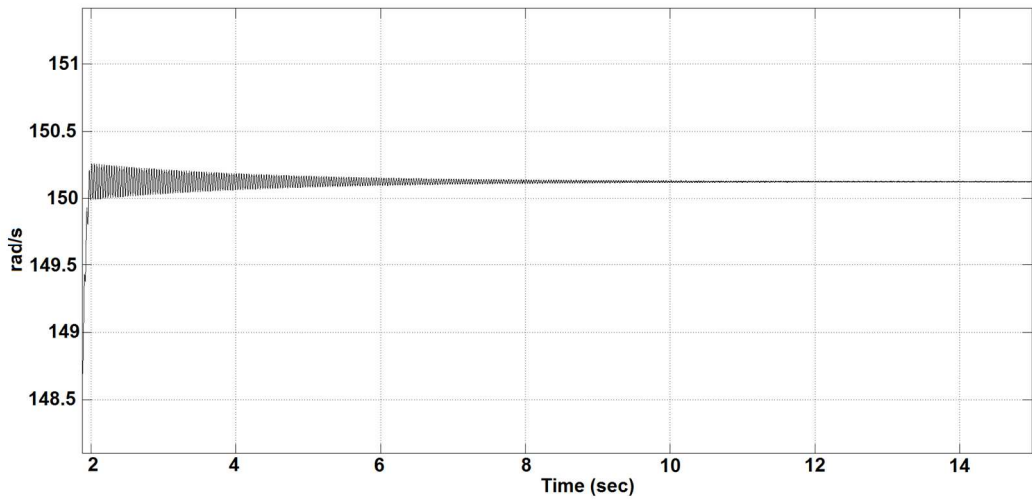


Figure 7.23. A Close Look at Velocity Curve of Gear.

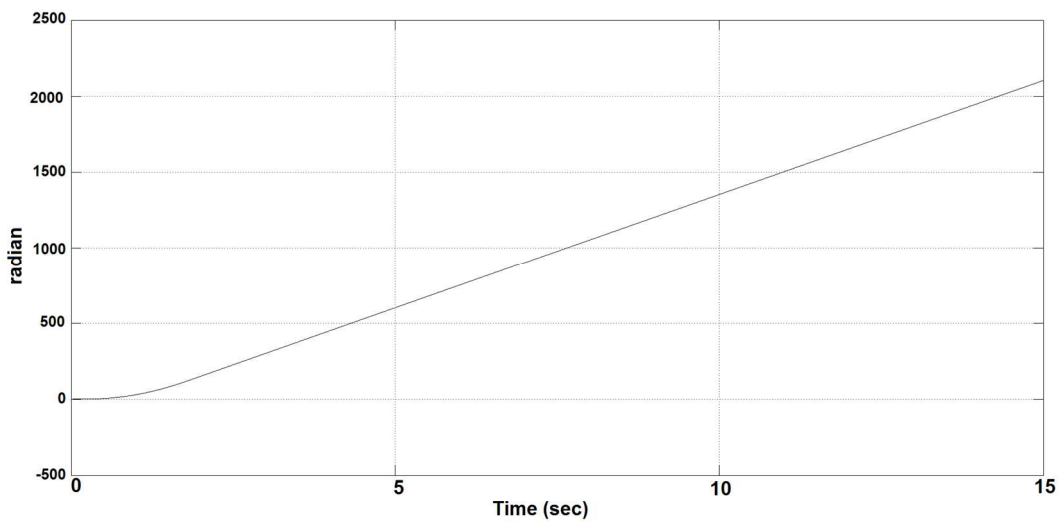


Figure 7.24. Position Curve of Gear.

7.3.3. Result of Case Study-3

The result of simulation of case 3 can be seen in Figures 7.25 to 7.32. In Figure 7.25, it is seen that in the starting times of motion when Transmission error is about 0.3×10^{-4} radian and this value in 10th second is 0.015×10^{-4} radian and in 15th second is about 0.0025×10^{-4} radian.

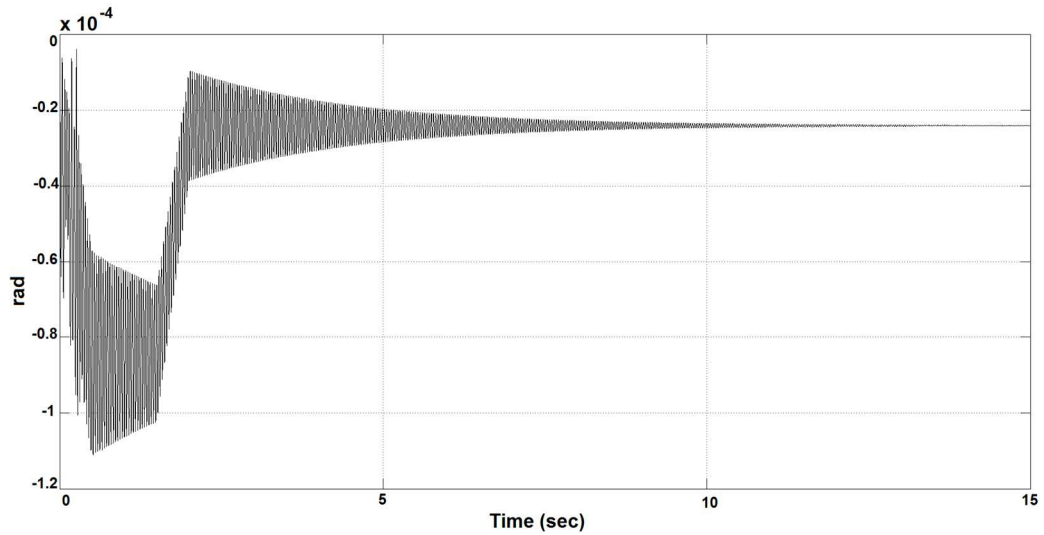


Figure 7.25. Transmission Error.

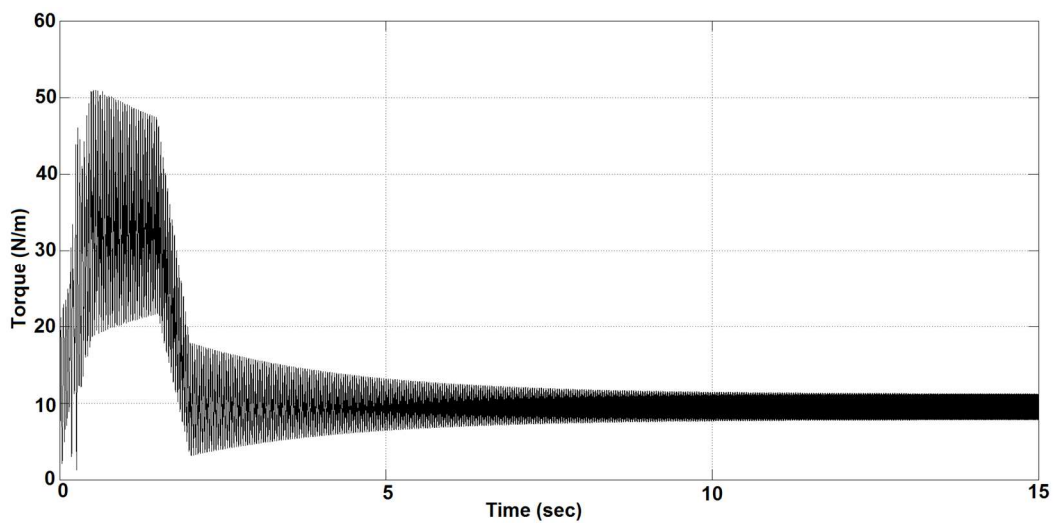


Figure 7.26. Input Torque.

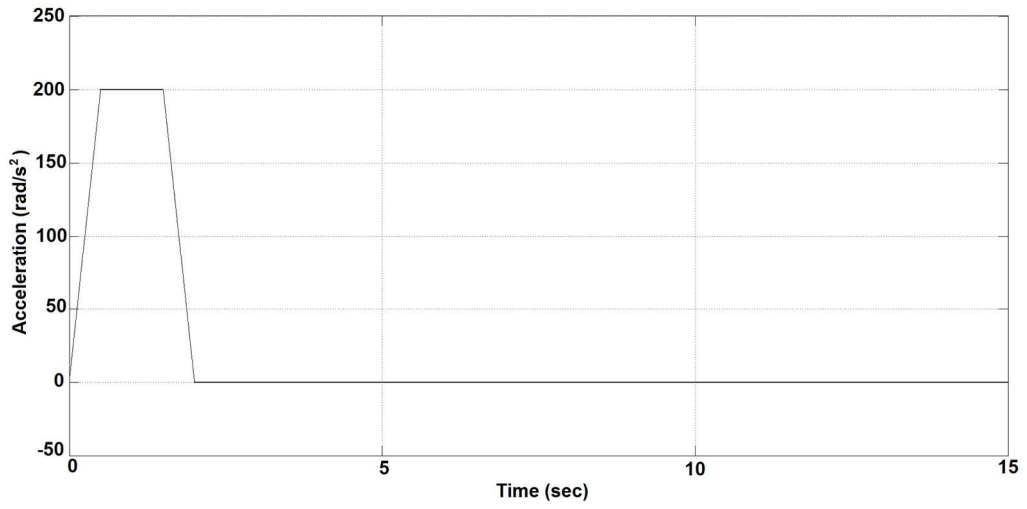


Figure 7.27. Acceleration Curve of Pinion.

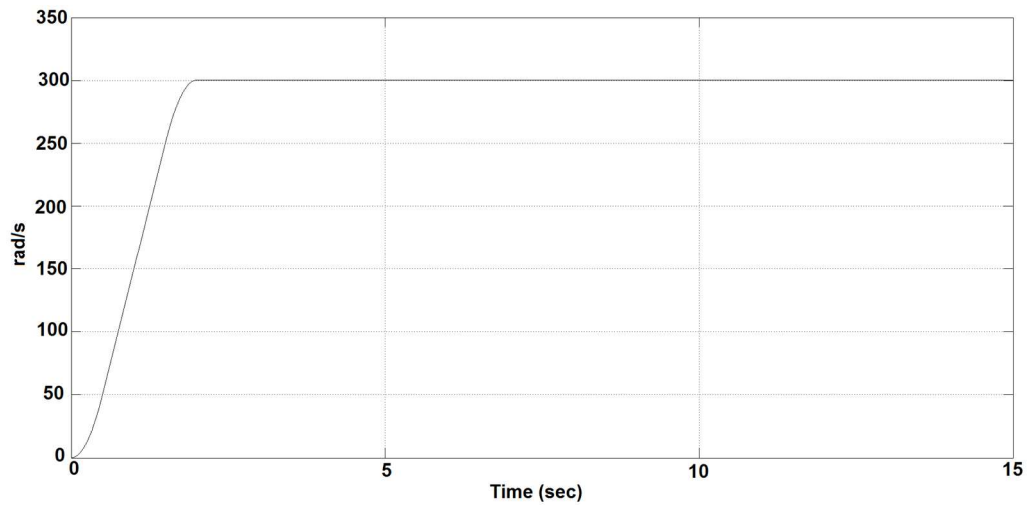


Figure 7.28. Velocity Curve of Pinion.

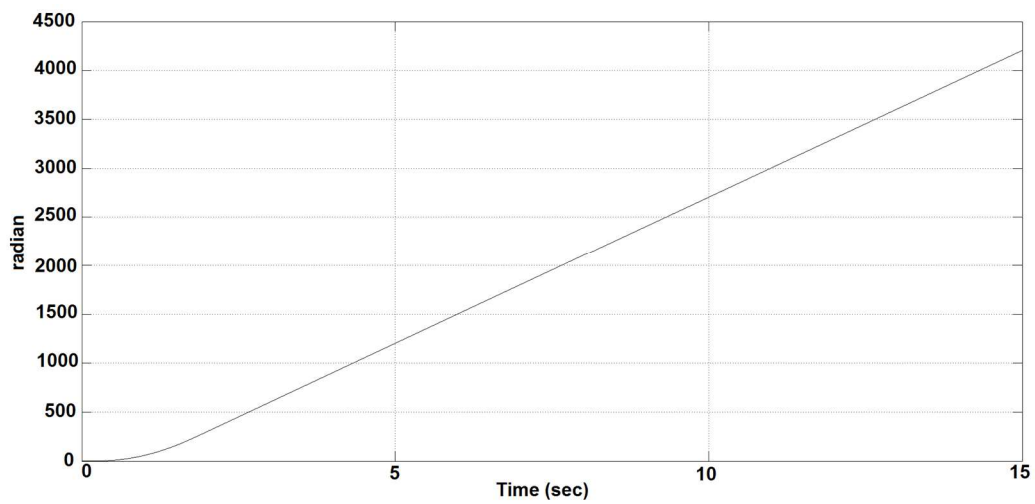


Figure 7.29. Position Curve of Pinion.

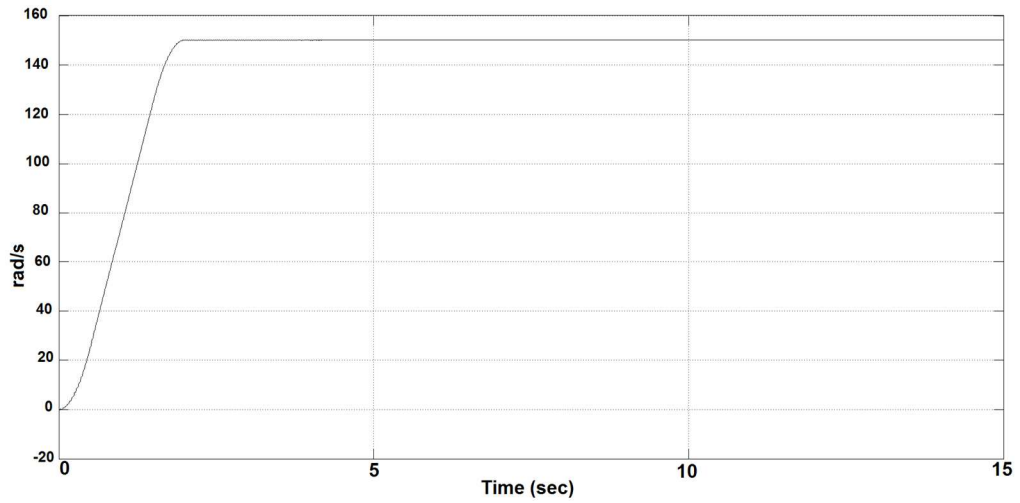


Figure 7.30. Velocity Curve of Gear.

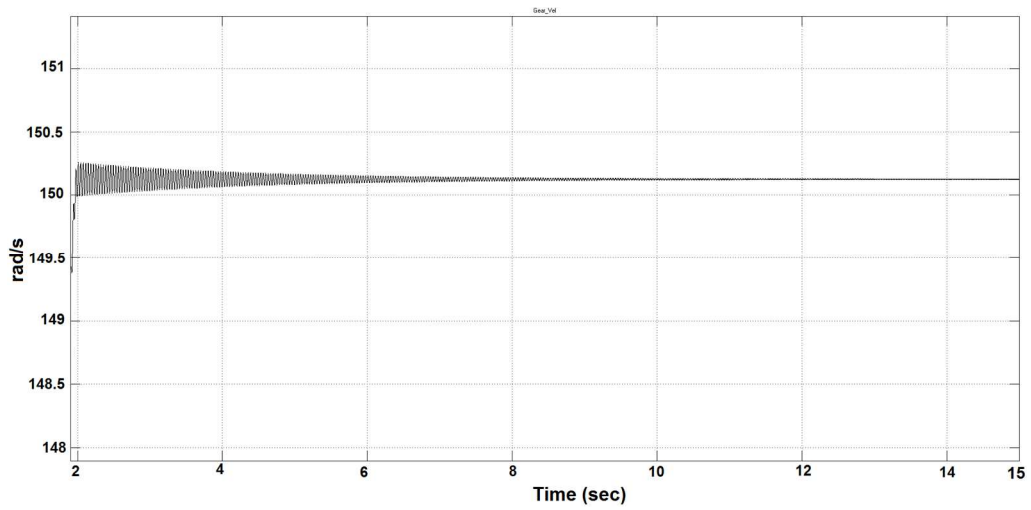


Figure 7.31. A Close Look at Velocity Curve of Gear.

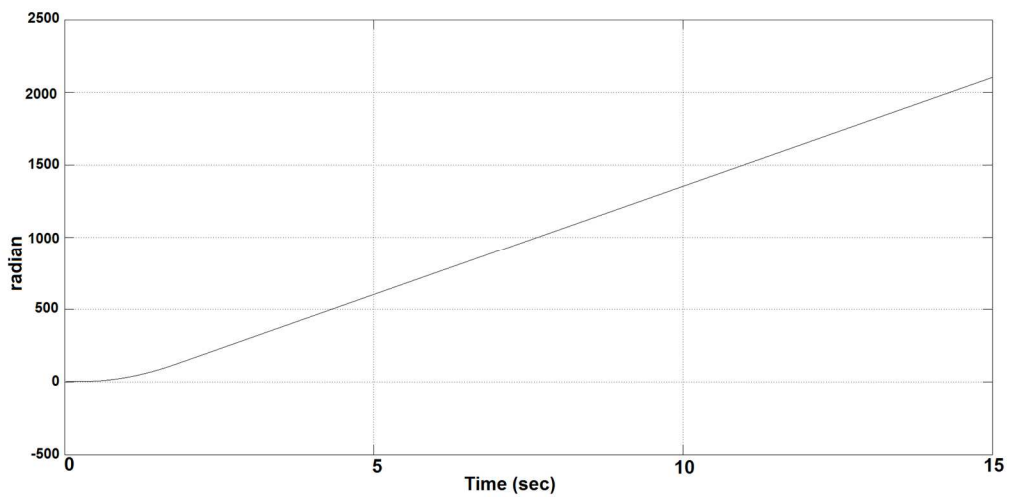


Figure 7.32. Position Curve of Gear.

7.4. Conclusion

By comparing results of simulations, it can be seen that by changing the system input and the type of input data, the quality of the system output can be easily determined. By examining the output of the system i.e. transmission error curve velocity curve and position curve in Figure 7.9, 7.14- 7.17 , 7.22- 7.25 and 7.30- 7.32, the system output can be seen in position curve and velocity curve completely is uniformly and without oscillation.

CHAPTER 8

Conclusion and Future Work

8.1. Conclusion and Future Work

In this study pair of spur gears with elastic modes was studied. The main goal of this study is to control the elastic mode of a spur gear to have a gear mechanism that runs silent and without transmission error. With this perspective in mind, a nonlinear controller with feed-forward loop was designed. A number of assumptions are made to realize such a nonlinear controller; it is assumed that nonlinear controller has got full access to the state of gear mechanism. Further, it is assumed that controller has got full access to the absolute angles of gears from a reference point. These absolute position information are necessary to compute the nonlinear mesh stiffness curve as a functions are difficult to meet in real life, it is not far from being true. For instance, the nonlinear stiffness curve can be computed in advance of operation by using a finite element software. Indeed of gear mechanism were analyzed by using ANSYS finite element software. Once this was done, nonlinear controller can cancel nonlinear forces that act on gear and pinion teeth. Thus, literally, system becomes a linear one, which opens up a room for application linear control techniques. Here, a simple form of pole-placement technique e.g. PI controller was used. It has been shown that the actuated part of a gear mechanism can be fully controlled, whereas unactuated part of the gear mechanism is at worst have a bounded-response. This bounded-response supports the idea of controlling a gear mechanism by a nonlinear controller.

Above the main goal and achievements of this study are reviewed. In addition to those things, a number of computational and theoretical subjects has also been studied in depth. First of all, a large number of spur gear mechanisms have been analyzed by ANSYS finite element software and their mesh controller for a spur gear mechanism has been discussed thoroughly.

Later in this work, to complete this study it can be worked with 2 and 3 stages gearboxes. Also, planetary gearboxes can be studied. The study can be continued on other types of gears. The gears which are widely used in industry, helical gears, bevel and helical bevel can be studied.

REFERENCES

- [1] Shoba Rani, T., & Khalandar, T.D. (2013), Spur gear. *Journal of Computational Engineering Research (IJCER)*. Retrieved January 29, 2015, from https://archive.org/stream/Httpijceronline.comindex.html/B0311010701_2_djvu.txt
- [2] Sirichai, S. (1999). *Torsional Properties of Spur Gears in Mesh Using Nonlinear Finite Element Analysis*. Doctoral Dissertation, Curtin University, Sydney.
- [3] Kahraman, A., & Blankenship, G. W. (1997). Experiments on Nonlinear Dynamic Behavior of an Oscillator with Clearance and Periodically Time-Varying Parameters. *ASME Journal of Applied Mechanics*, 64, 217–226.
- [4] Kahraman, A., & Singh, R. (1991). Interactions between time-varying mesh stiffness and clearance non-linearities in a geared system. *Journal of Sound and Vibration*, 146, 135–156.
- [5] Lin, J., & Parker, R.G. (2002). Mesh Stiffness Variation Instabilities in Two-Stage Gear Systems. *Journal of Vibration and Acoustics*, 124, 68-76.
- [6] Blankenship, G. W., & Kahraman, A. (1995). Steady State Forced Response of a Mechanical Oscillator with Combined Parametric Excitation and Clearance Type Non-linearity. *Journal of Vibration*, 185, 743–765.
- [7] Kahraman, A., & Blankenship, G. W. (1996). Interactions Between Commensurate Parametric and Forcing Excitations in a System with Clearance. *Journal of Vibration*, 194, 317–336.
- [8] Welbourn, D.B, (1979). Fundamental knowledge of gear noise: a survey. Retrieved March 14, 2015 from <http://trid.trb.org/view.aspx?id=199562>
- [9] Wang, J. (2003). *Numerical and experimental analysis of spur gear in mesh*. Doctoral Dissertation, Curtin University, Sydney.
- [10] Litvin, F.A., Lian, Q., & Kapelevich, A.L. (2000). Asymmetric modified spur gear drives: reduction of noise, localization of contact, simulation of meshing and stress analysis. *Journal of Computer methods in applied mechanics and engineering*, 188, 363-390.
- [11] Karpat, F., Ekwaro-Osire, S., & Karpar, E. (2012). A Computer program for dynamic load simulation of spur gears with asymmetric and symmetric teeth. *World Journal of Mechanics*, 2, 239-245.
- [12] Kahraman, A., Lim, J., & Ding, H. (2007). *A dynamic model of a spur gear pair with friction*. Paper presented at 12th IFToMM World Congress, Besançon, France.
- [13] Faggioni, M., Pellicano, F., Bertacchi, G., & Andrisano, A.O. (2007). *Dynamic optimization of spur gears*. Paper presented at the 12th FTToMM World Congress, Besançon, France.
- [14] Majtra, G. M. (2001). *Handbook of Gear Design*. Tata McGraw-Hill Publishing Company Limited, New Delhi.

- [15] Chen, Z., Shao, Y. (2011). Dynamic simulation of spur gear with tooth root crack propagating along tooth width and crack depth. *Journal of Engineering Failure Analysis*, 18, 2149–2164.
- [16] Wang, Q., Hu, P., Zhang, Y., Wang, Y., Pang, X., & Tong, C. (2014). A Model to Determine Mesh Characteristics in a Gear Pair with Tooth Profile Error. *Journal of Advances in Mechanical Engineering*, 2014.
- [17] Roy, M. R., Kumar, S. P., & Kiran, S.R. (2014). Contact pressure analysis of spur gear using FEA. *Journal of Advanced Engineering Applications*, 7(3), 27-41.
- [18] Tamminana, V. K., Kahraman, A., & Vijayakar, S. (2005). *A study of relationship between the dynamic factor and dynamic transmission error of spur gear pairs*. Paper presented at the ASME 2005 international design engineering technical conferences and computers and information in engineering conference, Long Beach, California.
- [19] Palmer, D., & Fish, M. (2012). Evaluation of methods for calculating effects of tip relief on transmission error, noise and stress in loaded spur gears. *Journal of Gear Technology*, 56-67.
- [20] Litvin, F.L., & Fuentes, A. (2004). *Gear Geometry and Applied Theory*. Cambridge University Press, Cambridge.
- [21] Kiekbusch, T., Sappok, D., Sauer, B., & Howard, I. (2011). Calculation of the Combined Torsional Mesh Stiffness of Spur Gears with Two- and Three-Dimensional Parametrical FE Models. *Journal of Mechanical Engineering*, 57, 810-818.
- [22] Andersson, A. (2000). An Analytical Study of the Effect of the Contact Ratio on the Spur Gear Dynamic Response. *Journal of Mechanical Design*, 122, 508-514.
- [23] Yang, D.C.H., & Sun, Z.S. (1985). A rotary model for spur gear dynamics. *Journal of mechanisms, transmissions, and automation in design*, 107(4), 529-535
- [24] Tian, X. (2004). *Dynamic simulation for system response of gearbox including localized gear faults*. Master of Science Dissertation, Alberta University, Alberta.
- [25] Autodesk Inventor Professional 2015 Program. Spur Gear tools Design application.
- [26] Seifried, R., (2014). *Dynamics of underactuated multibody systems: modeling, control and optimal design*. Springer, Switzerland
- [27] Al-Shyyab A. & Kahraman, A., (2005). Non-linear dynamic analysis of a multi-mesh gear train using multi-term harmonic balance method: sub-harmonic motions. *Journal of Sound and Vibration*, 279(1):417–451.
- [28] Amabili, M. & Rivola, A., (1997). Dynamic analysis of spur gear pairs: steady-state response and stability of the SDOF model with time-varying meshing damping. *Mechanical systems and signal processing*, 11(3):375–390.

- [29] Del Rincon, A.F., Viadero, F., Iglesias, M., García, P., De-Juan, A., & Sancibrian, R. (2013) A model for the study of meshing stiffness in spur gear transmissions. *Mechanism and Machine Theory*, 61:30–58.
- [30] Chen, Z., & Shao, Y. (2013). Mesh stiffness calculation of a spur gear pair with tooth profile modification and tooth root crack. *Mechanism and Machine Theory*, 62:63–74.
- [31] Theodossiades, S., & Natsiavas, S, (2000). Non-linear dynamics of gearpair systems with periodic stiffness and backlash. *Journal of Sound and vibration*, 229(2):287–310.
- [32] Velez, P., & Maatar, M. (1996). A mathematical model for analyzing the influence of shape deviations and mounting errors on gear dynamic behaviour. *Journal of Sound and Vibration*, 191(5): 629–660.
- [33] Faggioni, M., Samani, F.S., Bertacchi, G., & Pellicano, F. (2011). Dynamic optimization of spur gears. *Mechanism and machine theory*, 46 (4):544–557.
- [34] Chen, M., & Brennan, M. (2000). Active control of gear vibration using specially configured sensors and actuators. *Smart materials and structures*, 9(3):342.
- [35] Guan, Y.H., Shepard, W.S., & Lim, T.C. (2003). Direct hybrid adaptive control of gear pair vibration. *Journal of dynamic systems, measurement, and control*, 125(4):585–594.
- [36] Richards, D., & Pines, D.J. (2003). Passive reduction of gear mesh vibration using a periodic drive shaft. *Journal of Sound and Vibration*, 264(2):317–342.
- [37] Cheon, G.J. (2010). Numerical study on reducing the vibration of spur gear pairs with phasing. *Journal of sound and vibration*, 329 (19):3915–3927.
- [38] Temis, Y., Kozharinov, E., & Kalinin, D. (2015). Simulation of Gear Systems with Dynamic Analysis. The 14th IFToMM World Congress, Taipei, Taiwan.

CURRICULUM VITAE

Credentials

Name, Surname : Abbas KHOSHVAGHT PIRSOLTAN
Place of Birth : Tabriz
Marital Status : Married
e-mail : arazqartali@gmail.com
Address : Aydinlar Avenue, Iğde Alley, No: 8/10 Ankara-Turkey

Education

High School : Vahdat Industrial High School-Tabriz
BSc. : Rajae University-Tehran

Foreign Languages

Turkish (Azerbaijani Turkish) : Mother Tongue
Turkish (Turkey Turkish) : Fluent
English : Advanced
Arabic : Intermediate

Work Experience

Insol Inovative solutions Co. (Turkey) : 2013.06.01 up to now
J.T. Sahand Co. (Iran) : 2007.09.01 up to 2012.06.30
Air and Space Organization (Iran) : 2004 up to 2007

Areas of Experiences

Machine Design, Finite Element Analysis, Welding Inspection

Projects and Budgets

Publications

Oral and Poster Presentations

Pirsoltan. A. K., Altınkaynak, U. (2015). Paraplejik Hastaları Yürüten Giyilebilen Hibrid Robot Geliştirilmesi. Proje Park Biomed, 21 May, Kayseri, Turkey.

Patent

2014-GE-48475 document number and 2014/12943 application number by name "Bir giyilebilir Robot (An Exoskeleton Robot)" patented at Turkish Patent Institute.